Numerical Investigation on Forced Convection Heat Transfer over a Rotating Circular Cylinder Inside a Confined Channel

by

Md. Rakib Hossain

A dissertation submitted for the degree of **Master of Science** in the **Department of Mechanical Engineering**

Department of Mechanical Engineering

BANGLADESH UNIVERSITY OF ENGINEERING AND TECHNOLOGY

June 2021

The thesis titled "**Numerical Investigation on Forced Convection Heat Transfer over a Rotating Circular Cylinder Inside a Confined Channel**" submitted by **Md. Rakib Hossain**, St. Id: **1017102002**, Session: **October 2017**, has been accepted as satisfactory in partial fulfillment of requirement for the degree of **Master of Science in Mechanical Engineering** on June 20, 2021.

BOARD OF EXAMINERS

Dr. Mohammad Mamun Professor Dept. of Mechanical Engineering BUET, Dhaka-1000	**Chairman** (Supervisor)
Dr. Shaikh Reaz Ahmed Professor and Head Dept. of Mechanical Engineering BUET, Dhaka-1000	**Member** (Ex-officio)
Dr. Mohammad Arif Hasan Mamun Professor Dept. of Mechanical Engineering BUET, Dhaka-1000	**Member**
Dr. Sumon Saha Associate Professor Dept. of Mechanical Engineering BUET, Dhaka-1000	**Member**
Dr. A T M Hasan Zobeyer Professor and Head Dept. of Water Resource Engineering BUET, Dhaka-1000	**Member** (External)

Declaration of Authorship

I, Md. Rakib Hossain, declare that this thesis titled, "Numerical investigation on forced convection heat transfer over a rotating circular cylinder inside a confined channel" and the work presented in it is my own. I hereby confirm that:

- This work has been done completely or mainly while in candidature for a part of postgraduate degree at this University.
- This thesis or any part of this thesis has not been submitted elsewhere for any award or any degree or any diploma.
- Where I have consulted the published work of others, this is always clearly attributed.
- Where I have quoted from the work of others, the source is always given. With the exception of such quotations, this thesis is entirely my own work.
- I have acknowledged all main sources of help.

June 2021

Md. Rakib Hossain

ACKNOWLEDGEMENTS

Firstly, I would like to thank the Almighty Allah for blessing me with the accomplishment of this work.

I would like to express my sincere gratitude to my honorable supervisor, Dr. Mohammad Mamun, for his continuous support, encouragement, motivation and guidance throughout all phases of this M.Sc. Engg. study. It has been a great privilege and honor for me to work with him.

I would like to express my sincere gratitude to Dr. Sumon Saha for his precious advice and recommendations which have helped me tremendously to improve this research work.

I would like to thank the members of my thesis evaluation committee, Dr. Shaikh Reaz Ahmed, Dr. Mohammad Arif Hasan Mamun and Dr. A.T.M. Hasan Zobeyer for their valuable comments and suggestions.

Finally, I would like to thank my family for their encouragement and support, without which this dissertation and research would not have been possible.

“Research is to see what everybody else has seen,

And to think what nobody else has thought.”

-Dr. Albert Szent-Gyorgyi

ABSTRACT

Rotating cylinder flows are very important in aerodynamics and in engineering structures. Confined channel flow also has a wide range of applications including particles migration through veins, droplet dynamics and so on. The present study demonstrates a numerical investigation of forced convection heat transfer over a rotating hot circular cylinder vertically placed at the central axis of a confined horizontal channel for laminar and turbulent flow. The turbulent flow is investigated based on Reynolds Averaged Navier-Stokes (RANS) equations using the Shear Stress Transport (SST) model. Fully developed flow of air at ambient temperature is considered at the channel inlet for both laminar and turbulent flow cases, whereas the surface of the channel is kept insulated. The cylinder is rotating either in clockwise or counter-clockwise direction with a constant angular speed. The speed ratio, defined as the ratio between the cylinder's circumferential speed to the free stream speed, is varied along with the free stream speed. The governing mass, momentum and energy equations in non-dimensional form are solved numerically using Galerkin finite element method. For simultaneously solving those equations, segregated solution approach is applied, where multiple systems that depend on one another are solved separately in segregated steps. The modelling is performed in a steady and incompressible fluid flow. Parametric simulation is carried out over a range of mean flow Reynolds number based on the mean velocity of the working fluid within the range of $40 \leq Re \leq 2000$ for laminar flow and $3000 \leq Re \leq 10^7$ for turbulent flow. The variation of blockage ratio (β) is considered as 0.05, 0.1 and 0.2, whereas the rotational Reynolds number of the cylinder based on the peripheral velocity of the cylinder is set at Re_c = 4, 10, 20 and 30. The numerical results are visualized in terms of streamline plots, pressure contours and isosurface plots of thermal field. The distributions of coefficient of drag, coefficient of lift and average Nusselt number of the hot cylinder surface as a function of Reynolds number reveal a number of interesting observations from the present findings. From this study, it is found that rotational direction of the cylinder has negligible effect on thermal or flow fields and thus it doesn't affect the drag or lift coefficients and average Nusselt number. Although, the rotational speed of the cylinder has a significant influence on thermal or flow fields, it also doesn't affect any of the performance parameters. However, the downstream vorticity is greatly influenced by both the free stream velocity and the blockage ratio. Drag coefficients are higher for smallest cylinder both in laminar and turbulent flow whereas Lift coefficients are higher for laminar zone but no regular pattern is found for

turbulent flow. For laminar flow, *Nu* is greater for smallest cylinder but opposite for the case of turbulent flow. It is also found that the changes in *Re* and β significantly affect both the aerodynamic and the thermal performance of the confined channel. Drag coefficient decreases with the increase of Reynolds number while Lift coefficient approaches to zero for higher Reynolds number for laminar flow but for turbulent flow it shows arbitrary value around zero. And, *Nu* increases with the increase of Reynolds number up to a certain range in turbulent zone, after that following a decreasing pattern, it remains almost constant.

Contents

List of Figures

List of Tables

Abbreviations

CFD	Computational Fluid Dynamics
RANS	Reynolds Averaged Navier-Stokes
DNS	Direct numerical simulation
SST	Shear Stress Transport
FDM	Finite Difference Method
FVM	Finite Volume Method
FEM	Finite Element Method
CW	Clockwise
CCW	Counter Clockwise

Nomenclature

Symbols	Meaning	Unit
L	rectangular channel width	m
D	rectangular channel height	m
d	cylinder diameter	m
L_u	length from channel inlet	m
ω	angular speed	rad/s
β	blockage ratio	
u	x-axis velocity	m/s
v	y-axis velocity	m/s
ρ	density of fluid	kg/m^3
p	dimensional pressure	N/m^2
T	dimensional temperature	k
μ	dynamic viscosity	Pa*s
C_p	heat capacity at constant pressure	J/kg*k
$\mathrm{u_i}$	inflow velocity	m/s
T_c	ambient temperature	k
T_h	cylinder temperature	k
u_p	velocity of the cylinder	m/s
u_m	mean inflow velocity	m/s

Symbols	**Meaning**	**Unit**
α	Speed ratio	
Θ	dimensionless temperature	
Re	reynolds number	
Pr	prandtl number	
S_{ij}	strain rate tensor	
v_t	kinematic turbulent viscosity	m^2/s
k	turbulent kinetic energy	J/kg
ϵ	turbulent dissipation rate	m^2/s^3
μ_T	turbulent viscosity	Pa*s
ω	turbulent dissipation rate	m^2/s^3
C_D	drag coefficient	
C_L	lift coefficient	
Nu	average nusselt number	
F_D	drag force	N
F_L	lift force	N
A	projected area of the cylinder	m^2
Re_c	cylinder Reynolds number	

Chapter 1

Introduction

Heat transfer is such a branch of science that deals with the transfer of thermal energy. Heat transfer is very common in our day-to-day life. Different mechanical devices like Internal Combustion Turbines, Steam or Gas Turbines, air conditioners, refrigerators, etc., deal with the heat transfer. Transportation of heat by turbulent motion in many processes like chemical reactions, heat and mass transfer, and heat exchanger, etc., is of great importance from engineering viewpoint. This convection has several applications like nuclear reactor, electronics cooling, solar thermal technology, food processing industries and so on. Now-a-days, Computational Fluid Dynamics (CFD) have become a common tool for performing design and analysis of heat and mass transfer problems. There are many situations where the requirement of mean flow characteristics set by the designer becomes more essential than the behavior of flow and thermal fields. In that case, Reynolds Averaged Navier-Stokes (RANS) model can be chosen to perform numerical simulation within reasonable accuracy.

1.1 Convection Heat Transfer

Convection, also denoted as convective heat transfer, is the transfer of heat from one place to another by the motion of fluids. Convection is usually the dominant form of heat transfer in fluids. Convection is the most complex mechanism in comparison with other heat transfer mechanisms, namely conduction (heat diffusion) and radiation. Energy is transferred due to specific molecular motion (diffusion), along with by bulk or macroscopic motion of the fluid. In this motion a lot of molecules are moving collectively or as aggregates at any instant. Such motion in the presence of a temperature gradient increases the heat transfer. At aggregate condition, as the molecules retain their random motion, both the combination of energy transport by random motion of the molecules and by the bulk motion of the fluid is responsible for the total heat transfer. Depending on fluid motion, the convection can be classified as ‘natural’, ‘forced’ and ‘mixed’ convection.

1.1.1 Natural convection

Natural convection is a mechanism of heat transfer where the fluid motion is not influenced by any external source like fan or blower. In this mechanism, density of the fluid changes due to temperature gradient. This causes lighter hot fluid to move up and the relatively denser cold fluid to move close to the heated surface. Thus, a natural circulation of the fluid occurs, where the cold fluid moves up after being heated and again surrounding cold fluid fills the void. By this process thermal energy transfers from the heated surface to the relatively cold fluid layer. Natural convection is of great importance for its presence both in nature and engineering applications. Natural convection can be seen in the rising plume of hot air from fire, in the formation of microstructures during the cooling of molten metals and so on.

1.1.2 Forced Convection

Forced convection is such a type of heat transfer where the fluids are forced to move to increase the heat transfer. This force can be imposed by a fan, a pump, suction device, or other. As a result, heat transfer rate increases significantly compared to natural convection. By varying the fluid velocity, forced convection can be controlled, whereas natural convection occurs automatically. Forced convection has several applications like heat exchanger, pipe flow, and duct design in air conditioning system, steam turbines, lid driven cavity flow, etc.

1.1.3 Mixed convection

Mixed convection is the combination of natural convection and forced convection i.e., it occurs when both the natural convection and forced convection work together. This is the most common mode of heat transfer in practical situations. This is also defined by the occurrences where both buoyant forces and pressure forces interact. Several parameters like geometry, temperature, flow direction, flow velocity, etc. will define which type of convection (natural or forced) will dominate the mixed convection. This convection has several applications like thermal power plants, nuclear reactor, electronics cooling, solar thermal technology, food processing industries and so on.

1.2 Forced Convection Inside Channel

Forced convection inside a pipe or channel is a very popular problem. Generally, at the channel or pipe walls, the velocity of fluid becomes zero which means a no-slip condition. Flow patterns are greatly influenced by the surface of the channel or pipe. Inserting an obstacle inside the channel also affects the flow patterns significantly. Aerodynamic forces will generate on the surface of the obstacles with different heat transfer phenomenon if certain heating condition has been applied. However, if the obstacle shape is modified into triangular, trapezoidal, circular or any other complex shape, the pattern of forced convection may vary.

1.3 Laminar Flow

Laminar flow is a type of fluid flow where the fluid particles move smoothly or in regular paths comparing with that of turbulent flow. Laminar flow also known as streamline flow. In laminar flow, the flow properties at each point of the fluid remains constant. There is no cross-flow perpendicular to the direction of flow. Laminar flow is also characterized by high momentum diffusion and low momentum convection. It means that, viscous forces dominant over inertia force. Fluid flowing through a closed channel such as a pipe or between two flat plates, the flow may be laminar or turbulent depending on the velocity and viscosity of the fluid. At lower velocities laminar flow occur. The flow field is then determined by a non-dimensional parameter called the Reynolds number. This also depends on the dimension of the channel and the velocity, viscosity and density of the fluid. Laminar flow through a pipe occurs when the Reynolds number is below a threshold value of approximately 2,040.

1.4 Turbulent Flow

Most of the flows occurring in nature are turbulent by character, just like the production of smoke of any fire, tornado, cyclone, ocean current, etc. In fluid dynamics, turbulent flow is characterized by chaotic motion of the fluid. Turbulence is caused by excessive kinetic energy of a fluid that overcomes the damping effect of the fluid's viscosity. For this reason, turbulence is mainly visualized in low viscosity fluids. Turbulence is thus characterized by the following features:

- **Irregularity:** Turbulent flows are highly irregular in nature. For this, turbulent problems are normally treated as statistically. Turbulent flow is always chaotic. However, not all chaotic flows are turbulent.

- **Diffusivity:** The supply of energy in turbulent flows tends to accelerate the homogenization of fluid mixtures. The characteristic for which the enhanced mixing and increased rates of mass, momentum and energy transports is occurred in a flow is called "diffusivity".

- **Rotationality:** Turbulent flows always have some vorticity and are characterized by a strong 3-D vortex generation mechanism known as vortex stretching. In fluid dynamics, these vortices are associated with a corresponding increase of the component of vorticity in the stretching direction due to the conservation of angular momentum. On the other hand, turbulent energy cascade relies mainly on the vortex stretching to establish the structure function. In general, the stretching mechanism insinuates thinning of the vortices in the direction perpendicular to the stretching direction due to the conservation of volume of the fluid elements. For this reason, the radial length of the vortices decreases and the larger flow structures break down into smaller one. The process will continue until the small-scale structures are small enough that their kinetic energy can be changed by the fluid's molecular viscosity into heat. Thus, turbulence is always rotational and three-dimensional.
- **Dissipation:** To assist the turbulent flow, a permanent source of energy supply is required because turbulent dissipates rapidly as the kinetic energy has been changed into internal energy by viscous shear stress. Turbulent causes the formation of eddies of different length scales. Most of the kinetic energy of the turbulent motion has been occurred in the large-scale structures' region. The energy "cascades" from the large-scale structures to smaller one by an inertial and essentially inviscid mechanism. This process continues by creating smaller and smaller structures which produces a hierarchy of eddies. This process thus creates structures that are small enough that molecular diffusion becomes prominent and viscous dissipation of energy takes place finally. The scale at which this occurs is the Kolmogorov length scale.

Through this energy cascade, turbulent flow can be understood as a superposition of a spectrum of flow velocity oscillations and eddies with a mean flow. The eddies are mainly defined as coherent patterns of flow velocity, vorticity and pressure. Turbulent flows may be viewed as consisted of a full hierarchy of eddies over a wide range of length scales and the hierarchy can be explained by the energy spectrum that measures the energy in flow directions for each length scale (wavenumber). The scales in the energy cascade are normally uncontrollable and highly non-symmetric. Moreover, based on these length scales, eddies can be divided into three categories.

a) **Integral length scales:** This is the largest scales in the energy spectrum. Energy can be obtained by the mean flow from these eddies and also from each other. Thus, these are the energy production eddies that have most of the energy. They have the large flow velocity fluctuation and low frequency. Integral scales are greatly anisotropic and are determined in terms of the normalized two-point correlations of flow velocity. The maximum length of these scales is confined by the distinctive length of the apparatus. For instance, the largest integral length scale of the pipe flow problem is equal to the pipe diameter. For the case of atmospheric turbulence, this length can move up to the order of several hundred kilometers.

a) **Kolmogorov length scales:** These are the smallest scales ever in turbulent flow. At this scale, viscosity dominates and the turbulent kinetic energy is being dissipated into heat. For atmospheric motion, the typical values of the Kolmogorov length scale in which the large eddies have length scales on the order of kilometers, ranging from 0.1 to 10 millimeters.

b) **Taylor microscales:** The Taylor microscale is the intermediate length scale at which fluid viscosity greatly affects the behavior of turbulent eddies in the flow. This length scale is generally applied to turbulent flow that can be identified by a Kolmogorov spectrum of velocity fluctuations. In this kind of flow, length scales that are larger than the Taylor microscale are not affected by viscosity strongly. In the direction of flow, these larger length scales are generally referred to as the inertial range. The turbulent motions are subject to strong viscous forces below the Taylor microscale and kinetic energy is dissipated into heat. These shorter length scale motions are normally entitled as the dissipation range.

However, a total description of turbulent flow is one of the undefined problems in physics. Though it is possible to find some particular solutions of the Navier-Stokes's equations using the governing fluid motion, all such solutions are unable to finite disruptions at large Reynolds numbers. Dependence on the initial and boundary conditions creates the fluid flow irregular both in time and space so that a statistical information is needed. There is no useful analytical solutions of turbulent flows in geometries of engineering interest though statistical theories of turbulent flow have provided better understanding of the scaling laws in various flow regimes.

1.5 Direct Numerical Simulation

Direct numerical simulation (DNS) is such a simulation procedure in computational fluid dynamics (CFD) where the Navier–Stokes equations are solved numerically without any turbulence model. It means that the entire range of spatial and temporal scales of the turbulence must be determined. Every spatial scales of the turbulence must be determined with the help of the computational mesh, related with the motions having most of the kinetic energy. So, it can be concluded that DNS is very useful in developing of new models and the improvement of existing ones. However, DNS is limited to simple fluid flows and relatively lower range of Reynolds numbers.

1.6 Turbulence modelling

Turbulence modeling is the formation and utilize of a mathematical model to presage the effects of turbulence. Turbulence is an extremely complicated phenomenon by its nature. Besides any physical considerations, turbulence is by default three dimensional and time dependent. Thus, a great amount of information is required to describe the turbulent flow in total. Therefore, in building a mathematical model that approaches the physical behavior of turbulent flows, has far far less precision.

Since turbulence consists of random fluctuations of the various flow properties, a statistical approach is carried out for turbulence modeling. The objectives are best served by using the process introduced by O. Reynolds (1895) where all quantities are defined as the sum of mean and fluctuating parts. This procedure leads to the formulation of RANS equations for turbulent flow that is based on the adherences that the flow field over time have small, local oscillations that can be served in a time-averaged sense. Due to the nonlinearity of the Navier-Stokes equation, time averaging of the continuity and Navier-Stokes equations precedes to the appearance of momentum fluxes which act as apparent stresses throughout the flow.

The Navier–Stokes equations mainly govern the velocity and pressure field of a fluid flow. In case of turbulent flow, each of these quantities may be disintegrated into a mean part and a fluctuating part. By averaging the equations, we can find the Reynolds-averaged Navier–Stokes (RANS) equations, that govern the mean fluid flow. However, the nonlinearity of the Navier–Stokes equations signifies that the velocity fluctuations still come out in the RANS equations along with the presence of momentum fluxes that act as apparent stresses all over the flow. This demonstrates the issue of closure, i.e., establishing an adequate number of equations for all of the unknowns. Joseph Valentin Boussinesq was the first to look on the closure problem, by introducing the theory of eddy viscosity. In 1877 Boussinesq suggested relating the turbulence stresses to the mean fluid flow to define the system of equations. After that, Ludwig Prandtl proposed the additional concept of the mixing length along with the idea of boundary layer. For wall-bounded turbulent flows, the eddy viscosity should vary with distance from the boundary wall. In modern terminology, mixing-length model is referred as an algebraic model or a zero-equation model of turbulence. From the definition, an n-equation model presents a model that requires solution of n no. of differential equations in addition to conservation of mass, momentum and energy equations.

In this study, nine different turbulent models with RANS equations are used namely Algebraic yPlus, Length VELocity (L-VEL), k-ε, Realizable k-ε, k-ω, Shear Stress Transport (SST), Low Reynolds number k-ε, Spalart-Allmaras and v-2f. All of these models extend the Navier-Stokes equations with an additional turbulent viscosity term, but they differ by the calculation procedure.

1.6.1 Algebraic yPlus Model

The algebraic yPlus turbulence model is an algebraic turbulence model rested on the distance from the nearest boundary. The model is rested on Prandtl's mixing-length theory and is good for internal flows. It is so far less mesh sensitive than that of transport-equation models like Spalart-Allmaras or the k-ε model.

1.6.2 Length VELocity (L-VEL) Model

The L-VEL (Length-VELocity) turbulence model is also an algebraic turbulence model usually applied for electronic cooling applications. It is also less mesh sensitive than that of transport-equation models like Spalart-Allmaras or the k-ε model. It was evolved by Agonafer *et. al.* for internal fluid flows and uses an extension of the logarithmic law of the wall.

1.6.3 Spalart-Allmaras Model

The Spalart-Allmaras model appends a single additional variable namely Spalart-Allmaras viscosity and does not utilize any wall functions; it solves the whole flow field. The model was actually developed for aerodynamics applications and is beneficial in the fact that it solves only a single additional variable. For this reason, it is less memory-intensive than the other models which solve the flow field in the buffer layer. Experience also shows that this model does not exactly compute flow fields that exhibit shear flow, separated flow *etc*. Its benefit is that it is quite stable and shows better convergence.

1.6.4 *k-ε* Model

The k-ε model is one of the most applied turbulence models for industrial applications. This model contains the standard k-ε model. The model acquaints with two additional transport equations and two dependent variables; the turbulent dissipation rate, ε and the turbulent kinetic energy, k. The k-ε model is very famous for industrial purposes due to its good convergence criteria and relatively low memory necessities. It does not compute flow fields exactly that show adverse pressure gradients, strong curvature to the flow, or jet flow. It performs well for external flow problems around complex geometries.

1.6.5 *k-ω* Model

The k-ω model also solves for two dependent variables; the turbulent kinetic energy, k, and the dissipation per unit turbulent kinetic energy, ω. ω is also generally known as the specific dissipation rate. The execution of the k-ω model is same as the k-ε model. It also utilizes wall functions and therefore has sufficient memory requirements. Its converging is much more difficult and is quite sensitive to the initial guess of the solution. The k-ω model is helpful in many cases where the k-ε model is not accurate, such as internal fluid flows, flows that show strong curvature effect, separated flows, and jets.

1.6.6 Low Reynolds Number *k-ε* Model

When the accuracy of wall functions in the k-ε model is not sufficient, a low Reynolds number model can be used. "Low Reynolds number" appertains to the region close to the boundary wall where viscous effects dominate. Most low Reynolds number k-ε acclimates the turbulence transport equations by using damping functions. As it does not use wall functions, aerodynamic forces and heat flux can be modeled with higher accuracy.

1.6.7 Shear Stress Transport (SST) Model

To combine the uppishly behavior of the k-ω model at the near-wall region with the wholeness of the k-ε model, Menter *et. al.* introduced the SST (Shear Stress Transport) model that lies between the two. SST model in the CFD Module contains a few well-tested adjustments, such as production restrictors for both k and ω, the use of S instead of Ω in the restrictor for μ_T and a sharper cut-off for the cross-diffusion term. It is also a kind of low Reynolds number model, *i. e.* it does not apply wall functions.

1.6.8 *v2-f* Model

For the case of *v2-f* model, the turbulent viscosity is dependent on the velocity fluctuations, perpendicular to the streamlines. This phenomenon makes it possible to model turbulence anisotropy, and to distinct between low-Reynolds number effects and wall blockage. Global effects of the pressure fluctuations on the turbulent flow fields are contained by applying elliptic relaxation to the pressure strain term.

1.7 Turbulent Channel Flow and Heat Transfer

Channel flow can be modeled as internal flow where the confining walls change the hydrodynamic behavior of the fluid flow from an arbitrary state at the channel inlet to a definite state at the outlet. The flow may be laminar or turbulent depending on the flow velocity and fluid property. The flow may be turbulent when the Reynolds numbers are high enough depending on the geometry. If heat is applied on the wall, heat transfer occurs between the fluid bulk and solid wall. Heat may be provided to the wall either as constant wall heat flux or constant wall temperature difference. Due to turbulence in the flow, fluid particles show chaotic motion that increases the rate of energy and momentum exchange between the particles, thus accelerating the heat transfer and the friction coefficient. This friction coefficient also adds to the heat transfer. Moreover, the boundary conditions of the flow fields and the temperature fields also influence the turbulent heat transfer. Study of the turbulent flow and heat transfer over a rotating circular cylinder placed between a parallel channel are of great importance because of its essential nature in understanding the convective heat transfer between the fluid and solid boundary.

1.8 Motivation of the Present Study

Though DNS is the most accurate approach for analyzing turbulence, it is applicable only for simple physical geometries till now. But now-a-days, turbulent model is widely used in real life problems especially in the engineering sectors having many complex geometries. A few works have been done considering flow and heat transfer over rotating circular cylinder inside a confined channel. Most of the previous work deals with the constant speed ratio (ratio of the peripheral velocity of the rotating cylinder and the mean velocity of the working fluid) which means that the rotational speed of the cylinder is to be changed automatically with the change of mean flow Reynolds number which is not always the practical scenario of this type of problem. So, the present study of turbulence modeling of channel flow and heat transfer is mainly the observation of the practical scenario stated above.

1.9 Main Objectives of the Thesis

The main objectives of the present study are as follows:

- To find out the suitable turbulence model for the typical problem.
- To investigate the effect of rotational direction of the circular cylinder, the blockage ratio, the rotational speed of the cylinder as well as the change of mean velocity of the working fluid on the flow and the thermal characteristics of the confined channel.
- To observe the coefficient of drag, coefficient of lift and average Nusselt number of the hot cylinder surface as a function of Reynolds number.
- To find out the optimum condition of heat transfer.

1.10 Outline of the thesis

The primary goal of the present study is to investigate the effect of rotational direction of the circular cylinder, the blockage ratio, the rotational speed of the cylinder as well as the change of mean velocity of the working fluid on the flow and the thermal characteristics of the confined channel. This is presented in structured way for the easy readership and understanding. Before the main analysis, a proper theoretical background is provided on subject matter.

Chapter 1 discusses the theoretical aspects of the present analysis which contains a brief idea about convection, forced convection inside channel, laminar and turbulent flow, direct numerical simulation, turbulence modeling, turbulent channel flow and heat transfer. Finally, the application of present study and motivation of the present work are described. Objectives of the present work are also listed.

Chapter 2 encompasses sufficient literature review for the present work. This literature review is carried out on the basis of related physics, analysis procedure and geometry of the physical problem. Pertinent parameters, which are responsible for present work, are selected on the basis of the previous works.

Chapter 3 contains the mathematical modeling of the present study. The governing equations are also written both dimensional and non-dimensional forms. Appropriate boundary conditions are discussed. Turbulent kinetic energy and dissipation rate equation are shown for different turbulent models. Validation procedure is also discussed in details.

Chapter 4 represents formulation of the numerical methods. Firstly, general concept of CFD and numerical methods are discussed. After that, Galerkin weighted finite element formulation is shown for the present problem. Finally, code validation and grid independence test are described to ensure the numerical accuracy of the present work.

In **Chapter 5**, results and discussion are presented in a comprehensive way with related graphical analysis and contours. Effect of Reynolds number, blockage ratio, rotational direction and Reynolds number based on the circular cylinder on the variation of drag coefficient, lift coefficient and Nusselt numbers have been shown.

Chapter 6 summarizes the present work and concluding remarks are presented. Finally, further research scopes are presented for future research opportunities.

Chapter 2

Literature Review

This chapter commences by looking into both the experimental and numerical cases of flow past a circular cylinder in both the laminar and turbulent regimes. A great amount of interest has been found from the data and information obtained from these works. This literature review is split into four sections, laminar flow and heat transfer over a confined cylinder and rotating cylinder and same for the case of turbulent flow. The emphasis of the first two sections is entirely on the studies of laminar flow by both experimental and numerical methods. The latter two sections of the paper will compare the numerical models used for turbulent flows.

2.1 Laminar flow and Heat Transfer over a confined cylinder

Laminar flow past cylinders is a very interesting research topics from long since because of its importance in our day-to-day life. It has a wide range of applications in various branches like particle migration inside the veins, combustion including droplet dynamics and vaporization etc. The flow past a stationary cylinder inside a channel with the cylinder placed symmetrically at the center of the channel was studied by Chen et al. (1995). They focused on the nature and occurrence of the bifurcation from steady symmetric flow to the periodic shedding regime. Huang and Feng (1995) also investigated numerically flow over a circular cylinder confined between two parallel plates. In the study, the interplay among wall effects, elasticity, shear thinning and inertia is examined in detail.

Anagnostopoulos et al. (1996) studied the effect of blockage ratio on the vortices numerically. They have concluded that when the flow is steady, the size of the vortices decreases with the blockage ratio, while the spacing among the vorticities decrease in both directions with increasing blockage ratio when the flow is unsteady.

TABLE 2.1: Previous studies of laminar fluid flow in confined channel

Reference	Fluid	Confining Wall Boundary Conditions	Governing Parameters	Key findings
Zovatto and Pedrizetti (2001)	Any fluid	No slip	$100 \leq Re \leq 2000$	the transition from steady flow to a periodic vortex shedding regime happens at larger *Re* when the cylinder approaches to one wall
Chakraborty *et al.* (2004)	Air	Impervious wall	$0.1 \leq Re \leq 200$	total drag coefficient had been decreased with an increase in the blockage ratio for a definite value of the *Re*
Sahin and Owens (2004)	Any fluid	No slip	$0 \leq Re \leq 280$	identified the critical Reynolds numbers for different blockage ratios
Wen *et al.* (2004)	Air	No slip	$35 \leq \mathrm{Re} \leq 560$	the drag curve is in good agreement with the 2D computations of Henderson
Dipankar and Sengupta (2005)	Any fluid	Symmetry	$Re = 1200$	studied the the effect of gap (G) between the cylinder (of diameter D) and the wall, lift and drag coefficients
Kumar and Mittal (2006)	Any fluid	No slip	$0.005 \leq$ blockage ratio ≤ 0.125	with the increase of blockage ratio, the critical *Re* for the onset of the instability first decreases and then increases
Rehimi *et al.* (2008)	Air	Solid wall	$Re = 30$ - 277	showed experimentally the effect of channel confinement of a circular cylinder centered between two parallel walls
Singha and Sinhamahapatra (2010)	Air	No slip	$Re = 45, 100, 150, 200, 250$	validates that transition to vortex shedding regime is delayed when the channel walls are close to the cylinder
Sen *et al.* (2010)	Air	Slip and Towing tank boundary conditions	$Re \leq 40$	found the separation Reynolds number successfully

The unsteady momentum and heat transfer from an asymmetrically confined circular cylinder within a plane channel is investigated numerically by Mettu et al. (2006).

Rajani *et al.* (2013) also studied the unsteady laminar flow past a circular cylinder in a channel with fixed wall on both at top and bottom using OpenFOAM and studied the flow fields along with the pressure distributions. Nidhul *et al.* (2014) numerically investigated the effect of size of rectangular flow domain and grid spacing on flow past a circular cylinder at low Reynolds number. In the paper, the flow pattern and flow characteristics over a circular cylinder at low Reynolds number had been studied by means of vorticity magnitude contour, streamlines, coefficient of drag and change of x-component of velocity.

Sun *et al.* (2016) also investigated numerically the flow fields, lift coefficient, drag coefficient for laminar flow past a confined circular cylinder. Flow over a circular cylinder confined by walls with local waviness near the cylinder had been computed and the vortex shedding characteristics were studied by Deepakkumar *et al.* (2016). Among the four different locations considered in their study, the waviness located near the wake region effectively suppresses the shedding. Later, Mehdi *et al.* (2016) analyses fluid flow around around a 2-dimensional circular cylinder with Reynolds No of 200, 500, and 1000 with different angle of attack 0º, 5º, and 10º. In the study, the pressure coefficients, drag coefficients and vortex shedding for different Reynolds numbers and different angle of attack had been computed and compared with other numerical results that showed good agreement with the present results.

Zhang *et al.* (2016) study the laminar flow over a square cylinder confined within a channel conquered to a locally uniform blowing/suction speed placed both at the top and bottom channel walls. They have showed that wall blowing has a stabilizing effect on the flow, and the corresponding critical Reynolds number increases monotonically with increasing blowing velocity. Then, Mathupriya *et al.* (2018) investigated unsteady flow over a cylinder confined by two parallel walls using direct numerical simulation (DNS). They have concluded that different instability regimes are observed as the Re of the flow increases. Also, the confinement effects played a significant role in changing the properties of the wake.

Doreti and Dineshkumar (2018) later investigated various control techniques to reduce vortex induced vibrations, drag and lift force acting on circular cylinder in-order to prevent structural damage and discussed the effect of those techniques in modifying the wake flow structure is

2.2 Laminar flow and Heat Transfer over a rotating cylinder

TABLE 2.2: Previous work of laminar flow over a rotating cylinder

Reference	Fluid	Confining Wall Boundary Conditions	Governing Parameters	Speed Ratio	Key findings
M. B. Glauert (1957)	Any fluid	----	----	constant	circulation increase indefinitely with the increase of rotational speed
Ingham (1983)	Any fluid	Solid wall	*Re* = 5, 20	Constant; 0, 0.1, 0.2, 0.3, 0.4, 0.5	effects of using different boundary conditions on the stream-function at large distances from the cylinder are presented and discussed
Ingham and Tang (1990)	Any fluid	Solid wall	*Re* = 5, 20	Constant; 0, 0.1, 0.2, 0.4, 0.5, 1, 3, 5	investigated steady and unsteady flow past a rotating circular cylinder respectively for different Reynolds number and speed ratio
Tang and Ingham (1991)	Any fluid	Solid wall	*Re* = 60, 100	Constant; 0 ≤ Speed Ratio ≤ 1	extend the Reynolds number range for reliable data on the steady flow, particularly with regard to the lift and drag coefficients.
Chew *et al.* (1995)	Any fluid	Solid wall	*Re* = 1000	Constant; 0 - 6	showed that the present method can be used to calculate not only the global characteristics of the separated flow, but also the precise evolution with time of the fine structure of the flow field
Kang *et al.* (1999)	Any fluid	No slip	*Re* = 40, 60, 100, 160	Constant 0 ≤ Speed Ratio ≤ 2.5	With increasing speed ratio, the mean lift increases linearly and the mean drag decreases, which differ significantly from those predicted by the potential flow theory
F. H. Barnes (2000)	Water	Solid wall	*Re* = 50, 55, 60, 65	Constant 0 ≤ Speed Ratio ≤ 1.2	measurements were made to determine the α value at which shedding is suppressed for Reynolds numbers between 50 and 65

highlighted in this work. Later, Cavanagh and wulandana (2019) studied the flow effects at Reynolds numbers of 20, 50, 200, and 500 in the steady laminar and periodic shedding regimes. They have found that for stationary case, the length of the recirculation zone is independent of the number of ridges, while the drag coefficient generally increases as the number of ridges increases. Then, Jagad *et al.* (2018) investigated the flow over a circular cylinder embedded on different spherical and cylindrical surfaces at a fixed Reynolds number of 100 and concluded that the effect of surface curvature is insignificant on drag coefficient, lift coefficient and Strouhal number.

Tokumaru and Dimotakis (1993) also studied the same as Ingham and Tang (1990). Stojkovic *et al.* (2002) numerically investigated two-dimensional laminar flow over a circular cylinder rotating with a fixed angular velocity and concluded that the mean drag had been decreased with increasing circumferential speed of the cylinder. Stojkovic *et al.* (2003) and K. M. Lam (2009) investigated vortex shedding for flow past a rotating circular cylinder with different Reynolds number and rotational speed. Later, Mittal and Kumar (2003) performed similar numerical investigation and showed that the results from the stability analysis for the rotating cylinder were in very good agreement with those from direct numerical simulations. They concluded that the flow became unstable for speed ratio within $4.3 < \alpha < 4.8$. Cliffe and Taveneer (2004) concluded that the critical flow rate where the instability generates can be increased by rotating the cylinder about its own axis, and that at a fixed flow rate the vortex street can be removed entirely by sufficiently large rotation.

After that, Snagmo Kang (2006) and Sojoudi and Saha (2013) studied numerically uniform shear and shear thinning and thickening respectively over a rotating circular cylinder. Kumar *et al.* (2011) investigated flow past a rotating circular cylinder experimentally and showed that Strouhal number measurements and global wake patterns agree well with previous work. Flow past rotating circular cylinders near a wall in the low Reynolds number regime was studied by Rao *et al.* (2011). The wake-wall interactions were investigated in detail, for different wall heights and rotational rates by Shaafi *et al.* (2017). Later, Sengupta and Patidar (2018) numerically investigated flow past a cylinder executing rotary oscillation for $Re = 250 - 400$ using two-dimensional (2D) stream function-vorticity formulation. They proved that their results match more accurately with experimental results both qualitatively and quantitively.

Badr *et al.* (1989) also studied the steady and unsteady flows past a circular cylinder rotating with constant angular velocity and translating with constant linear velocity. They have concluded that the values of the steady-state lift, drag and moment coefficients from the two methods are found to be in good agreement.

Apart from fluid flow, Paramane and Sharma (2009), Paramane and Sharma (2010) numerically investigated heat transfer across a rotating circular cylinder maintained at constant temperature and uniform heat flux respectively to observe flow patterns, Nusselt numbers for different Reynolds numbers and blockage ratios. Prasad *et al.* (2011) extended the similar works in order to analyze the combined effect of channel-confinement and cylinder rotation on the flow and heat transfer across a cylinder for various blockage ratio, rotational velocity and Reynolds number. Similarly, the effects of Prandtl number on the heat transfer characteristics of an unconfined rotating circular cylinder are investigated for varying rotation rate for different Reynolds number and Prandtl numbers are investigated by Sharma and Dhiman (2012). Sharma *et al.* (2015) also investigated temperature distribution and heat transfer for uniform wall temperature condition for flow past a rotating cylinder. They had described the effect of vortex shedding, drag and lift characteristics and concluded that the heat transfer rate increases with increasing Reynolds number.

2.3 Turbulent flow and Heat Transfer over a confined cylinder

A. Roshko (1961) investigated the flow past a circular cylinder experimentally for Reynolds number from 10^6 to 10^7 and concluded that the drag coefficient increases from its low supercritical value to a value 0.7 at Re = 3.5 x 10^6 and then becomes constant. Yazdi and Khoshnevis (2018) experimentally studied the effect of sub critical Reynolds number of the flow across an elliptic cylinder and observed lower turbulence intensity and velocity defect parameters. Ford and Winroth (2019) also studied experimentally the scaling and topology of confined bluff-body flows for Re = 10^4 to 10^5 and found that flow topology changes substantially between short and long tailed geometries.

Experimental investigation of flow past a circular cylinder in a pipe is studied by Arumuru *et al.* (2020) to understand the effect of Reynolds number and blockage ratios. They concluded that in the turbulent regime, the upstream flow becomes fully turbulent, and the Strouhal

TABLE 2.3: Previous work of turbulent flow over a circular cylinder in a confined channel

Reference	Fluid	Confining Wall Boundary Conditions	Governing Parameters	Key findings
Islam and Raghavan (2006)	Air	No slip	$Re = 100000$	laminar model works very well up to Re of 10^5 and the discrepancy between the present approach and experiments increases with Re beyond this value
Benim *et al.* (2007)	Air	Symmetry	$Re = 10^4$ to 5×10^6	predict the boundary layer transition and the associated drag coefficient reduction
Rahman *et al.* (2007)	Air	Periodic	$Re = 1000$, 3900	computed the pressure and drag coefficients for different Reynolds numbers and compared with experimental and other numerical results
Parnaudeau *et al.* (2008)	Air	Solid wall	$Re = 3900$	Both the numerical and experimental results are found to be in good agreement with previous large eddy simulation data
Ong *et al.* (2009)	Air	Impervious wall	$Re = 10^6$, 2×10^6, 3.6×10^6	satisfactory results for engineering design purposes are found for high Reynolds number flows around a circular cylinder in the supercritical and upper-transition flow regimes, i.e. Re > 10^6.
Yagmur *et al.* (2015)	Air	Solid wall	$Re = 5000$, 10000	the numerical and experimental results were in good agreement in case of the instantaneous and time-averaged flow field patterns of vorticity, velocity component along streamwise direction and streamline topology
Yuce and Kareem (2016)	Air	No slip	$Re \leq 4\times10^6$	Wake downstream of the square cylinder was found to be much more turbulent than that of the circular one
Daneshi M. (2016)	Air	No slip	$Re = 10^6$, 2×10^6, 4×10^6	the frequencies of the drag and lift coefficients obtained theoretically agreed well with the experimental results

number remains constant. The spanwise pressure distribution is influenced due to the blockage effects near the wall. Later, Maryami et al. (2020) studied experimentally the unsteady pressure exerted on the surface of a round cylinder in smooth and turbulent flows and shown that an increase in the length scale of the flow structures increases the spanwise correlation length of the flow structures at the vortex shedding frequency at the stagnation point, while at the cylinder base, the spanwise correlation length decreases at the vortex shedding frequency.

Tabata and Fujima (1991) then studied numerically the flow past a circular cylinder using finite element method and discussed the effect of the subdivision of the boundary layer upon flow patterns and drag coefficients. Tutar and Holdo (2001) numerically observed flow around a circular cylinder in sub-critical flow regime using two groups of turbulence models and showed that the finite element method (FEM) can also be used with confidence for this type of flow. Young and Ooi (2004) numerically investigated the effect of the turbulent length scale at the inlet and found that the variations of up to 14% were noted in the flow properties such as mean drag and Strouhal number, but large discrepancy between experimental and computational results had been remained.

Dong and Karniadakis (2005) presented the results of direct numerical simulations (DNS) for turbulent flows over a stationary circular cylinder and over a rigid cylinder imposing forced harmonic oscillations at Reynolds number Re = 10,000. They have compared their data with experimental one and showed that the simulation has captured the physical quantities and the statistics of the cylinder wake correctly. The roughness effects on the flow past a circular cylinder were investigated numerically by Rodriguez *et al.* (2016) and Xie and Wang (2016). Pang *et al.* (2016) investigated high Reynolds number flow around a cylindrical bluff body and concluded that the k-ω (SST) model is supercilious to other two-equation RANS models and is capable of capturing the effects of surface roughness. The curvature correction modification to the k-ω (SST) model further amends this model.

Later, Plata *et al.* (2018) numerically investigated flow past a circular cylinder using a multiscale discontinuous Galerkin method for Re = 20000 and 140000 and found an overall good agreement with the reference CFD in terms of integral flow quantities and near-wake statistics. Then, Turbulent flow characteristics around a circular cylinder was studied by Yao *et al.* (2019) to show the effect on the drag coefficient, lift coefficient and the distribution of the wind pressure. Kumar and Singh (2020) also studied numerically the flow past a cylindrical bluff body at sub-critical Reynolds number and observed that at fixed *Re*, the drag coefficient (C_D) increases with an increase in the blockage ratio while decrease with increasing *Re* for a fixed value of blockage ratio. After that, Ooi et al. (2020) numerically investigated the effect of blockage ratio for *Re* = 3900 and concluded that at higher blockage ratios, an adverse pressure gradient develops and the boundary layer on the channel walls separates and interacts with the cylinder wake.

Sowoud *et al.* (2020) studied the turbulent flow past a cylinder for different Reynolds number and showed both qualitative and quantative results. Then the super hydrophobicity on the flow past a circular cylinder in various flow regimes are investigated using particle image velocimetry-based experiments was studied by Sooraj *et al.* (2020). They concluded that the surface modification can reduce the drag coefficient and have a profound effect on the near wake.

Using the technique of large eddy simulation flow over a circular cylinder at Reynolds number 3900 is studied numerically by Kravchenko and Moin (2000). They have studied the impact of numerical resolution on the shear layer transition and found that the power spectra of velocity fluctuations are in excellent agreement with the experimental data. Breuer (2000) also using the same technique of LES, evaluated the applicability of LES for practically relevant high-*Re* flows and investigated the influence of sub-grid scale modeling and grid resolution on the quality of the predicted results. Catalano *et al.* (2003) also used the LES modelling flow around a circular cylinder in the supercritical regime and compared the data with RANS solutions and experimental data and concluded that LES solutions are shown to be considerably more accurate than the RANS results.

Rodriguez *et al.* (2015) and Sidebottom *et al.* (2015) used the LES modelling to investigate the flow topology, vortex shedding process and to assess the effect of four numerical parameters namely sub-grid scale (SGS) turbulence models, wall models, discretization of the advective terms in the governing equations, and grid resolution respectively. Zhang et al. (2019) numerically investigated turbulent flow and noise sources on a circular cylinder in the critical regime by LES. The far-field noise obtained in the study by both direct computation and acoustic analogy shows a dominant vortex shedding tone, but with additional broadband sources in the cylinder wake.

2.4 Turbulent flow and Heat Transfer over a rotating cylinder

TABLE 2.4: Previous work of turbulent flow over a rotating cylinder

Reference	Fluid	Confining Wall Boundary Conditions	Governing Parameters	Speed Ratio	Key findings
Badr *et al.* (1990)	Any fluid	Solid wall	$10^3 \leq Re \leq 10^4$	Constant; 0.5, 1, 3	there is admirable agreement between both the numerical and experimental results for all speed ratios considered, except for the highest rotation rate.
Cheng *et al.* (1994)	Any fluid	Solid wall	$Re = 6\times10^3$	Constant; 0, 0.1, 0.2, 0.3	calculated values for different separation positions, the drag and lift force coefficients, the velocity and the pressure distribution on the cylinder surface are found to good agreement with the published experimental data
Nair *et al.* (1998)	Any fluid	No slip	$Re = 3800$	Constant; 0.5, 1, 3	concluded that their finite-difference method is found to be accurate and fast as compared with other published results
Dierich *et al.* (1998)	Any fluid	Solid wall	$Re = 1.5\times10^4$ to 10^5	variable	Shown that the universal logarithmic velocity distribution is still valid near the wall.
Chou M. H. (2000)	Air	No slip	$Re = 10^3$ and 10^4	Constant; ≤ 3	showed the flow field and calculated time dependent lift and drag coefficients
. Elmiligui *et al.* (2004)	Air	periodic	$Re = 50000$	Constant; 0, 0.2, 0.4, 0.6, 0.8, 1	predicted the drag coefficient, lift coefficient and the Strouhal number and commented that modified PANS model was the most accurate
Takayama and Aoki (2004)	Air	Solid wall	$Re = 0.4\times10^5$ to 1.8×10^5	Constant; 0 to 1	concluded that both the drag and lift coefficients with arc grooves increases with the increasing spin ratio

Sanjital and Goldstein (2004) studied the forced convection heat transfer from a circular cylinder for a wide range of Reynolds number and Prandtl number. They had proposed an empirical correlation for identifying the overall heat transfer from the cylinder. Later, Shao and Zhang (2006) presented both the RANS and LES modelling to simulate the flow over a circular cylinder at a Reynolds number of 5800, that is based on free-stream velocity and the diameter of cylinder. They have investigated both the velocity field and the temperature field and analogized with the experimental measurements. Lastly, Ma and Duan (2020) investigated the flow similarities and heat transfer around a circular cylinder for a wide range of Reynolds number and showed the effect on drag coefficient, lift coefficient and Nusselt number.

Direct Numerical Simulation of Turbulent flow around a rotating circular cylinder was studied by Hwang *et al.* (2007). They have computed the turbulent kinetic energy and found to be similar to that in plane channel flow as well as in pipe and zero pressure gradient boundary layer flows. Cheng and Luo (2007) then studied the effect of wall confinement for flow around a rotating circular cylinder and observed that the mean drag coefficient increases monotonically with the gap between the cylinder and the wall.

Dol *et al.* (2008) then experimentally investigated periodic vortex shedding from a rotating circular cylinder for Reynolds number of 9000 for velocity ratios between 0 and 2.7. They have observed that the convection speeds of the two rows of vortices differ while the spacing ratio diminishes and increased inequality of the two separated shear layers leads to weaker vortices in the near wake region. S. J. Karabelas (2010) then studied the Large Eddy Simulation of high-Reynolds number flow past a rotating cylinder with different spin ratios. He had concluded that as the spin ratio increases, the mean drag decreases and the flow is also stabilized. He also proved the LES computations could be accurate for high-Re sub-critical flows. Now, Karabelas *et al.* (2012) studied the same but using the RANS equations via finite volume method. They had found that load coefficients were inversely proportional to the Reynolds number for most of the examined rotational rates.

The flow past a rotating cylinder at supercritical Reynolds number has been studied using the computational fluid dynamic methods by Yao *et al.* (2016). They have analyzed the variation of flow field around a rotating cylinder and showed the variations of lift and drag coefficients. After that, Mgaidi *et al.* (2018) and Yazdi *et al.* (2019) analyzed the flow around a rotating circular cylinder at subcritical regime of Reynolds number by both experimentally and numerically. Mgaidi *et al.* (2018) have mainly focused on the lift coefficients and compared their numerical values with the experimental data they have found. Their experimental data matches best with the SST models.

Yazdi *et al.* (2019) also used the SST models for numerical study and investigated Strouhal number, drag coefficient and flow pattern for different Reynolds number and spin ratios. They have found that with increasing the rotation ratio, the drag coefficient is decreased and also, by increasing the rotation ratio, the positions of the stagnation and separation points are changed. Lastly, Chen *et al.* (2020) experimentally investigated the whirl and generated forces of rotating cylinders in still water and suggested that the frequency of the DFW (Different Frequency Whirl) may equal multiple times or one-multiple times that of the rotating frequency: the whirl direction of the DFW with multiple times the frequency of the rotating frequency is the same as the rotating direction.

Ozerdem (2000) experimentally measured the convective heat transfer coefficient for a rotating horizontal cylinder and proposed a correlation between the Nusselt number and turbulent Reynolds number for a range of Reynolds number. Ouali et al. (2006) also investigated convective heat transfer coefficient experimentally for flow past a circular cylinder. Correlations between the Nusselt number with the axial and rotational Reynolds numbers are proposed. Later, Eighnam (2014) investigated heat transfer from a rotating cylinder by both experimentally and numerically to establish a correlation connecting to Nusselt number and Reynolds number.

Chapter 3

Mathematical Formulation

For any kind of numerical problem, it is necessary to model the problem mathematically. Any physical system can be modeled using one or more algebraic or differential equations. After that, these equations have to be solved using appropriate initial and/or boundary conditions found from the physical problem. Hence, mathematical modeling is the most important part to obtain the accurate and realistic solution of the physical problem.

3.1 Physical Problem

The details of the rectangular shaped cavity are shown in figure 3.1. The computational domain is presented in Cartesian coordinate having its origin at the center of the cylinder. The rectangular channel has a width of $L = 3D$, where D is the diameter of the channel. The circular cylinder of diameter d is centrally placed inside the channel at a distance of $Lu = 1.2D$ from the channel inlet. The cylinder is rotating at an angular speed of ω either clockwise (CW) or counterclockwise (CCW) direction and the surface of the cylinder is kept at a high temperature Th. Three different diameters of the cylinder are selected and hence, the blockage ratio (β) is varied as $\beta = d/D = 0.05$, 0.1 and 0.2 respectively.

3.2 Mathematical modelling

Mathematical modeling consists of governing equations and boundary conditions for the present problem. At first, dimensional governing equations are formulated from the physical system along with appropriate boundary conditions. Later, few scales are applied to the governing equations and boundary conditions to convert them in non-dimensional form. Different models are available to evaluate the thermo-physical properties of air as a single phase. Among them, Laminar flow and SST (Shear Stress Transport) model for turbulent flow are considered for the present problem.

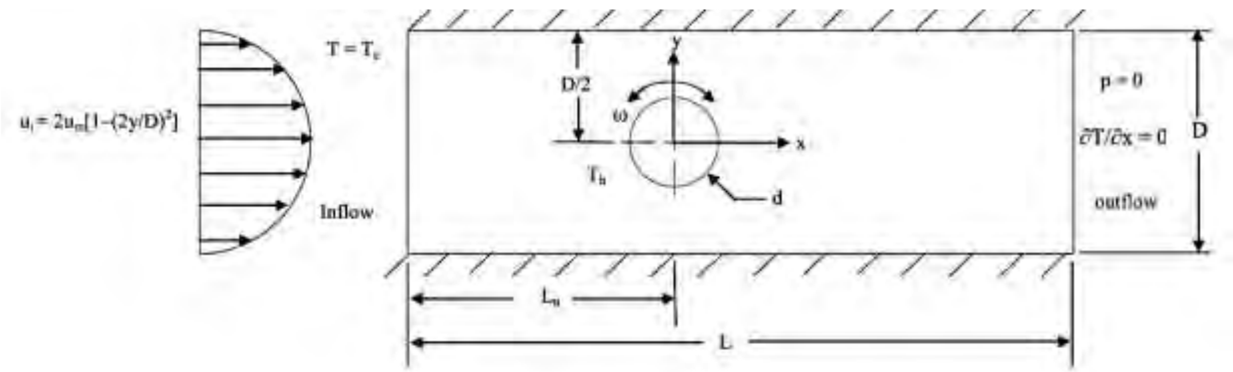

FIGURE 3.1: Schematic diagram (2D) of the rectangular channel with a rotating circular cylinder in Cartesian coordinate system.

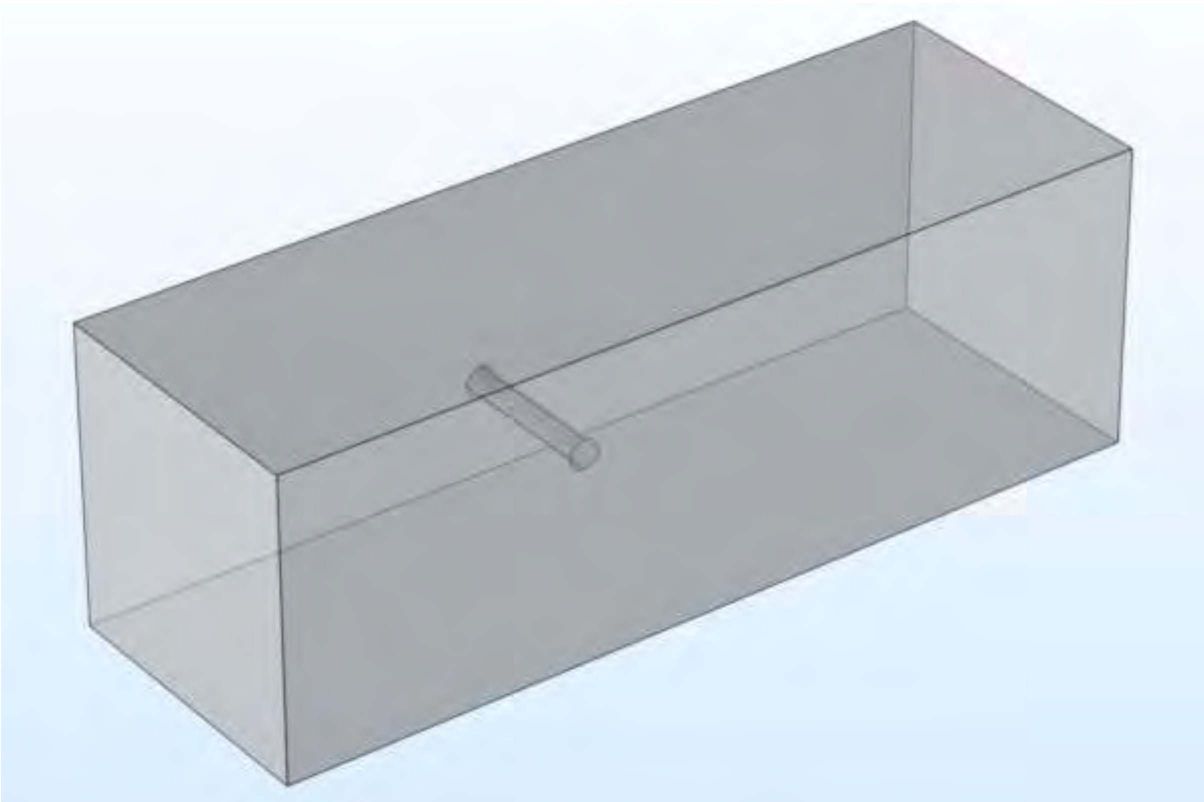

FIGURE 3.2: 3D view of the schematic diagram

3.2.1 Laminar Flow Governing equations

The working fluid in the channel is considered as air and the thermo-physical properties of air are taken to be constant. The radiation and the buoyancy effects along with viscous dissipation are neglected in this study. Radiation heat transfer is very much negligible than the convective heat transfer in this case. And as air is used as the working fluid in our study with smaller cylinder so we can ignore the effect of buoyancy as well as the viscous dissipation. The flow inside the channel is assumed to be two-dimensional, steady, laminar/turbulent, and incompressible and hence, the mass, momentum and energy conservation equations in dimensional form are written as follows given by Sun *et al.* [16]:

Continuity equation:

$$\frac{\partial u}{\partial x}+\frac{\partial v}{\partial y}=0, \tag{3.1}$$

x-momentum equation:

$$\rho\left(u\frac{\partial u}{\partial x}+v\frac{\partial u}{\partial y}\right)=-\frac{\partial p}{\partial x}+\mu\left(\frac{\partial^2 u}{\partial x^2}+\frac{\partial^2 u}{\partial y^2}\right), \tag{3.2}$$

y-momentum equation:

$$\rho\left(u\frac{\partial v}{\partial x}+v\frac{\partial v}{\partial y}\right)=-\frac{\partial p}{\partial y}+\mu\left(\frac{\partial^2 v}{\partial x^2}+\frac{\partial^2 v}{\partial y^2}\right), \tag{3.3}$$

Energy equation:

$$\rho C_p\left(u\frac{\partial T}{\partial x}+v\frac{\partial T}{\partial y}\right)=k\left(\frac{\partial^2 T}{\partial x^2}+\frac{\partial^2 T}{\partial y^2}\right), \tag{3.4}$$

Where, x and y are the dimensional cartesian coordinates, u and v are the dimensional velocity components in the x and y directions respectively, p is the dimensional pressure, T is the dimensional temperature, ρ is the density of fluid and μ is the dynamic viscosity and C_p is the heat capacity at constant pressure.

3.2.2 Boundary conditions

Boundary conditions are necessary for solving the governing equations. In the present study, no-slip boundary condition is imposed on the wall surface of the channel, whereas a parabolic inflow velocity u_i for laminar flow of the working fluid maintained at an ambient temperature Tc ($< T_h$) is considered at the channel inlet. Outflow boundary condition for both flow and thermal fields are maintained at the exit of the channel. The boundary conditions of present problem are presented dimensionally in table 3.1.

TABLE 3.1: Boundary conditions of the present model in dimensional form

Boundary Wall(s)	Thermal Field	Flow Field
Inlet	$T = T_c$	$u = 2(1-4y^2)$
Outlet	$\partial T/\partial x = 0$	$p = 0$
Channel Surface	$\partial T/\partial y = 0$	$u = v = 0$
Rotating cylinder wall	$T = T_h$	$u = \pm 2\alpha y$, $v = \mp 2\alpha x$

Here, $\alpha = \frac{u_p}{u_m}$, where u_p is the velocity of cylinder and u_m is the mean inflow velocity. (+) ve sign of U and (-) ve sign of V is for CW rotation and (-) ve sign of U and (+) ve sign of V is for CCW rotation of the cylinder.

3.3 Dimensional Analysis for Laminar Flow

For convection problems, it is very common to present the governing equations in dimensionless form. Generally, the variables of the equations are normalized by a reference value. As a result, the governing equations takes a non-dimensional form. The non-dimensional analysis is advantageous over dimensional analysis as it reduces the physical experiment. For this purpose, some non-dimensional governing parameters are formed using the physical variables.

3.3.1 Non- dimensional scales

The following reference or characteristic parameters are chosen for obtaining the scales for the present problem.

$$L_{ref} = D, \mathrm{U}_{\mathrm{ref}} = u_m, \mathrm{P}_{ref} = \rho U_{ref}^{\;2}, T_{ref} = T_c \tag{3.5}$$

Where, L_{ref} is the reference characteristic length, U_{ref} is the reference velocity, P_{ref} is the reference pressure and T_{ref} is the reference temperature.

The following scales are applied to (3.1) - (3.4) to obtain the non-dimensional form of the governing equations. These scales are represented by means of their reference properties.

$$X = \frac{x}{D}, Y = \frac{y}{D}, U = \frac{u}{u_m}, V = \frac{v}{u_m}, \Theta = \frac{T - T_c}{T_h - T_c}, P = \frac{p}{\rho u_m^{\;2}}, \mathrm{Re} = \frac{u_m D}{\nu}, \mathrm{Pr} = \frac{\mu C_p}{k} \tag{3.6}$$

Where, u_m is the mean velocity at inlet, X and Y are the dimensionless coordinates, U and V are the dimensionless velocity components in the X and Y directions respectively, P is the dimensionless pressure, Θ is the dimensionless temperature, Again, T_h is the highest temperature and T_c is the lowest temperature.

3.3.2 Laminar Flow Non-dimensional governing parameters

In order to reduce the number of physical variables in dimensional analysis, non-dimensional parameters are used. The non-dimensional parameters that govern the present problem are stated below:

Reynolds number (*Re*): The Reynolds number is the ratio of inertial force to viscous force. It helps to predict flow patterns in different fluid flow situations. At low Reynolds numbers, flows tend to be dominated by laminar (sheet-like) flow, while at high Reynolds numbers flows tend to be turbulent. As the Reynolds number increased, the inertia forces become dominant and small disturbances in the fluid may be amplified to cause the transition from laminar to turbulent flow. Reynolds number is expressed as [67]:

$$\mathrm{Re} = \frac{U_\alpha D}{\mu} \tag{3.7}$$

Where, U_∞ is the free stream velocity, D is the diameter of the channel and μ is the dynamic viscosity of fluid.

Prandtl number (*Pr*): This is the ratio of molecular diffusivity of momentum to molecular diffusivity of heat. It represents the relative importance of momentum and energy transport by the diffusion process. Pr relates the relative thickness of the hydrodynamic and thermal boundary layers. Pr is the connecting link between the velocity field and thermal field. The

Prandtl number is expressed as [44]:

$$\mathrm{Pr} = \frac{\mu C_p}{k} \tag{3.8}$$

Here, k is the thermal conductivity of the fluid.

3.3.3 Non-dimensional governing equations

Applying scales and governing parameter mentioned above, dimensional governing equations ((3.1) - (3.4)) yields to the following form:

Continuity equation:

$$\frac{\partial U}{\partial X}+\frac{\partial V}{\partial Y}=0, \tag{3.9}$$

X-momentum equation:

$$U\frac{\partial U}{\partial X}+V\frac{\partial U}{\partial Y}=-\frac{\partial P}{\partial X}+\frac{1}{\mathrm{Re}}\left(\frac{\partial^2 U}{\partial X^2}+\frac{\partial^2 U}{\partial Y^2}\right), \tag{3.10}$$

Y-momentum equation:

$$U\frac{\partial V}{\partial X}+V\frac{\partial V}{\partial Y}=-\frac{\partial P}{\partial Y}+\frac{1}{\mathrm{Re}}\left(\frac{\partial^2 V}{\partial X^2}+\frac{\partial^2 V}{\partial Y^2}\right), \tag{3.11}$$

Energy equation:

$$U\frac{\partial \Theta}{\partial X}+V\frac{\partial \Theta}{\partial Y}=\frac{1}{\mathrm{Re}\,\mathrm{Pr}}\left(\frac{\partial^2 \Theta}{\partial X^2}+\frac{\partial^2 \Theta}{\partial Y^2}\right), \tag{3.12}$$

3.3.4 Non-dimensional boundary conditions

Boundary conditions for the present problem in the non-dimensional form are presented in the table 3.2. From the dimensional boundary conditions presented in §3.2.2 and by applying scales (see §3.3.1) these non-dimensional boundary conditions are achieved.

TABLE 3.2: Non-dimensional boundary conditions of the present problem.

Boundary Wall(s)	Thermal Field	Flow Field
Inlet	$\Theta = 0$	$U = 2(1-4Y^2)$
Outlet	$\partial\Theta/\partial X = 0$	$P = 0$
Channel Surface	$\partial\Theta/\partial Y = 0$	$U = V = 0$
Rotating cylinder wall	$\Theta = 1$	$U = \pm\, 2\,\alpha Y,\ V = \mp\, 2\,\alpha X$

3.4 Turbulent Flow governing equations

Turbulent velocity u_i can be decomposed into an average component U_i and fluctuating component u_i' *i. e.* $u_i = U_i + u_i'$. Here, i=1,2 denotes the x, y directions. Similarly turbulent pressure *p* can be split into average component *P* and fluctuating component p'. The stationary turbulent flow field is governed by incompressible RANS equations for turbulent flow which can be written as below given by Sidebottom *et al.* [79]:

Continuity equation:

$$\frac{\partial U_j}{\partial x_j} = 0, \tag{3.13}$$

Momentum equation:

$$\rho U_j \frac{\partial U_i}{\partial x_j} = -\frac{\partial P}{\partial x_i} + \frac{\partial}{\partial x_j}\left(2\mu S_{ij} - \overline{\rho u_i' u_j'}\right) + f_i, \tag{3.14}$$

Energy equation:

$$\rho \mathrm{C_p} U_j \frac{\partial T}{\partial x_j} = k \frac{\partial^2 T}{\partial x_j{}^2}, \tag{3.15}$$

Where, the strain rate tensor, $S_{ij} = \frac{1}{2}\left(\frac{\partial U_i}{\partial x_j} + \frac{\partial U_j}{\partial x_i}\right)$. Volume force is denoted by f_i which has two components along two axes. The volume force is considered zero in all directions for the present study. In equation 3.14 the component $\tau_{ij} = -\overline{\rho u_i' u_j'}$ is the turbulent Reynold's stresses. It has six components in three-dimensional analysis and three components in two-dimensional analysis. This causes the presence of more unknown variables than the number of equations and make the system of governing equations not solvable. To overcome this problem different turbulent models are used. From Boussinesq hypothesis, $\tau_{ij} = -\overline{\rho u_i' u_j'} = 2\mu_t S_{ij}$, where μ_t is called turbulent viscosity or eddy viscosity. A Kinematic turbulent viscosity, ν_t can also be defined, $\nu_t = \frac{\mu_t}{\rho}$ whose unit is m^2 / s.

3.5 Turbulent Models

There are different turbulent models which can be categorized as: Zero Equation Models, One Equation Model and Two Equation Models. We are interested mainly on the last one, the Two Equation Models. Corresponding dimensional equation of some two equation models are stated below:

3.5.1 *k* - *ϵ* Model

The model introduces two additional transport equations and two dependent variables; the turbulent kinetic energy, *k,* and the turbulent dissipation rate, ϵ. [103]. The turbulent viscosity is modeled as:

$$\mu_T = \rho C_\mu \frac{k^2}{\varepsilon}, \tag{3.16}$$

The transport equation for k is expressed as

$$\rho U_j \frac{\partial k}{\partial x_j} = \frac{\partial}{\partial x_j}\left[\left(\mu + \frac{\mu_T}{\sigma_k}\right)\frac{\partial k}{\partial x_j}\right] + 2\mu_T S_{ij}\frac{\partial U_i}{\partial x_j} - \rho\varepsilon, \tag{3.17}$$

The transport equation for ϵ is expressed as

$$\rho U_j \frac{\partial \varepsilon}{\partial x_j} = \frac{\partial}{\partial x_j}\left[\left(\mu + \frac{\mu_T}{\sigma_\varepsilon}\right)\frac{\partial \varepsilon}{\partial x_j}\right] + 2\mu_T S_{ij} C_{\varepsilon 1}\frac{\varepsilon}{k}\frac{\partial U_i}{\partial x_j} - C_{\varepsilon 2}\rho\frac{\varepsilon^2}{k}, \tag{3.18}$$

The empirical optimum values of model constants are

$$C_\mu = 0.09, C_{\varepsilon 1} = 1.44, C_{\varepsilon 2} = 1.92, \sigma_k = 1.0, \sigma_\varepsilon = 1.3 \tag{3.19}$$

3.5.2 *k* – *ω* Model

The k- ω model solves for the turbulent kinetic energy, k and for the dissipation per unit turbulent kinetic energy, ω. Here, ω is also commonly known as the specific dissipation rate. The CFD Module that is deployed in present study has the Wilcox (1994) revised k - ω model. In this turbulence model, the turbulent viscosity is expressed as

$$\mu_t = \rho \frac{k}{\omega}, \tag{3.20}$$

The turbulent energy equation is expressed as

$$\rho U_j \frac{\partial k}{\partial x_j} = \frac{\partial}{\partial x_j}\left[\left(\mu + \sigma_k{}^* \mu_T\right)\frac{\partial k}{\partial x_j}\right] + 2\mu_T S_{ij}\frac{\partial U_i}{\partial x_j} - \rho\beta_0{}^* k\omega, \tag{3.21}$$

and the specific dissipation rate equation is expressed as

$$\rho U_j \frac{\partial \omega}{\partial x_j} = \frac{\partial}{\partial x_j}\left[\left(\mu + \sigma_\omega \mu_T\right)\frac{\partial \omega}{\partial x_j}\right] + 2\alpha\mu_T S_{ij}\frac{\omega}{k}\frac{\partial U_i}{\partial x_j} - \rho\beta_0\omega^2, \tag{3.22}$$

The optimum empirical values of model constants are used as

$$\begin{gathered}\alpha = \frac{13}{25}, \beta = \beta_0 f_\beta, \beta^* = \beta_0{}^* f_\beta, \sigma = \frac{1}{2}, \sigma^* = \frac{1}{2}, \\ \beta_0 = \frac{13}{125}, f_\beta = \frac{1+70\chi_\omega}{1+80\chi_\omega}, \chi_\omega = \left|\frac{\Omega_{ij}\Omega_{jk}S_{ki}}{\left(\beta_0 * \omega\right)^3}\right|, \beta_0{}^* = \frac{9}{100}\end{gathered} \tag{3.23}$$

3.5.3 SST Model

The SST model is a combination of the *k-ε* model in the free stream and the *k-ω* model near the walls [105]. It is also a low Reynolds number model, i.e., it does not apply wall functions. Low Reynolds number refers to the region close to the wall where viscous effect dominates. In this model, equations are formulated in terms k and ω. The turbulent viscosity is expressed as

$$\mu_T = \frac{\rho a_2 k}{\max\left(a_2\omega, S f_{v2}\right)}, \tag{3.24}$$

where, S is the characteristic magnitude of the mean velocity gradients and is obtained from

$$S = \sqrt{2S_{ij}S_{ij}}, \tag{3.25}$$

Turbulent energy equation is expressed as

$$\rho U_j \frac{\partial k}{\partial x_j} = \frac{\partial}{\partial x_j}\left[\left(\mu + \sigma_k \mu_T\right)\frac{\partial k}{\partial x_j}\right] + P - \rho\beta_0{}^* k\omega, \tag{3.26}$$

Specific dissipation rate equation is expressed as

$$\rho U_j \frac{\partial \omega}{\partial x_j} = \frac{\partial}{\partial x_j}\left[\left(\mu + \sigma_\omega \mu_T\right)\frac{\partial \omega}{\partial x_j}\right] + 2\left(1 - f_{v1}\right)\frac{\sigma_{\omega 2}\rho}{\omega}\frac{\partial \omega}{\partial x_j}\frac{\partial k}{\partial x_j} + \frac{\rho\gamma}{\mu_T}P - \rho\beta_0\omega^2, \tag{3.27}$$

Where,

$$P = \min\left(2\mu_T S_{ij}\frac{\partial U_i}{\partial x_j}, 10\rho\beta_0^* k\omega\right), \tag{3.28}$$

The model constants are defined through interpolation of appropriate inner and outer values a as

$$\phi = f_{v1}\phi_1 + \left(1 - f_{v1}\right)\phi_2, \tag{3.29}$$

Where, $\phi = \beta, \gamma, \sigma_k, \alpha_\omega$.

The interpolation functions are defined as

$$f_{v1} = \tanh\left(\theta_1^4\right),$$

$$\theta_1 = \min\left[\max\left(\frac{\sqrt{k}}{\beta_0^*\omega l_\omega}, \frac{500\mu}{\rho\omega l_\omega^2}\right), \frac{4\rho\sigma_{\omega 2}k}{CD_{k\omega}l_\omega^2}\right],$$

$$CD_{k\omega} = \max\left(\frac{2\rho\sigma_{\omega 2}}{\omega}\frac{\partial\omega}{\partial x_i}\frac{\partial k}{\partial x_i}, 10^{-10}\right), \tag{3.30}$$

and

$$f_{v2} = \tanh\left(\theta_2^2\right),$$

$$\theta_2 = \max\left(\frac{2\sqrt{k}}{\beta_0^2\omega l_\omega}, \frac{500\mu}{\rho\omega l_\omega^2}\right), \tag{3.31}$$

3.5.4 Low Reynolds Number *k* - *ϵ* Model

The low Reynolds number *k-ε* model is similar to the *k-ε* model, but does not need wall functions: it can solve for the flow everywhere [106]. It is a logical extension of the k-ε model and shares many of its advantages, but generally requires a denser mesh; not only at walls, but everywhere its low Reynolds number properties kick in and dampen the turbulence. The low Reynolds number *k-ε* model can compute lift and drag forces and heat fluxes can be modeled with higher accuracy compared to the *k-ε* model. The turbulent viscosity is expressed as

$$\mu_T = \rho C_\mu \frac{k^2}{\varepsilon} f_\mu\left(\rho, \mu, k, \varepsilon, l_\omega\right), \tag{3.32}$$

Turbulent energy equation is expressed as

$$\rho U_j \frac{\partial k}{\partial x_j} = \frac{\partial}{\partial x_j}\left[\left(\mu + \frac{\mu_T}{\sigma_k}\right)\frac{\partial k}{\partial x_j}\right] + 2\mu_T S_{ij}\frac{\partial U_i}{\partial x_j} - \rho\varepsilon, \tag{3.33}$$

Dissipation rate equation is expressed as

$$\rho U_j \frac{\partial \varepsilon}{\partial x_j} = \frac{\partial}{\partial x_j}\left[\left(\mu + \frac{\mu_T}{\sigma_\varepsilon}\right)\frac{\partial \varepsilon}{\partial x_j}\right] + 2\mu_T S_{ij} C_{\varepsilon 1}\frac{\varepsilon}{k}\frac{\partial U_i}{\partial x_j} - C_{\varepsilon 2}\rho\frac{\varepsilon^2}{k} f_\varepsilon\left(\rho,\mu,k,\varepsilon,l_\omega\right), \tag{3.34}$$

Where,

$$\begin{aligned} f_\mu &= \left(1 - e^{-l^*/14}\right)^2\left(1 + \frac{5}{R_t^{3/4}} e^{-\left(R_t/200\right)^2}\right), \\ f_\varepsilon &= \left(1 - e^{-l^*/3.1}\right)^2\left(1 - 0.3e^{-\left(R_t/6.5\right)^2}\right), \\ l^* &= \left(\rho u_\varepsilon l_\omega\right)/\mu, R_t = \rho k^2/\left(\mu\varepsilon\right), u_\varepsilon = \left(\mu\varepsilon/\rho\right)^{1/4}, \end{aligned} \tag{3.35}$$

Where, l_ω is the distance to the closest wall. The closure constants are used as

$$C_\mu = 0.09, C_{\varepsilon 1} = 1.5, C_{\varepsilon 2} = 1.9, \sigma_k = 1.4, \sigma_\varepsilon = 1.4 \tag{3.36}$$

3.6 Dimensional Analysis for Turbulent Flow

Here, channel height D is the reference length and mean velocity u_m is the reference velocity. The dimensional parameters are then defined as

$$x_i^* = \frac{x_i}{D}; U_i^* = \frac{U_i}{u_m}; P^* = \frac{P}{\rho u_m^{\,2}}; \Theta = \frac{T - T_c}{T_h - T_c}, \tag{3.37}$$

Here, x_i^* is the non-dimensional co-ordinates, U_i^* is non-dimensional average velocity; both of them have two components in 2D co-ordinate system. Θ is non-dimensional temperature and P^* is non-dimensional average pressure. By using these parameters, the steady, incompressible RANS equations for turbulent flow can be obtained in non-dimensional form as [107]:

Continuity equation:

$$\frac{\partial U_j^{\,*}}{\partial x_j^{\,*}} = 0, \tag{3.38}$$

Momentum equation:

$$U_j^{\ *}\frac{\partial U_i^*}{\partial x_j^{\ *}} = -\frac{\partial P^*}{\partial x_i^{\ *}} + \frac{2}{\mathrm{Re}}\frac{\partial}{\partial x_j^{\ *}}\left(\left(1+\frac{\upsilon_T}{\upsilon}\right)S_{ij}^{\ *}\right) + f_i^*, \tag{3.39}$$

Energy equation:

$$U_j^{\ *}\frac{\partial \Theta}{\partial x_j^{\ *}} = \frac{1}{\mathrm{Re}\,\mathrm{Pr}}\frac{\partial^2 \Theta}{\partial x_j^{\ *2}}, \tag{3.40}$$

where, dimensionless strain-rate tensor, $S_{ij}^{\ *} = \frac{1}{2}\left(\frac{\partial U_i^*}{\partial x_j^{\ *}} + \frac{\partial U_j^{\ *}}{\partial x_i^{\ *}}\right)$, dimensionless Reynolds number, $\mathrm{Re} = \frac{u_m D}{\upsilon}$, dimensionless stream wise force, $f_1^* = f_2^* = f_3^* = 0$, and dimensionless Prandtl number, $\mathrm{Pr} = \frac{\upsilon}{\alpha}$.

3.6.1 Non-dimensional Boundary Conditions

The non-dimensional boundary conditions for turbulent flow in listed below:

TABLE 3.3: Non-dimensional boundary conditions of the present problem for turbulent flow.

Boundary Wall(s)	Thermal Field	Flow Field
Inlet	$\Theta = 0$	$U_1^* = 2\left(1-4x_2^{*2}\right)$
Outlet	$\partial\Theta/\partial x_1^{\ *} = 0$	$P^* = 0$
Channel Surface	$\partial\Theta/\partial x_2^{\ *} = 0$	$U_1^* = U_2^* = 0$
Rotating cylinder wall	$\Theta = 1$	$U_1^* = 2\alpha x_2^{\ *}, U_2^* = 2\alpha x_1^*$

3.7 Non-dimensional turbulent Models

3.7.1 *k* - *ϵ* Model

According to this model the dimensionless turbulent energy equation can be expressed as [107]

$$U_j^* \frac{\partial k^*}{\partial x_j^*} = \frac{1}{\mathrm{Re}} \frac{\partial}{\partial x_j^*} \left[\left(1 + \frac{\upsilon_T^*}{\sigma_k} \right) \frac{\partial k^*}{\partial x_j^*} \right] + \frac{2}{\mathrm{Re}} \upsilon_T^* S_{ij}^* \frac{\partial U_i^*}{\partial x_j^*} - \varepsilon^*, \tag{3.41}$$

Dimensionless dissipation rate equation can be written as

$$U_j^* \frac{\partial \varepsilon^*}{\partial x_j^*} = \frac{1}{\mathrm{Re}} \frac{\partial}{\partial x_j^*} \left[\left(1 + \frac{\upsilon_T^*}{\sigma_\varepsilon} \right) \frac{\partial \varepsilon^*}{\partial x_j^*} \right] + \frac{2}{\mathrm{Re}} C_{\varepsilon 1} \upsilon_T^* S_{ij}^* \frac{\varepsilon^*}{k^*} \frac{\partial U_i^*}{\partial x_j^*} - \frac{1}{\mathrm{Re}} C_{\varepsilon 2} \frac{\varepsilon^{*2}}{k^*}, \tag{3.42}$$

3.7.2 *k* – *ω* Model

The dimensionless turbulent energy equation can be written as [107]

$$U_j^* \frac{\partial k^*}{\partial x_j^*} = \frac{1}{\mathrm{Re}} \frac{\partial}{\partial x_j^*} \left[\left(1 + \sigma_k^* \upsilon_T^* \right) \frac{\partial k^*}{\partial x_j^*} \right] + \frac{2}{\mathrm{Re}} \upsilon_T^* S_{ij}^* \frac{\partial U_i^*}{\partial x_j^*} - \beta_0^* k^* \omega^*, \tag{3.43}$$

Dimensionless dissipation rate equation can be written as

$$U_j^* \frac{\partial \omega^*}{\partial x_j^*} = \frac{1}{\mathrm{Re}} \frac{\partial}{\partial x_j^*} \left[\left(1 + \sigma_\omega \upsilon_T^* \right) \frac{\partial \omega^*}{\partial x_j^*} \right] + \frac{2}{\mathrm{Re}} \sigma_\omega \upsilon_T^* S_{ij}^* \frac{\omega^*}{k^*} \frac{\partial U_i^*}{\partial x_j^*} - \beta_0 \omega^{*2}, \tag{3.44}$$

3.7.3 SST Model

Dimensionless turbulent energy equation can be expressed as [107]

$$U_j^* \frac{\partial k^*}{\partial x_j^*} = \frac{1}{\mathrm{Re}} \frac{\partial}{\partial x_j^*} \left[\left(1 + \sigma_k \upsilon_T^* \right) \frac{\partial k^*}{\partial x_j^*} \right] + P^* - \beta_0^* k^* \omega^*, \tag{3.45}$$

Dimensionless dissipation rate equation can be expressed as

$$U_j^* \frac{\partial \omega^*}{\partial x_j^*} = \frac{1}{\mathrm{Re}} \frac{\partial}{\partial x_j^*} \left[\left(1 + \sigma_\omega \upsilon_T^* \right) \frac{\partial \omega^*}{\partial x_j^*} \right] + 2 \left(1 - f_{v1} \right) \frac{\sigma_{\omega 2}}{\omega^*} \frac{\partial \omega^*}{\partial x_j^*} \frac{\partial k^*}{\partial x_j^*} + \frac{\gamma}{\mu_T} P^* - \beta_0 \omega^{*2} \tag{3.46}$$

3.7.4 Low Reynolds Number *k* – *ω* Model

Dimensionless turbulent energy equation can be expressed as [107]

$$U_j^{\,*}\frac{\partial k^*}{\partial x_j^{\,*}}=\frac{1}{\mathrm{Re}}\frac{\partial}{\partial x_j^{\,*}}\left[\left(1+\frac{\upsilon_T}{\sigma_k}\right)\frac{\partial k^*}{\partial x_j^{\,*}}\right]+\frac{2}{\mathrm{Re}}\upsilon_T S_{ij}^{\,*}\frac{\partial U_i^*}{\partial x_j^{\,*}}-\varepsilon^*, \tag{3.47}$$

Dimensionless dissipation rate equation can be expressed as

$$U_j^{\,*}\frac{\partial \varepsilon^*}{\partial x_j^{\,*}}=\frac{1}{\mathrm{Re}}\frac{\partial}{\partial x_j^{\,*}}\left[\left(1+\frac{\upsilon_T}{\sigma_\varepsilon}\right)\frac{\partial \varepsilon^*}{\partial x_j^{\,*}}\right]+\frac{2}{\mathrm{Re}}C_{\varepsilon 1}\upsilon_T S_{ij}\frac{\varepsilon^*}{k^*}\frac{\partial U_i^*}{\partial x_j^{\,*}}-C_{\varepsilon 2}\frac{\varepsilon^{*2}}{k^*}f_\varepsilon\left(\rho,\mu,k,\varepsilon,l_\omega\right), \tag{3.48}$$

Chapter 4

Computational Method

We can solve a problem by three different ways namely experimental, numerical and analytical approach. When the equations are more complex, numerical approach is more preferable than analytical one. In this chapter, a brief discussion of numerical method is presented. Among different numerical methods, finite element method (Galerkin weighted residual method) is applied for the present problem.

4.1 Computational Fluid Dynamics

Computational fluid dynamics (CFD) is a branch of fluid mechanics that uses numerical analysis and data structures to analyze and solve problems that involve fluid flows. Computers are used to perform the calculations needed to simulate the free-stream flow of the fluid, and the interaction of the fluid (liquids and gases) with surfaces defined by boundary conditions. The fundamental basis of almost all CFD problems is the Navier–Stokes equations, which define many single-phase (gas or liquid, but not both) fluid flows. These equations can be made simple by removing viscosity terms to yield the Euler equations. Further simplification, by removing vorticity terms yields the full potential equations. Finally, for small perturbations in subsonic and supersonic flows, (not transonic or hypersonic) these equations can be linearized to yield the linearized potential equations. CFD provides a qualitative and even quantitative prediction of fluid flows by means of mathematical modeling through formulation of equations, numerical methods through discretization and solution techniques and software tools with solvers, pre and post processing utilities.

Different types of numerical solution procedure are available and among them finite difference, finite element, finite volume, spectral element methods are very popular. All this method can be applied to find out the numerical solution. However, proper choice of the method can reduce the computational time and ensure better numerical accuracy. Although Finite Element Methods have certain limitations, advanced techniques are adopted to overcome those limitations and keep the numerical error in reasonable limit. The numerical solution techniques are getting popular day by day due to their attractive features.

4.2 Finite Element Method

The finite element method (FEM) has been used for solving differential equations in different engineering and mathematical modeling. The term finite element was first introduced by Clough in 1960. In the early1960s, this method is used by engineers for approximate solutions of problems in stress analysis, fluid flow, heat transfer, and other areas. The FEM is a particular numerical method for solving partial differential equations in two or three space variables. To solve a problem, the FEM subdivides a large system into smaller, simpler parts that are called finite elements. This is done by a particular space discretization in the space dimensions, which is enforced by the construction of mesh inside the object: the numerical domain for the solution, which has a certain number of points. Finally, the finite element formulation of a boundary value problem results in a system of algebraic equations. The method approximates the unknown variables at the domain. The simple equations that model these finite elements are then assembled into a larger system of equations that models the entire problem. The FEM then uses variational or weighted residual or direct methods from the calculus to approximate a solution by minimizing an associated error function.

4.2.1 Advantages of Finite Element Method

The advantages of FEM over other methods are stated below:

- Finite Element Method is well-suited for complex geometry than FDM.
- It can handle a wide variety of engineering problems: Solid Mechanics, Fluids, Heat Transfer, Dynamics, Electrostatic problems etc.
- FEM can handle complex restraints and complex loading: Point load, Element load etc. compared with other numerical methods.
- Writing computer codes on FEM is structured and straight forward.
- Conventional numerical solvers can be used to solve the equations generated by FEM.
- FEM has the ability to combine different kinds of functions that estimate the solution within each element which is nearly impossible with FDM or FVM.

4.3 Numerical Formulation

For the present investigation, Finite element method is used to solve the governing equations. Since FEM is based on unstructured grids, this method is very useful for engineering applications related with complex flow fields. The application of this technique is well documented by Zienkiewicz, Taylor, and Zhu (2005). In the present study, non-linear parametric solution method is chosen to solve the governing equations. Triangular mesh arrangement is implemented in the present investigation with finer mesh near the cylinder surface. Six noded triangular elements (Figure 4.1) are used in this investigation to smoothly capture the non-linear variations of the field variables. The continuity, momentum and energy equations are solved using the Galerkin finite element method. In this study, Energy equation is a passive scalar transport equation. The flow field is being solved by using RANS equation and turbulent model equation is used to solve energy equation and to have thermal field solution. The continuity equation is used as a constraint due to mass conservation and this constraint may be used to obtain the pressure distribution (Basak & Ayappa, 2001).

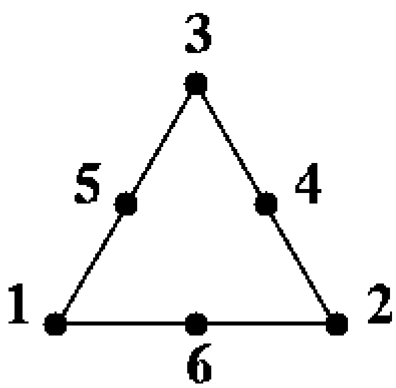

FIGURE 4.1: Six noded triangular mesh element (https://www.cs.cmu.edu/~quake/triangle.highorder.html)

4.4 Discretization of Equations

In order to get the correct forms of the boundary conditions, the governing mass and momentum equations must be written in conservation form as it allows the partial integration to be carried out correctly (T. J. Chung, 2002). Thus, we can write:

Continuity equation:

$$v_{i,i} = 0, \tag{4.1}$$

Momentum equations:

$$\frac{\partial}{\partial x_i}\left(\rho v_i v_j - \sigma_{ij}\right) = 0, \tag{4.2}$$

Where, σ_{ij} is the total stress tensor.

$$\sigma_{ij} = -p\delta_{ij} + \tau_{ij} = -p\delta_{ij} + \mu\left(v_{i,j} + v_{j,i}\right), \tag{4.3}$$

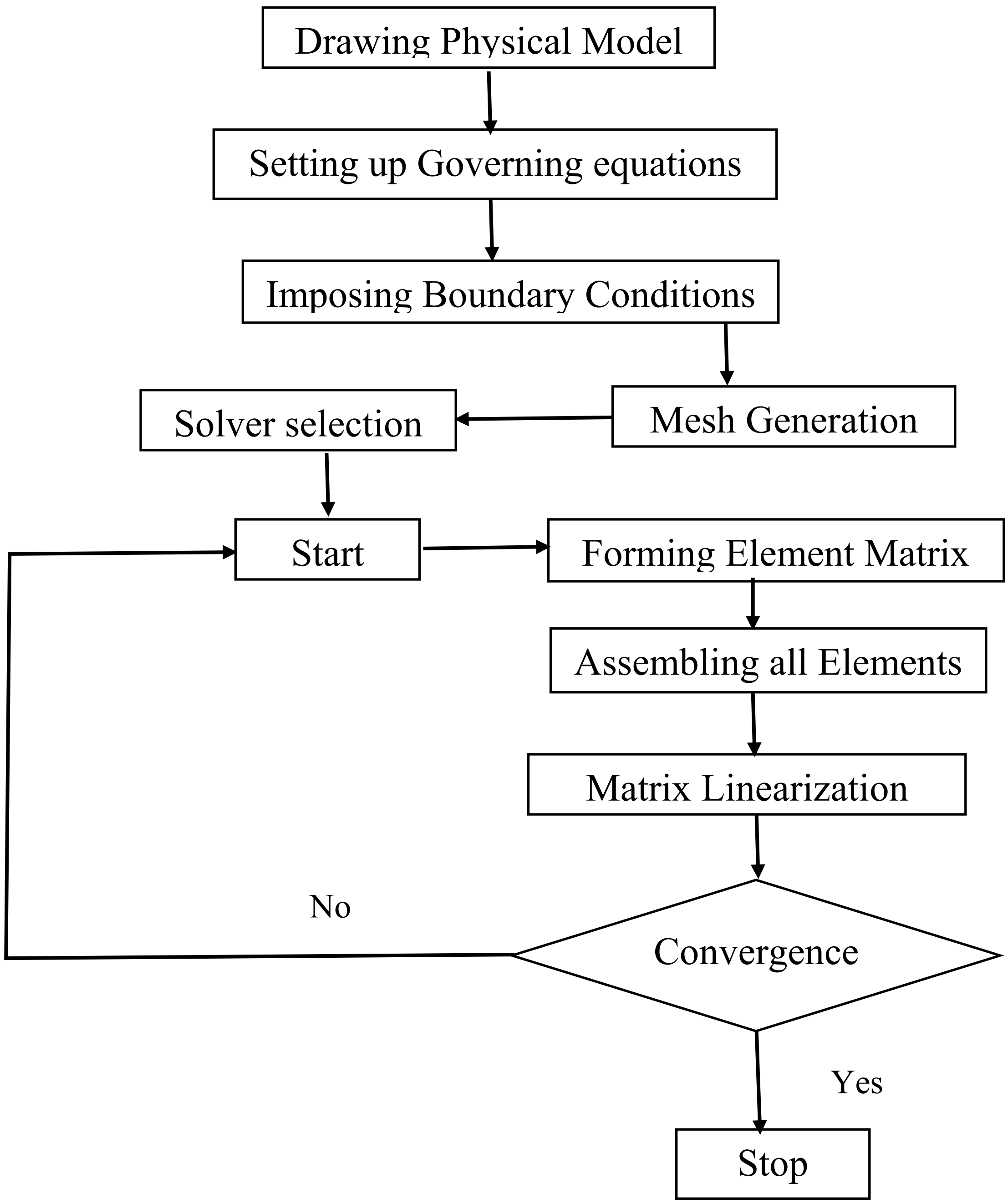

FIGURE 4.2: Flow chart of Computational Procedure

4.5 Calculation of performance parameters

Important non-dimensional parameters such as Drag coefficient (C_D), lift coefficient (C_L) and average Nusselt number (Nu) along the surface of the rotating cylinder for isothermal heating are calculated as [16]

$$C_D = \frac{F_D}{\frac{1}{2}\rho u_m{}^2 A}, C_L = \frac{F_L}{\frac{1}{2}\rho u_m{}^2 A}, Nu = \frac{1}{\pi\beta}\int_0^{\pi\beta}\left(\frac{\partial\Theta}{\partial N}\right)_s dS, \tag{4.28}$$

Where, F_D is the drag force, F_L is the lift force, A is the projected area and of the cylinder and S is the arc length of the cylinder surface.

4.6 Mesh Generation

As stated earlier, the computational domain is, at first, discretized by applying triangular mesh elements. The entire domain is discretized by non-uniform unstructured triangular mesh elements. Each triangular element has six nodes (see figure 4.1). More fine mesh has been used near the boundary of the cylinder. Also, the meshing is done in such a manner so that there is no singular point in the computational domain. Then varying number of mesh elements, the grid independence test has been accomplished and 15570 elements has been considered for the current study since there is insignificant change in the drag coefficient, lift coefficient and average Nusselt number with the improvement of finer grid. It must be noted that, meshes are finer near the wall to increase accuracy of flow prediction as the different parameter's gradient is higher in near wall region.

Table 4.1: Some of the main mesh parameters

Mesh parameters	**values**
Maximum element size	0.005 m
Minimum element size	6×10^{-5} m
Maximum element growth rate	1.1

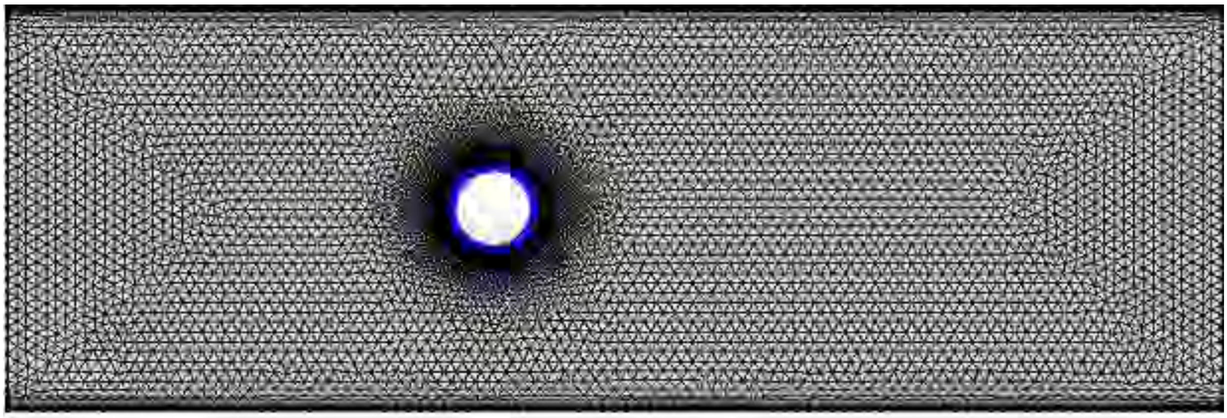

(a)

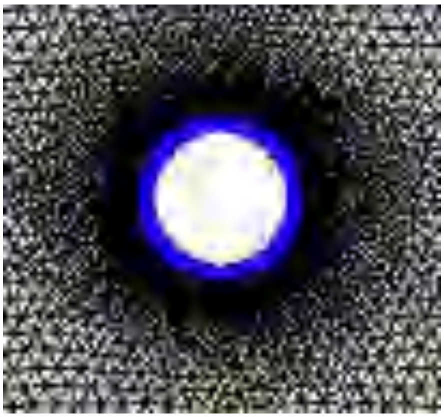

(b)

(c)

FIGURE 4.3: (a) Mesh structures for the entire domain, (b) mesh around the cylinder, (c) mesh near longitudinal wall

4.7 Model Validation

Model validation has been done in numerical procedure to check the reliability of the present scheme. The validation has been performed for both the laminar and turbulent flow separately. Moreover, grid validation has also been performed to select the suitable mesh elements.

4.7.1 Model Validation for Laminar Flow

Firstly, the present model is compared with the results of Prasad *et al.* (2011) on the basis of drag coefficient, lift coefficient and nusselt number for Re = 40-100. The present numerical solutions are in good agreement with the published result of Prasad *et al.* (2011) on a numerical simulation of convection over a rotating circular cylinder inside a rectangular channel with the combined effect of fluid flow and heat transfer. The comparison has been shown in Fig. 4.4.

4.7.2 Grid Independence Test

Mesh resolution sensitivity were tested for laminar flow with Re_c = 4, blockage ratio = 0.1, Re = 500 and considering CCW rotation. Five sets of meshes are taken into consideration for the present problem. Number of triangular elements considered as 1660, 3018, 7378, 15570 and 36634. Differences in the values of drag coefficient, lift coefficient and Nusselt number decreases with increasing meshes which are listed in the table 4.1 below:

By comparing the data shown in table 4.1, 15570 elements are taken for this study. As further increase of elements will only increase the computational cost.

The same grid combination has been taken into consideration for turbulent flow too.

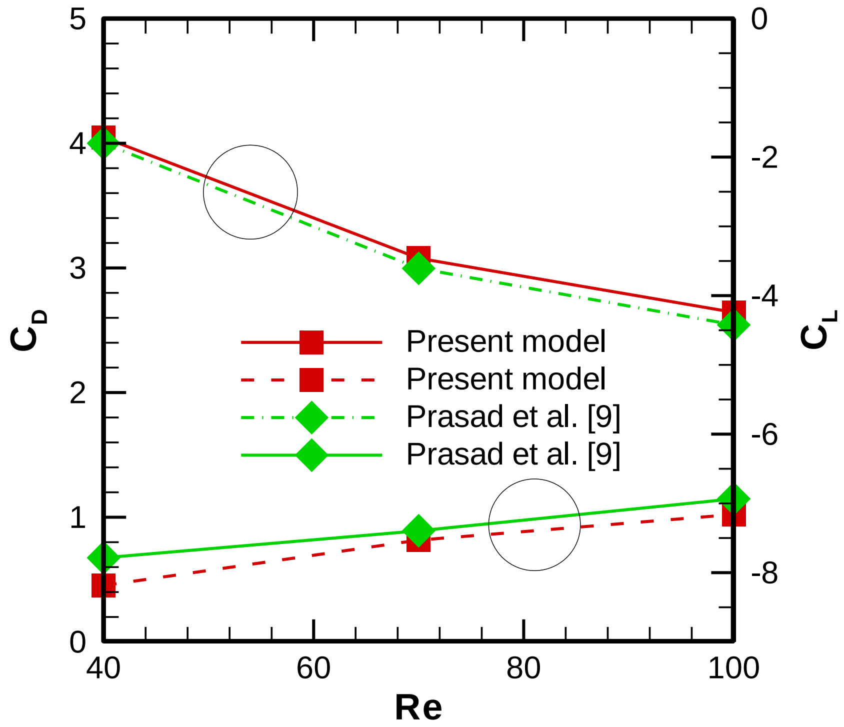

(a)

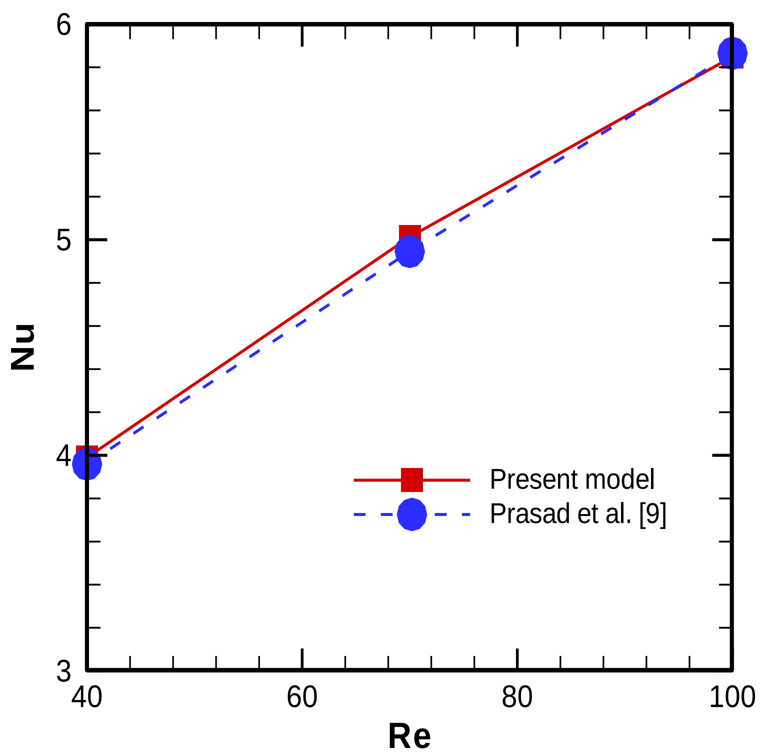

(b)

FIGURE 4.4: Comparison between the Present solution and the result of Prasad *et al.* [2011] in terms of (a) C_D, C_L and (b) Nu for various Re with $\beta = 0.3$ and $\alpha = 2$.

Table 4.2: Grid independence test for laminar flow

Number of meshes	Drag coefficient	Lift coefficient	Nusselt number
1660	4.69489004	-0.1366207	12.5639032
3018	4.298109482	-0.447083934	13.8047709
7378	4.364347295	-0.523352884	14.660012
15570	4.372705083	-0.507143595	15.0382573
36634	4.372705083	-0.507143595	15.0382573

4.8 Turbulence Modelling

Previous studies show that out of two equations RANS model, the Shear Stress Transport (SST) model suited best for the present study of flow past a rotating circular cylinder confined in a channel [97, 98]. SST model has got the superiority over other two equations model as it combines the behavior of the *k-ω* model at the near-wall region with the well converging *k-ε* model.

4.8.1 Model Validation for Turbulent Flow

For turbulent flow, the present model is compared with the results of Mgaidi *et al.* (2018) on the basis of lift coefficient for speed ratio from 0.6 to 1.1 and *Re* from 1.5×10^5 to 2.14×10^5. The present work is well close to the results of Mgaidi *et al.* (2018) on a numerical simulation of turbulent flow over a rotating circular cylinder in a confined channel. A maximum error of approximately 8% is found from the present data. Probable reason for this deviation might be the use of different CFD tool. Also, the published results of Mgaidi *et al.* (2018) have large deviation with their experimental study.

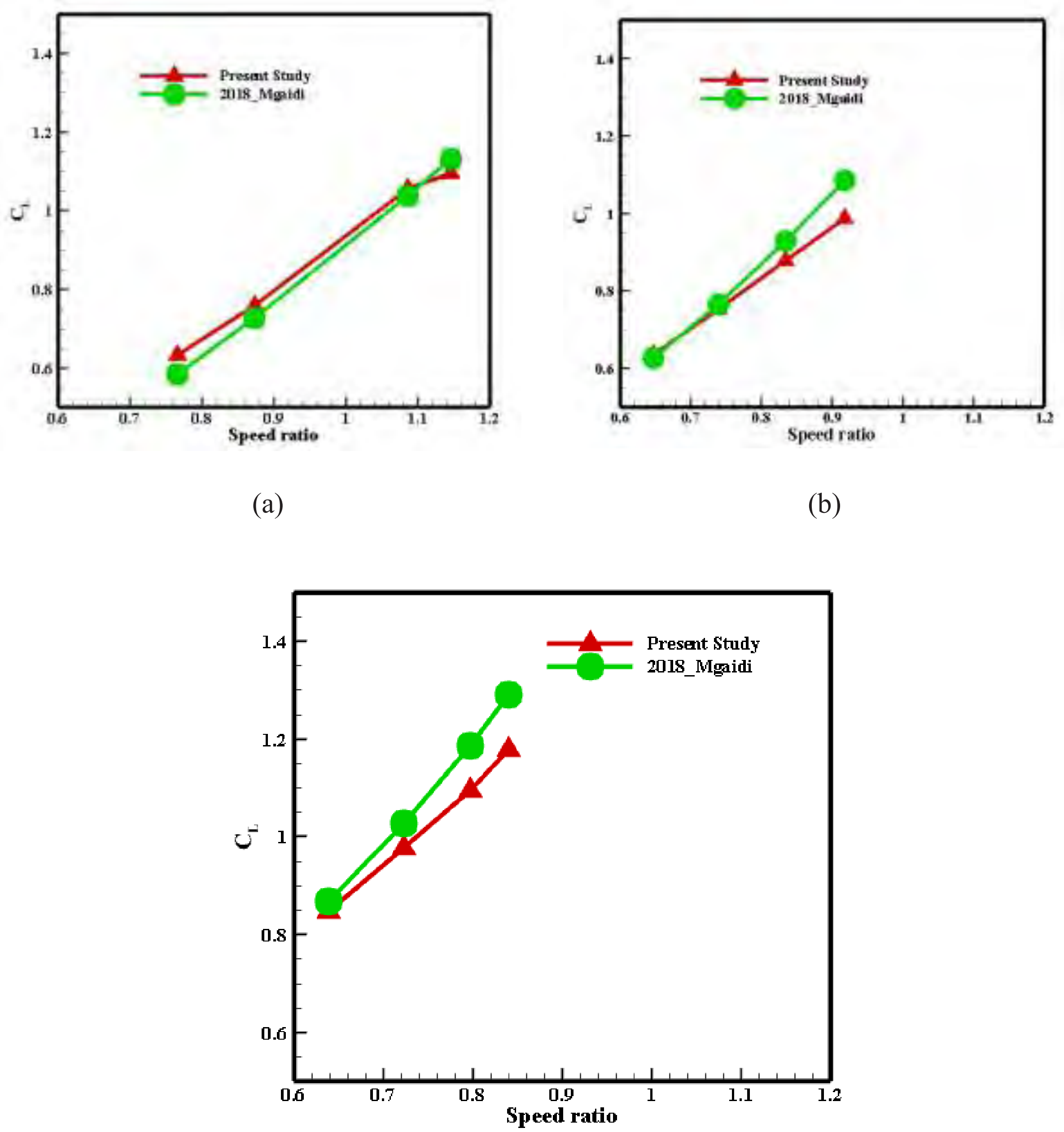

(a) (b)

(c)

FIGURE 4.5: Comparison between the Present solution and the result of Mgaidi *et al.* (2018) in terms of lift coefficient for (a) U =11 m/s, (b) U =13 m/s, and (c) U =15 m/s.

Chapter 5

Results and Discussions

The main objective of the present study is to investigate the effect of rotational direction of the circular cylinder, the blockage ratio, the rotational speed of the cylinder as well as the change of mean velocity of the working fluid on the flow and the thermal characteristics of the confined channel. Special attention is given to keep the speed ratio (ratio of the peripheral velocity of the rotating cylinder and the mean velocity of the working fluid) varies with Reynolds numbers, whereas all previous works dealt with the constant speed ratio. Since constant value of speed ratio makes the rotational speed of the cylinder to be changed automatically with the change of mean flow Reynolds number which is not always the practical scenario of this type of problem. In this study, we'll observe the distributions of coefficient of drag, coefficient of lift and variations of average Nusselt number of the hot cylinder surface as a function of Reynolds number. The Reynolds number for laminar flow has been changed from 40 to 2000 and from 3000 to 10000000 for turbulent flow. Moreover, the cylinder Reynolds number (defined by the rotational speed of the cylinder) varies from 4 to 30 and the blockage ratio from 0.05 to 0.2. Selected numerical results of the present problem in terms of streamline plots, pressure contour, and isosurface plots of temperature are taken into consideration to visualize the flow and the thermal fields.

5.1 Laminar Flow

Parametric simulation is carried out in the range of $40 \leq Re \leq 2000$, $4 \leq Re_c \leq 30$ and $\beta = 0.05$, 0.1, 0.2. The results are described in terms of streamline plots, pressure contour, and isosurface plots of temperature, distributions of drag and lift coefficients and variations of Nusselt number of the hot cylinder surface as a function of Reynolds number. Figure 5.1 shows the variation of isosurface plots of temperature with the change of mean flow Reynolds number for different combinations of cylinder rotational direction and speed, and blockage ratio. The top two rows of Fig. 5.1 (a) reveal the fact that the direction of rotation of the cylinder has little impact on thermal fields. As the whole surface of the cylinder is kept at constant temperature, so rotation doesn't make any effect on thermal fields. However, with the increase of mean flow Reynolds

5.1.1 Isosurface plots

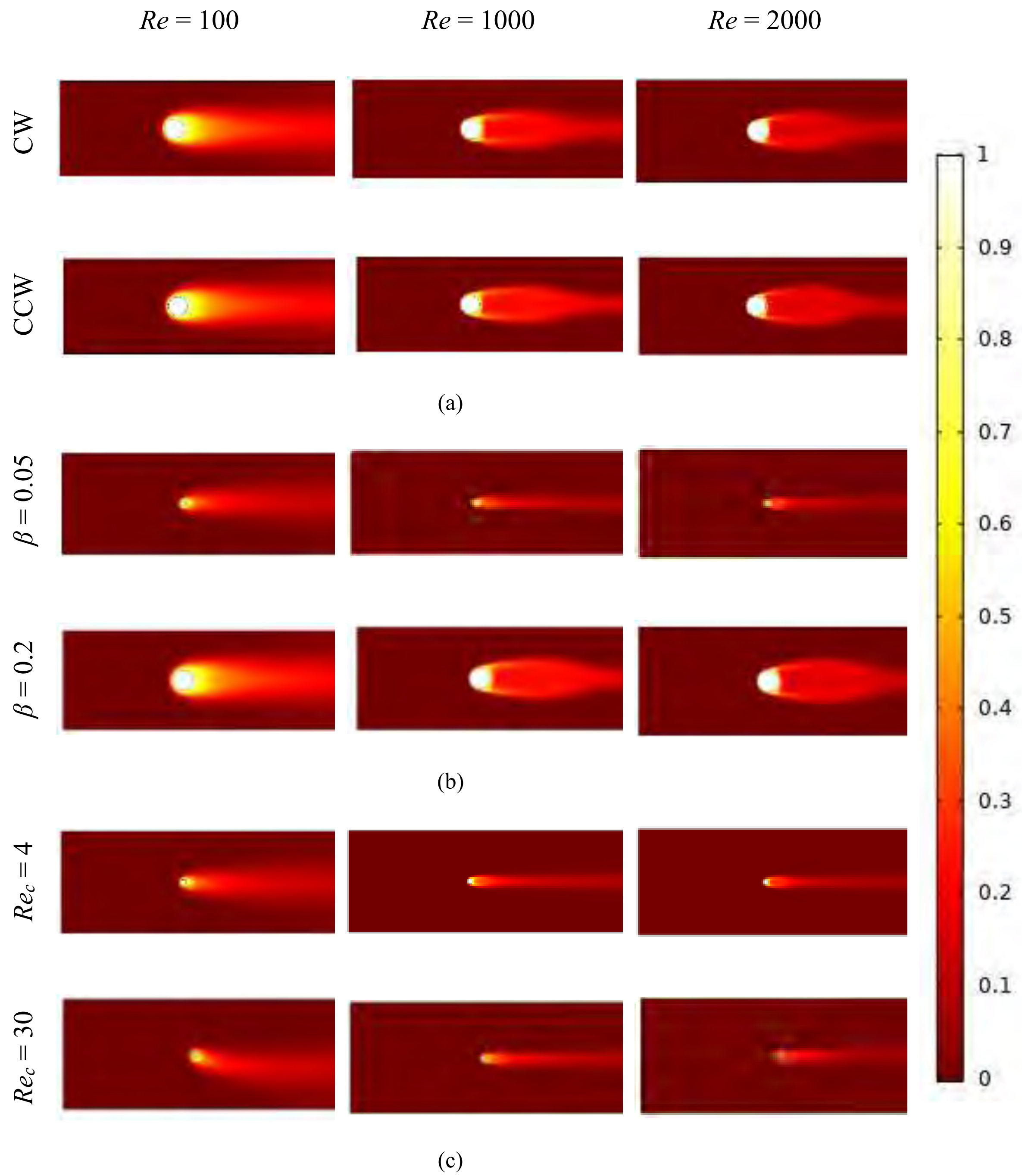

FIGURE 5.1: Effects of mean flow Reynolds number and (a) direction of cylinder rotation for $Re_c = 4$ and $\beta = 0.2$, (b) blockage ratio for $Re_c = 4$ and CCW direction of cylinder rotation and (c) rotational Reynolds number of the cylinder for $\beta = 0.05$ and CW direction of cylinder rotation on isosurface plots of temperature.

number, the shape of the isosurface plots changes sharply since the incoming cold air blows over the rotating hot cylinder at a faster speed for higher *Re*. The thermal fields at the downstream of the channel significantly depend on the blockage ratio and the rotational Reynolds number of the cylinder at low *Re*. This is clearly evident in Fig. 5.1 (b) and (c). However, at higher *Re*, the change of blockage ratio still contributes to affect the thermal fields, whereas the change of Re_c on the region of high temperature inside the channel appears to be insignificant. Because at higher *Re*, incoming air blows so fast that it can neutralize the effect of relatively smaller rotational speed of the cylinder. Hence, only the blockage ratio of the cylinder plays dominant role on the thermo-fluid characteristics inside the channel.

5.1.2 Streamline plots

In order to visualize the flow fields inside the channel, the streamline plots for various combinations of geometrical and flow parameters are presented in Fig. 5.2. Figure 5.2 (a) shows the variation of streamline plots with the change of rotational directions (CW and CCW) of the cylinder and mean flow Reynolds number. It is observed that streamline plots are significantly changed with the increase of incoming air velocity. In the mean free stream, for inviscid flow over a rotating cylinder, rotation causes recirculation of fluid around the cylinder as also observed by Prasad *et al.* [9], which, in turns, results in the formation of the eddies at the downstream of the cylinder. Due to low pressure region at the downstream, some detached eddies are formed. The fact that the rotational direction does not affect the flow fields significantly can be visualized from Fig. 5.2 (a). Figure 5.2 (b) demonstrates the effect of cylinder size in terms of blockage ratio on the streamline plots and it can be concluded that

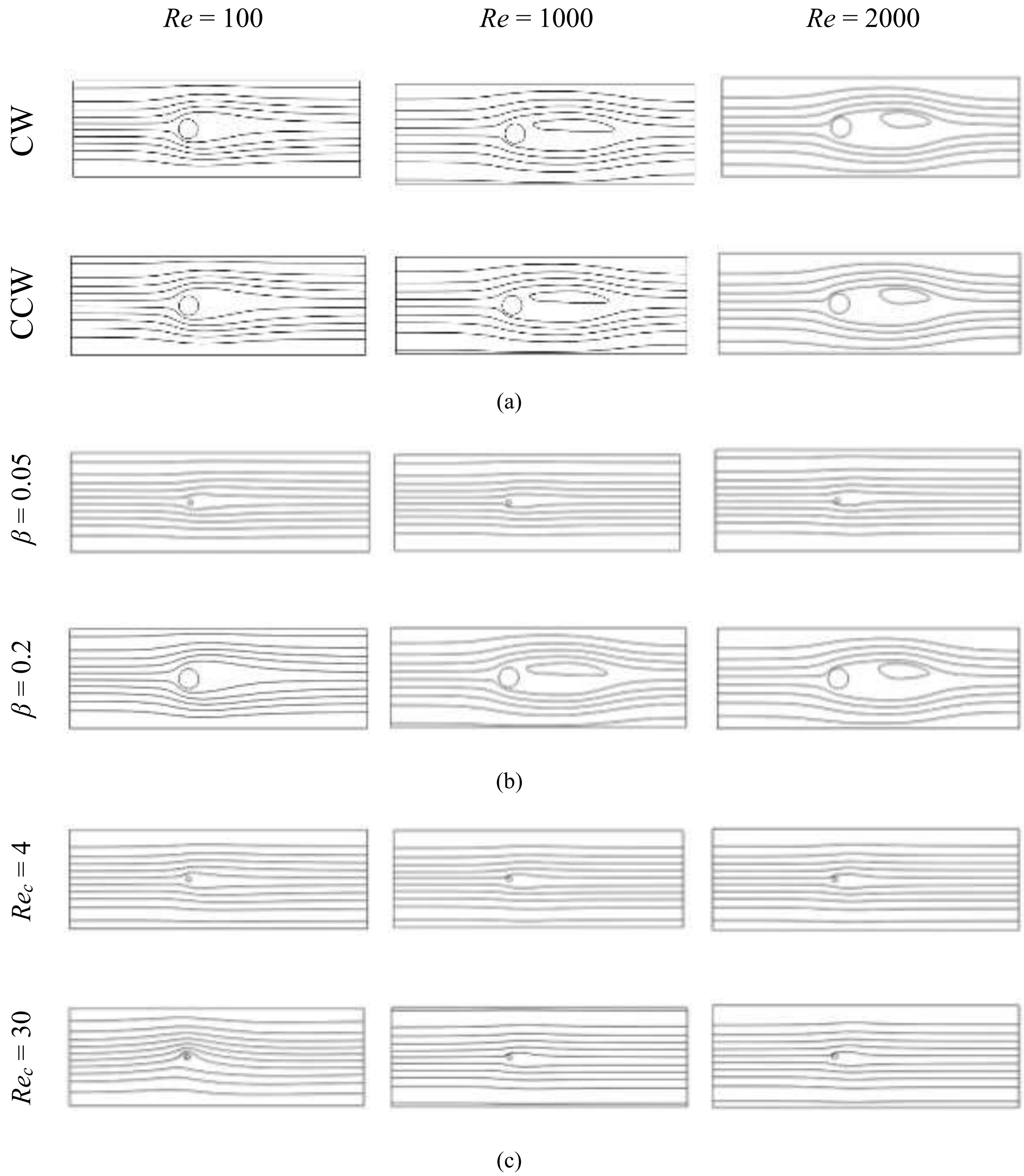

FIGURE 5.2: Effects of mean flow Reynolds number and (a) direction of cylinder rotation for $Re_c = 4$ and $\beta = 0.2$, (b) blockage ratio for $Re_c = 4$ and CCW direction of cylinder rotation and (c) rotational Reynolds number of the cylinder for $\beta = 0.05$ and CW direction of cylinder rotation on streamline plots.

eddies are increased for the larger one as flow restriction increases with the increasing size of the cylinder. So, the downstream pattern is significantly changed due to the increasing size of the cylinder. Due to the enhanced effect of Re_c, the streamlines representing the flow fields are shifted further towards the wall of the channel which can be noticed from Fig. 5.2 (c). Here, it is moving towards the bottom surface of the channel since CW direction of cylinder rotation has been taken into consideration. But for higher *Re*, this effect is reduced due to the enhanced effect of free stream velocity.

5.1.3 Pressure contour

Figure 5.3 shows the variation of pressure with the change of mean flow Reynolds number for different combinations of cylinder rotational direction and speed, and blockage ratio. Figure 5.2 (a) shows that direction of rotation of the cylinder has little impact on pressure fields which are in the range of 10^{-3} Pa. The pressure is maximum on the surface of the cylinder and eventually decreases. Figure 5.3 (b) depicts that with the increase of blockage ratio, pressure field changes significantly especially at the downstream. By increasing the diameter of the cylinder, actually flow separation at the downstream increases because of the higher flow restrictions which results in such kind of changes. The fact that with the increasing rotational speed, the pressure field varies just near the cylinder wall can be proved from fig. 5.3 (c). Because with the increasing rotational speed, air strikes much on the surface. As a result, pressure increases.

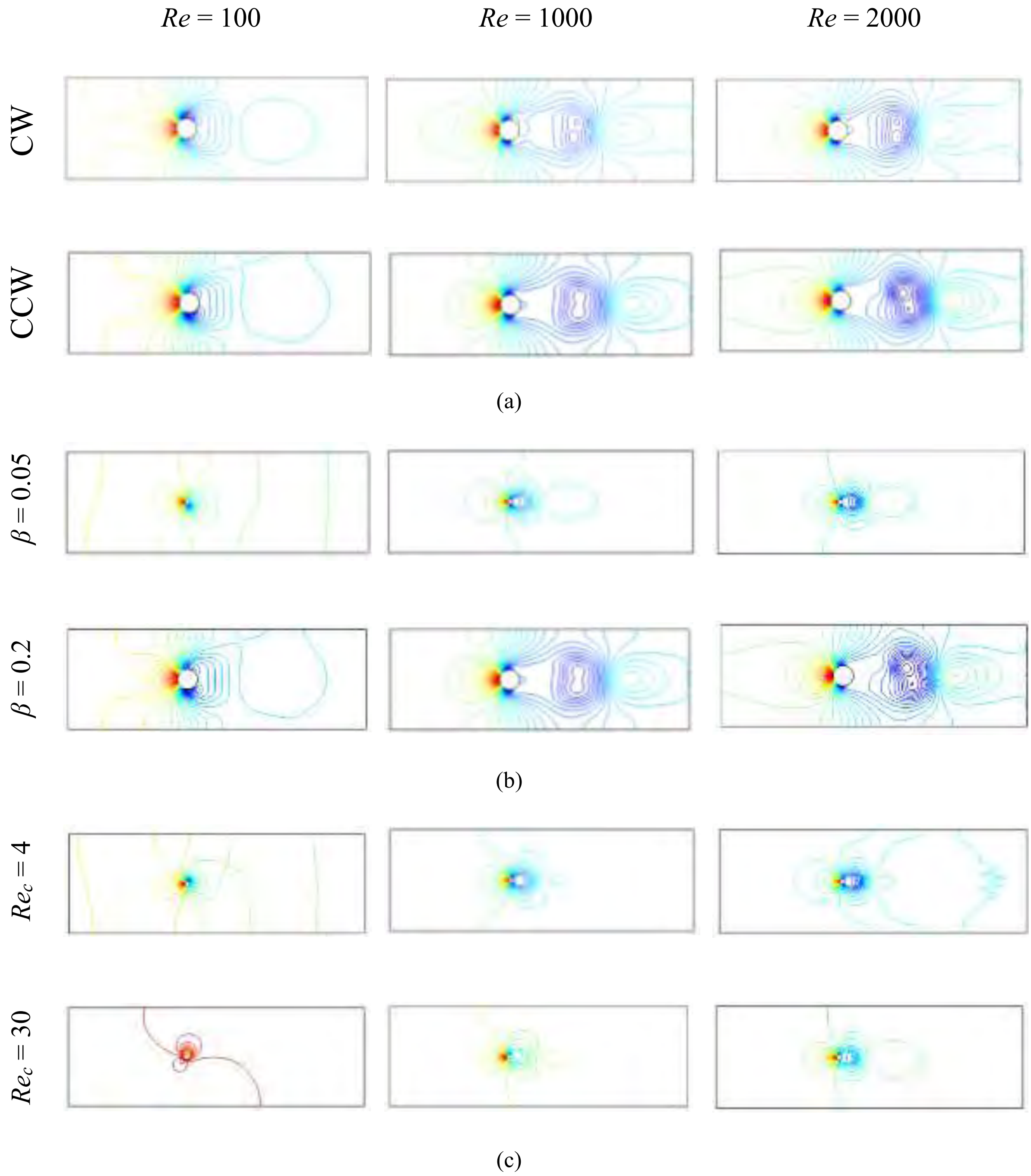

FIGURE 5.3: Effects of mean flow Reynolds number and (a) direction of cylinder rotation for $Re_c = 4$ and $\beta = 0.2$, (b) blockage ratio for $Re_c = 4$ and CCW direction of cylinder rotation and (c) rotational Reynolds number of the cylinder for $\beta = 0.05$ and CW direction of cylinder rotation on pressure contours.

5.1.4 Variations of Performance parameters

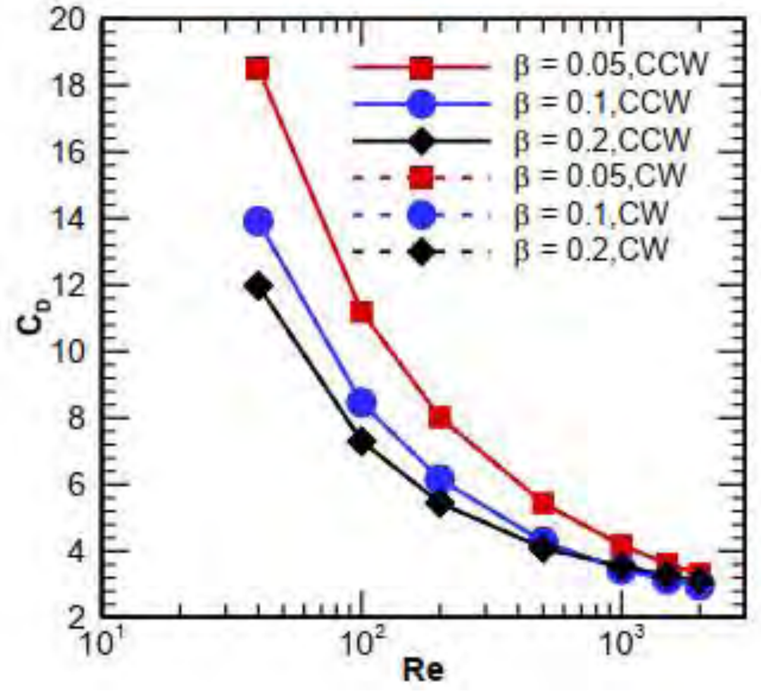

(a)

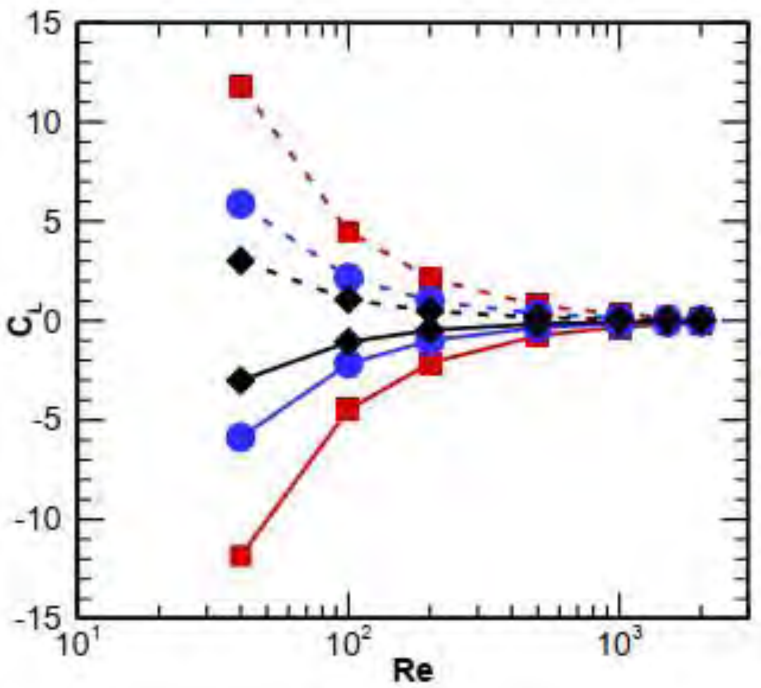

(b)

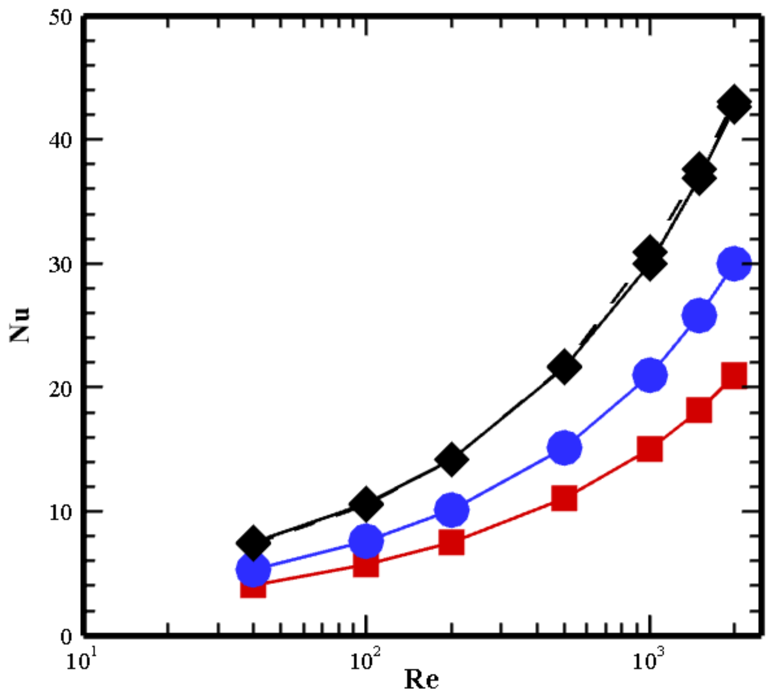

(c)

FIGURE 5.4: Variation of C_D, C_L and Nu as a function of Re for different β and both CW and CCW rotational direction of the cylinder at $Re_c = 4$.

The variations of C_D, C_L and Nu as a function of Re are displayed in Fig. 5.4 (a), (b) and (c) respectively. The decreasing trend of the variation of C_D and the increasing trend of Nu are observed with increasing mean flow Reynolds number. There are two types of drag, one is the skin-friction drag and another is the viscous pressure drag. Both of them are proportional to the velocity of the fluid velocity [111] whereas the drag coefficient is inversely proportional to the same velocity. For this reason, drag coefficient decreases with increasing Re. And Nu also increases as with increasing mean flow Reynolds number, greater amount of fluid moves over the cylinder surface and it takes more heat from the surface. For a fixed Re_c, it is found that both CW and CCW directions of rotation do not alter the values of C_D and Nu. Moreover, the absolute values of C_L remain the same, but with the opposite sign due to the change of the rotational direction of the cylinder. On the other hand, the change of blockage ratio contributes significantly to the change of both C_D and C_L at higher Re. As the size of the cylinder increases, it becomes more difficult to generate lift. The rotation of the cylinder might affect the drag coefficient to be decreased with increasing Re. Besides, the value of Nu decreases gradually

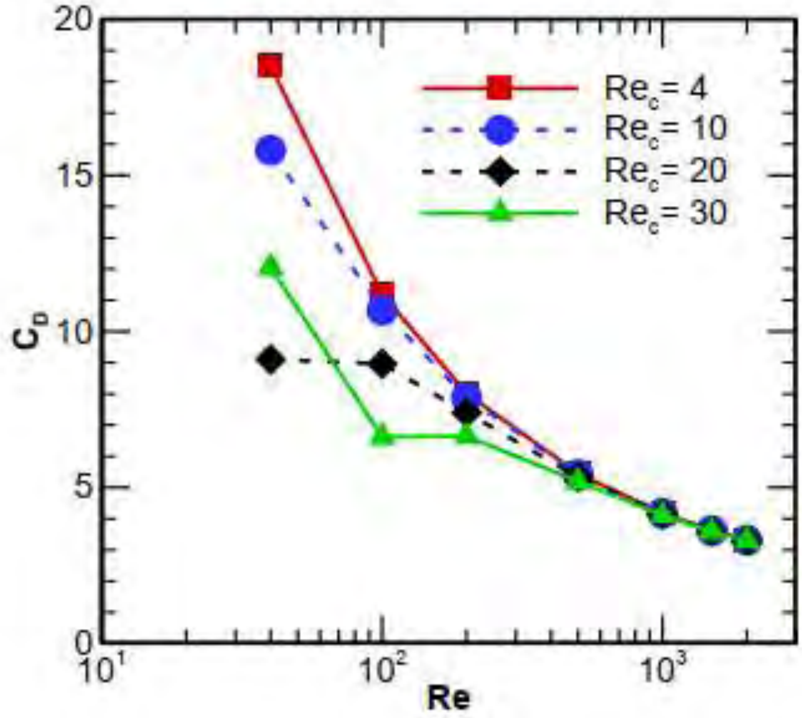

20
15
10
5
0
C_D
10^1
10^2
10^3
Re
$Re_c= 4$
$Re_c= 10$
$Re_c= 20$
$Re_c= 30$

(a)

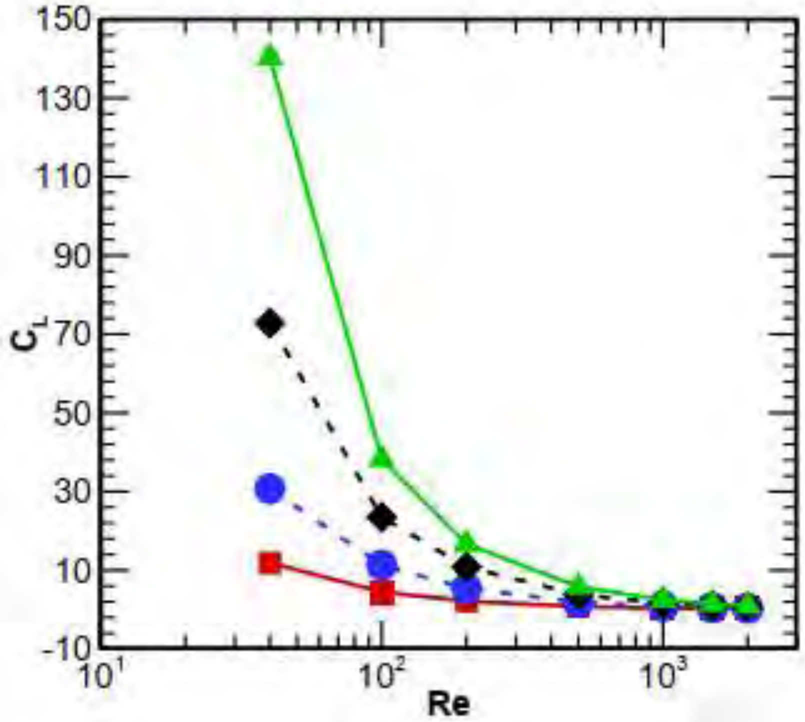

150
130
110
90
70
50
30
10
-10
C_L
10^1
10^2
10^3
Re

(b)

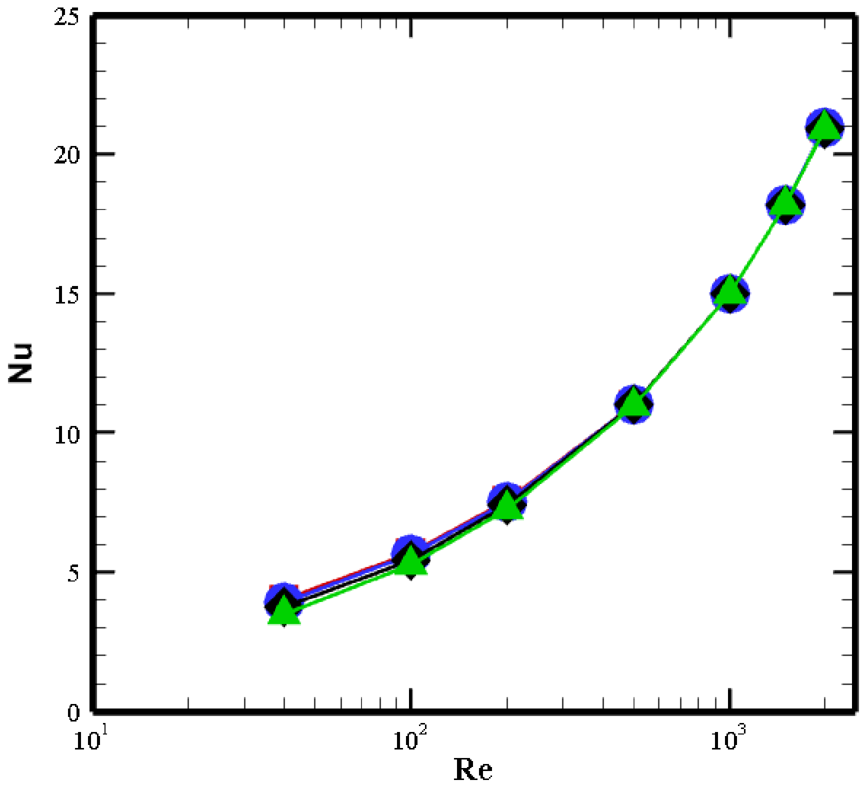

(c)

FIGURE 5.5: Variation of C_D, C_L and Nu as a function of Re for different Re_c at β = 0.05 and CW rotational direction of the cylinder.

with increasing β. The rotation of the cylinder probably causes the fluid to pass over the cylinder without any effective heat transfer and exertion of pressure force on the surface of the cylinder. From Fig. 5.4, it is obvious that heat transfer is highest for the smallest blockage ratio, β = 0.05. For this reason, Fig. 5.5 is drawn to analyze the effect of Re_c on C_D, C_L and Nu at β = 0.05. It can be concluded that the values of C_D, C_L are almost the same, but a little discrepancy is shown for higher Re_c at low Re. Moreover, with the increase of Re_c, C_D decreases but C_L increases. The flow separation occurs in the flow field for rotating cylinder rather on the surface for the stationary cylinder. This causes the pressure drag coefficient to be decreased with further increase of the rotational velocity [46]. And as the cylinder gets rotated, the fluid above the cylinder gets decelerated whereas the fluid below the cylinder gets accelerated. This causes the pressure above the cylinder to be increased with a decrease of pressure at the bottom. For this reason, the lift coefficient increases with increasing rotational velocity [46]. However, the value of Nu remains exactly the same for different values Re_c. This reveals that heat transfer does not change with increasing Re_c within the selected range.

5.2 Turbulent Flow

Parametric simulation is carried out in the range of $3000 \leq Re \leq 10000000$, $4 \leq Re_c \leq 30$ and $\beta = 0.05, 0.1, 0.2$. The results are described in terms of streamline plots, pressure contour, and isosurface plots of temperature, distributions of drag and lift coefficients and variations of Nusselt number of the hot cylinder surface as a function of Reynolds number.

5.2.1 Isosurface plots

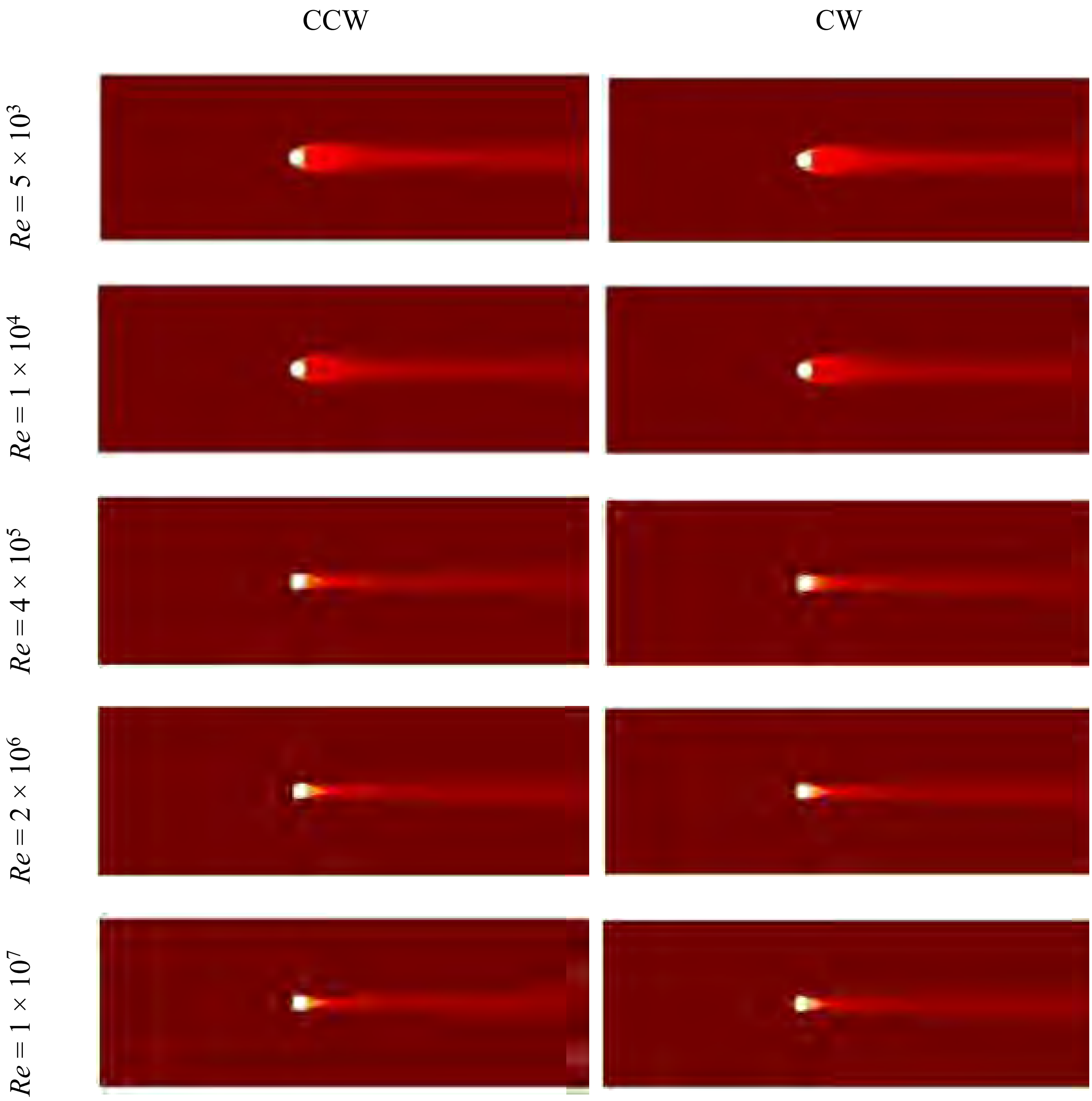

(a)

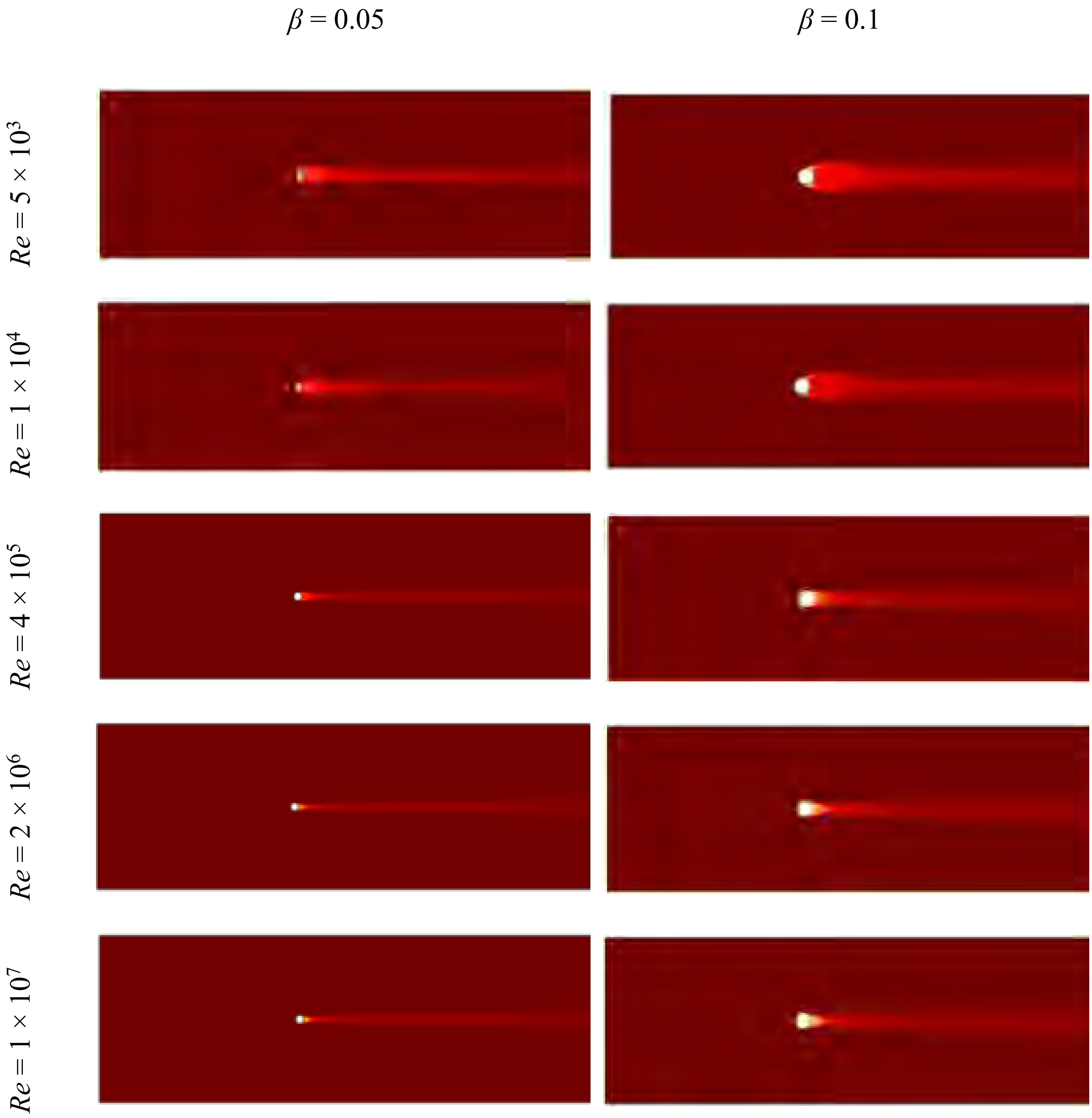
$\beta = 0.05$
$\beta = 0.1$
$Re = 5 \times 10^3$
$Re = 1 \times 10^4$
$Re = 4 \times 10^5$
$Re = 2 \times 10^6$
$Re = 1 \times 10^7$

(b)

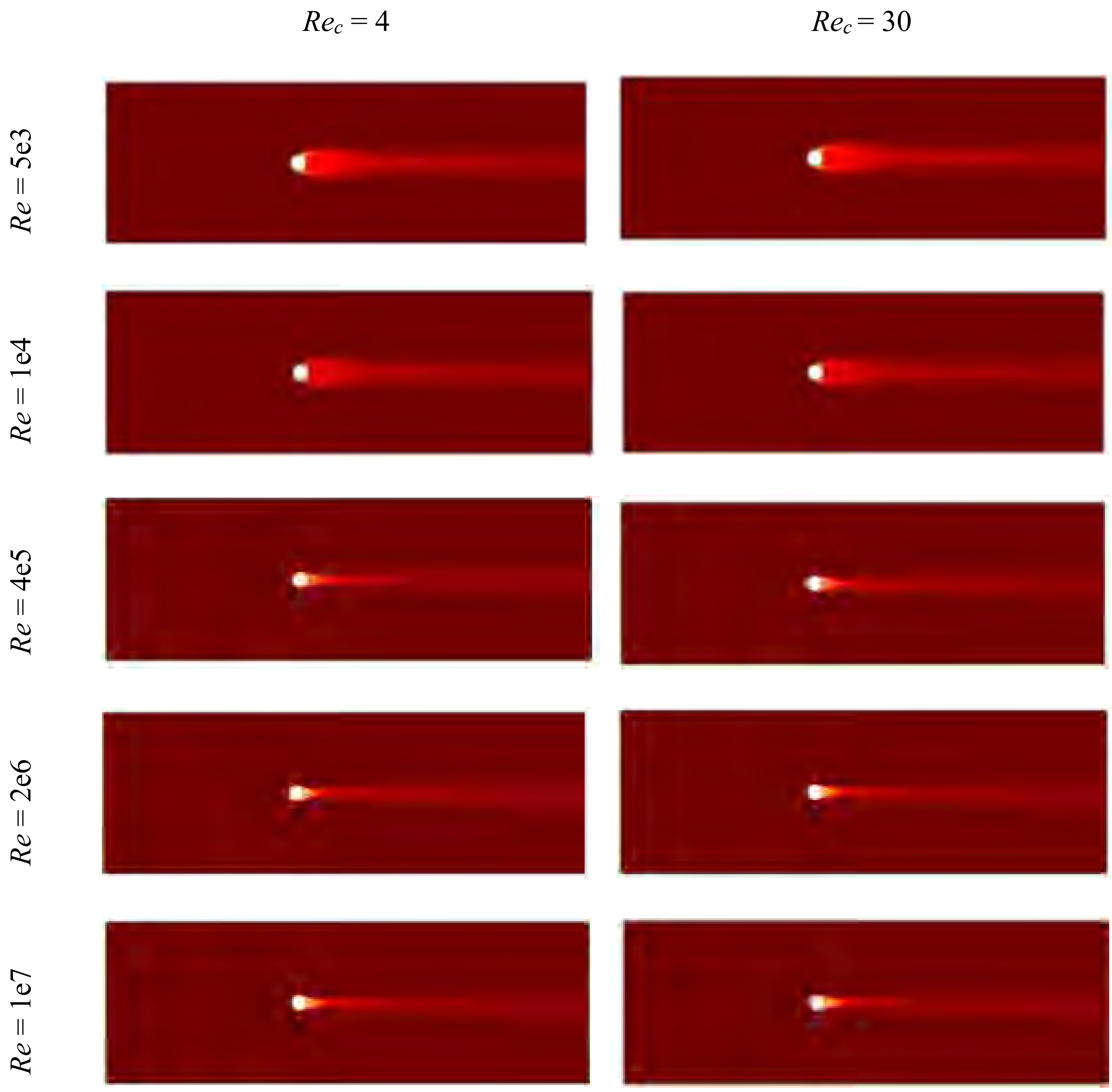

(c)

FIGURE 5.6: Effects of mean flow Reynolds number and (a) direction of cylinder rotation for $Re_c = 10$ and $\beta = 0.1$, (b) blockage ratio for $Re_c = 10$ and CW direction of cylinder rotation and (c) rotational Reynolds number of the cylinder for $\beta = 0.1$ and CCW direction of cylinder rotation on isosurface plots of temperature.

5.2.2 Streamline plots

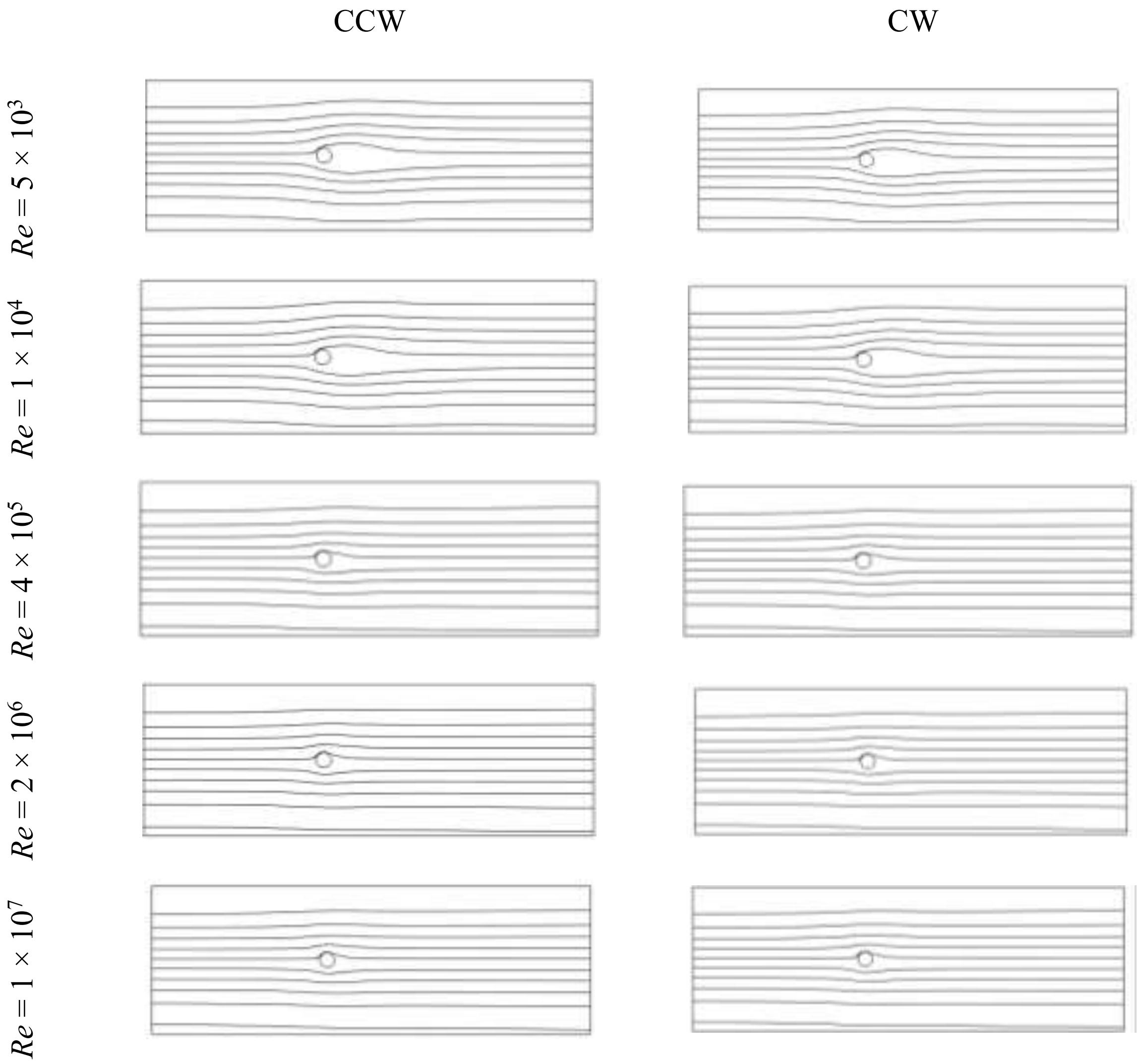

(a)

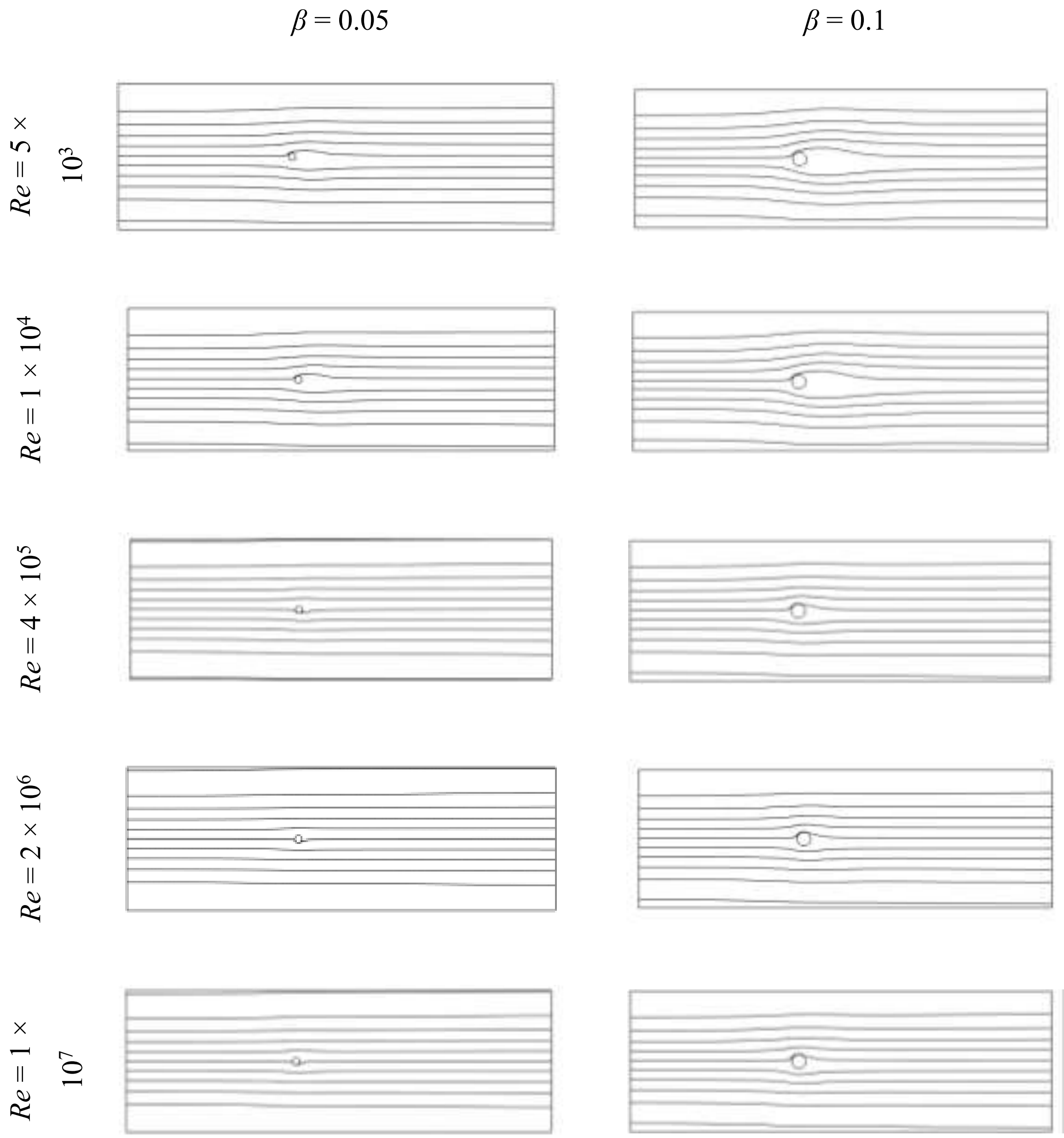
$\beta = 0.05$
$\beta = 0.1$
$Re = 5 \times 10^3$
$Re = 1 \times 10^4$
$Re = 4 \times 10^5$
$Re = 2 \times 10^6$
$Re = 1 \times 10^7$

(b)

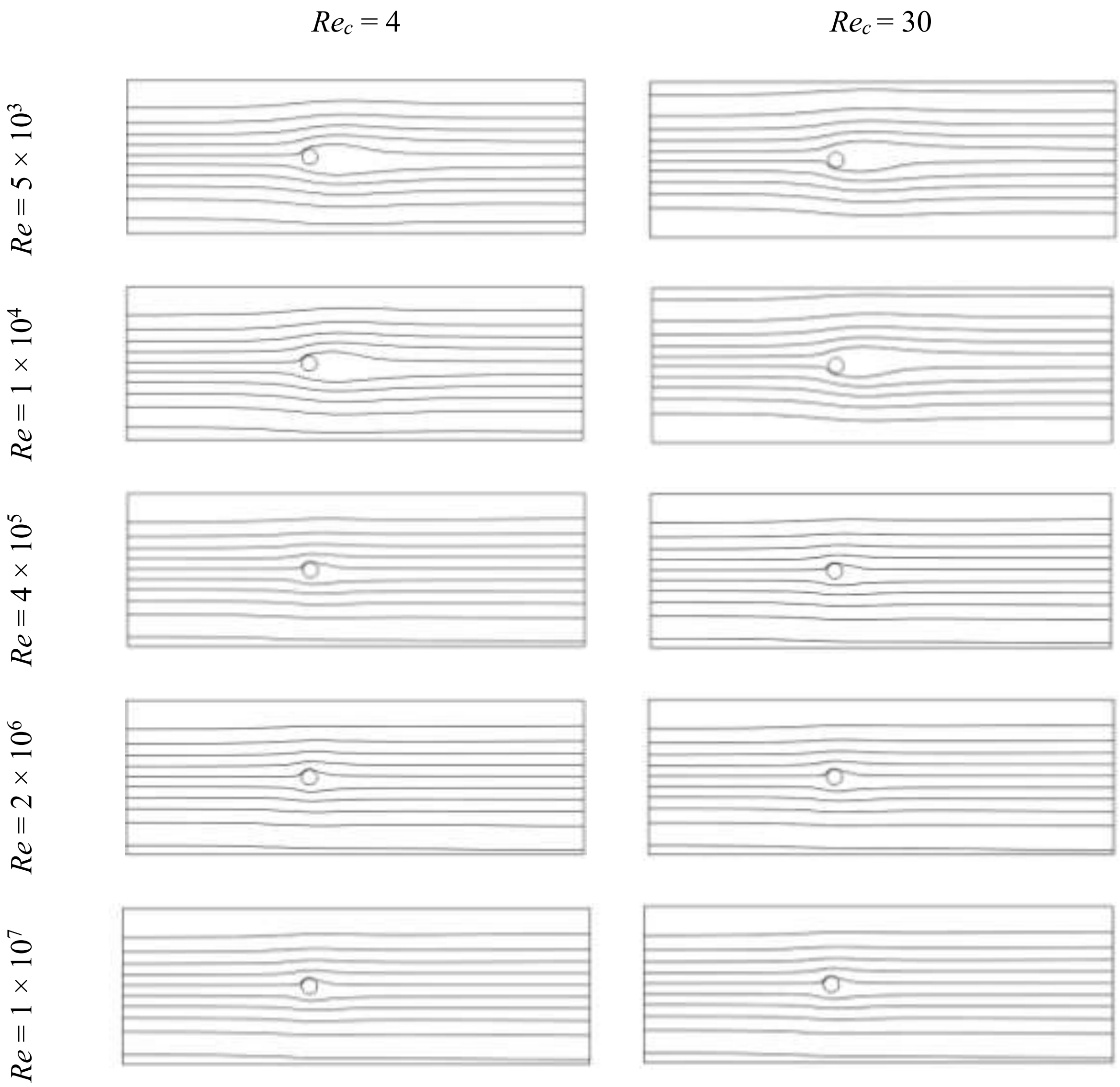

(c)

FIGURE 5.7: Effects of mean flow Reynolds number and (a) direction of cylinder rotation for $Re_c = 10$ and $\beta = 0.1$, (b) blockage ratio for $Re_c = 10$ and CW direction of cylinder rotation and (c) rotational Reynolds number of the cylinder for $\beta = 0.1$ and CW direction of cylinder rotation on streamline plots.

5.2.3 Pressure contours

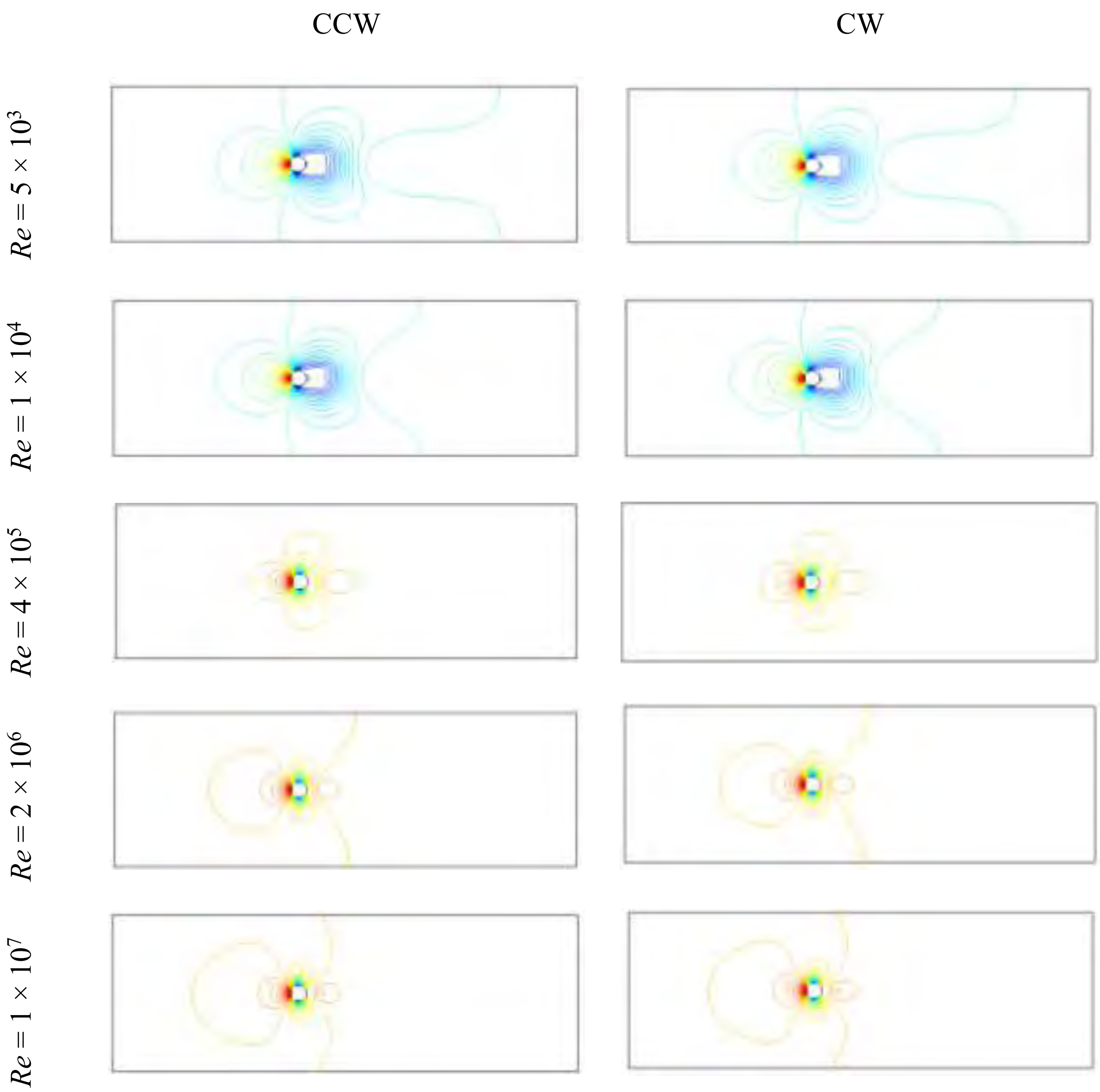

(a)

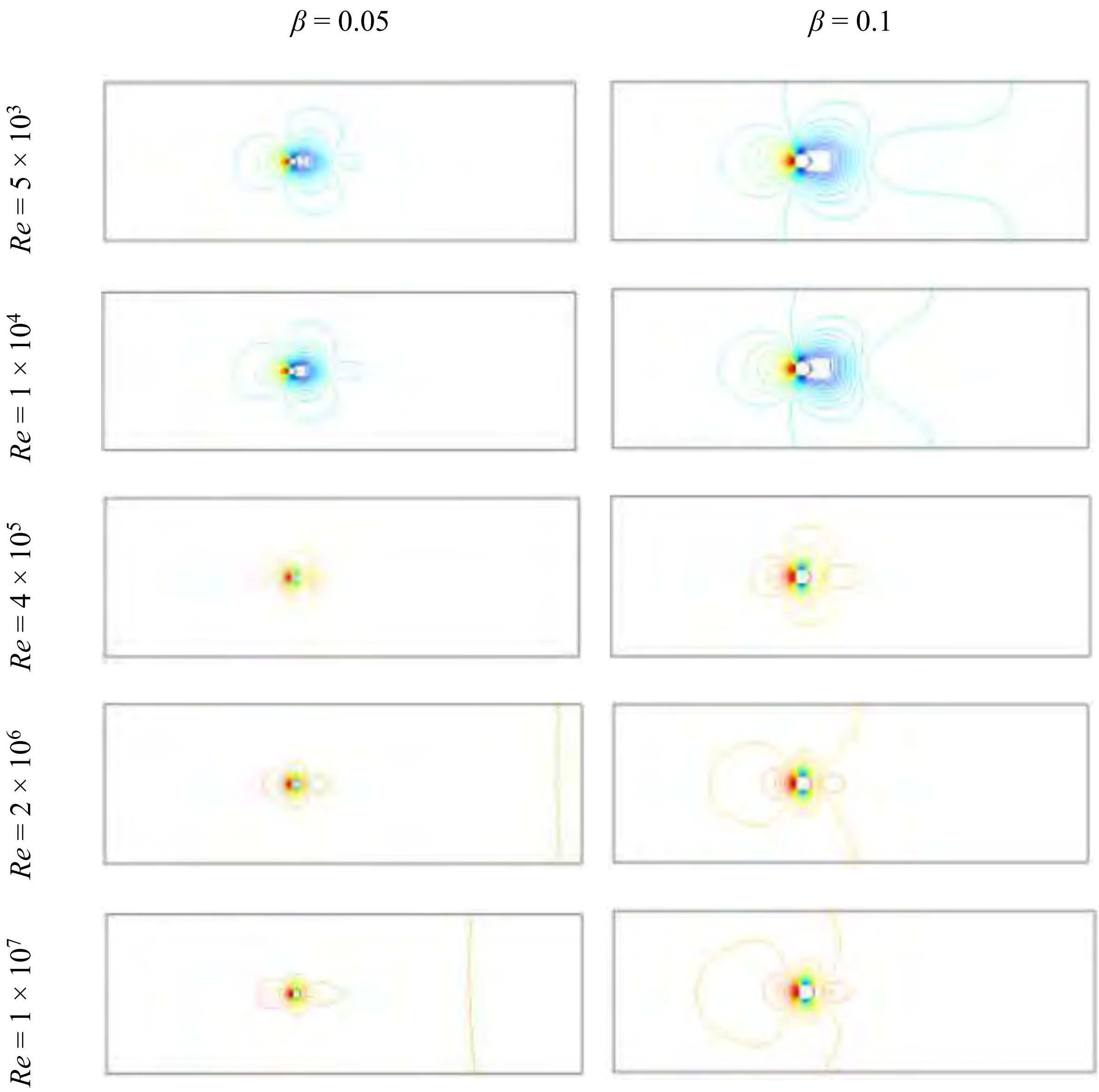

$\beta = 0.05$
$\beta = 0.1$
$Re = 5 \times 10^3$
$Re = 1 \times 10^4$
$Re = 4 \times 10^5$
$Re = 2 \times 10^6$
$Re = 1 \times 10^7$

(b)

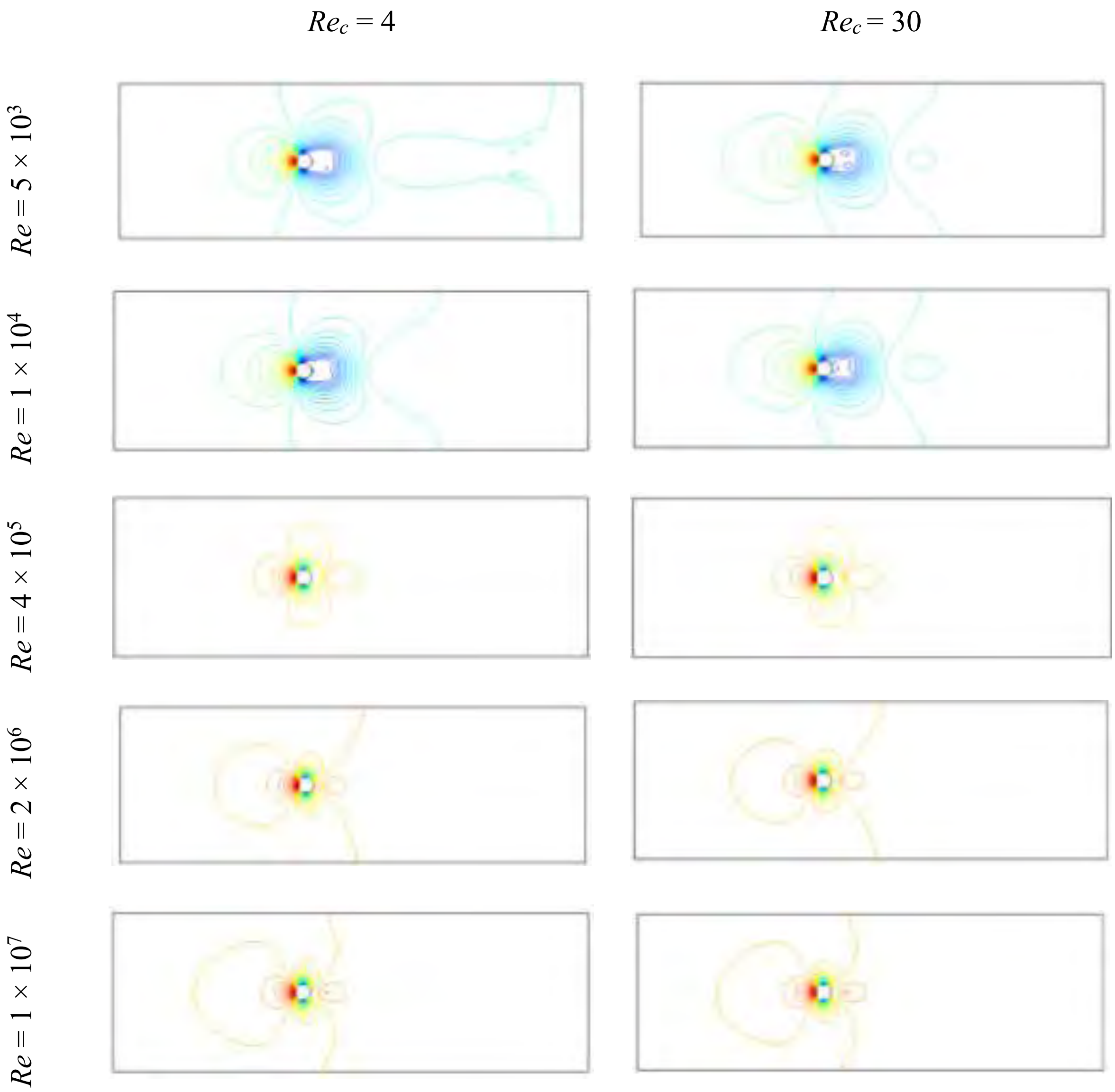

(c)

FIGURE 5.8: Effects of mean flow Reynolds number and (a) direction of cylinder rotation for $Re_c = 10$ and $\beta = 0.1$, (b) blockage ratio for $Re_c = 10$ and CW direction of cylinder rotation and (c) rotational Reynolds number of the cylinder for $\beta = 0.1$ and CCW direction of cylinder rotation on pressure contours.

Figure 5.6 shows the variation of isosurface plots of temperature with the change of mean flow Reynolds number for different combinations of cylinder rotational direction and speed, and blockage ratio. Figure 5.6 (a) reveals that the rotational direction of cylinder has no or little effect on the thermal flow fields. As the object is a symmetric one, so there is no such effect of rotational direction. However, for higher Reynolds number (*Re*), the separation region at the downstream becomes narrower because of the much higher speeds of incoming cold air with constant rotational speed. For this, downstream field changes significantly with increasing *Re*. The thermal field that is also greatly influenced by changing the blockage ratio as shown in Fig. 5.6 (b). For higher blockage ratio, separation region becomes larger as expected. Because, flow restriction and surface area of the hot surface increases with the increasing size of the cylinder. The change of Re_c on the region of high temperature inside the channel appears to be insignificant. Hence, the blockage ratio and the Reynolds number plays dominant role on the thermo-fluid characteristics inside the channel.

In order to visualize the flow fields inside the channel, the streamline plots for various combinations of geometrical and flow parameters are presented in Fig. 5.7. Figure 5.7 (a) depicts the variation of streamline plots with the change of rotational directions (CW and CCW) of the cylinder and mean flow Reynolds number. There is no significant change in thermal fields for rotational direction of the cylinder because the mean flow velocity of fluid is large enough to overcome the effect of rotational velocity. It is also observed that streamline plots are significantly changed with the increase of incoming air velocity just for the same reason as laminar flow fields. Figure 5.7 (b) demonstrates the effect of cylinder size in terms of blockage ratio on the streamline plots and it can be concluded that separations are higher for the larger one as flow restriction increases with the increasing size of the cylinder. The fact that the streamline changes a little with the increasing Re_c, is shown in Fig. 5.7 (c). But for higher values of *Re*, this effect of Re_c has been vanished. This is because the mean flow Reynolds number (*Re*) dominates over Re_c when velocity is higher.

And Fig. 5.8 depicts the effects of mean flow Reynolds number, rotational direction of the cylinder, blockage ratio and the cylinder Reynolds number on the pressure contours. The fact that the rotational direction of cylinder can't affect the pressure field so much, is found from Fig. 5.8 (a). Pressure field changes significantly with increasing blockage ratios especially at the downstream of the flow. This is shown in Fig. 5.8 (b). As flow restrictions are increasing with the increase of blockage ratios, so it is very much practical to have different field for

5.2.4 Variations of Performance parameters

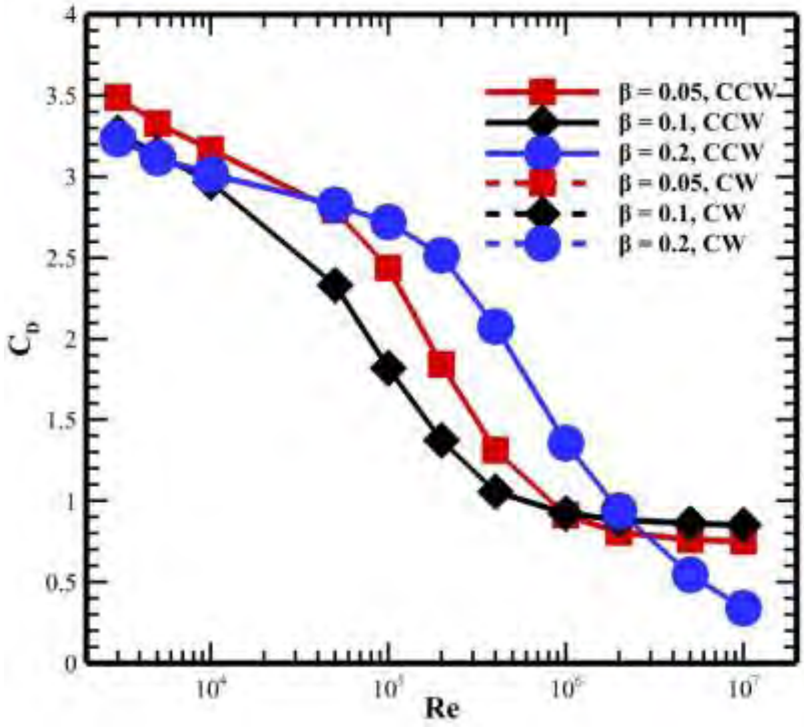

(a)

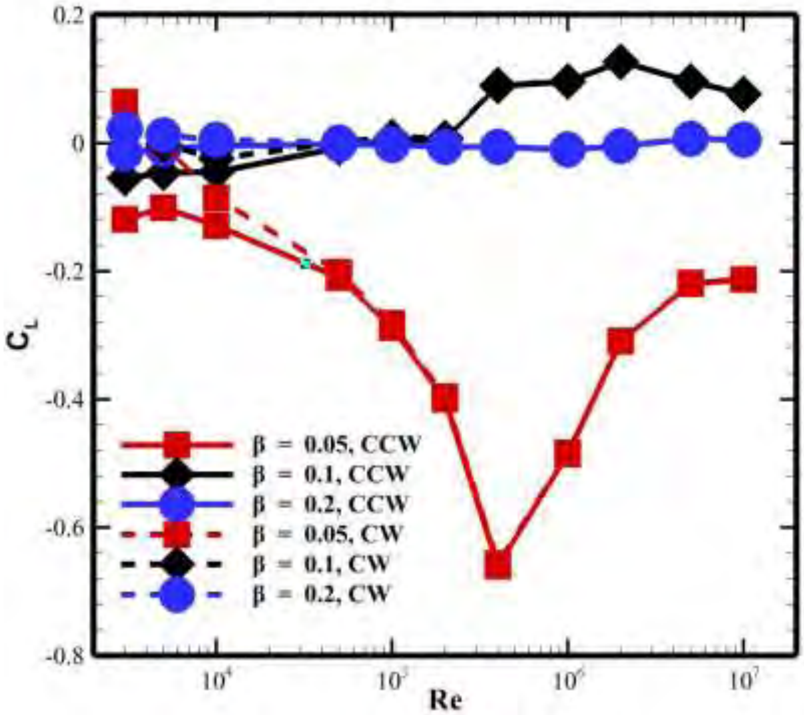

(b)

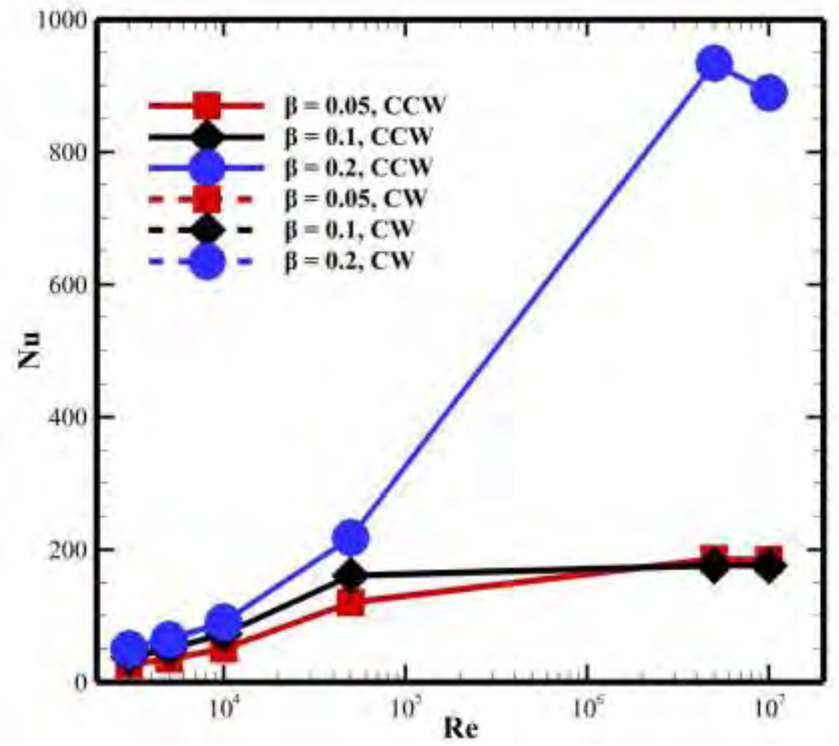

(c)

FIGURE 5.9: Variations of (a) C_D, (b) C_L and (c) *Nu* for different Reynolds number, blockage ratio and rotational direction of the cylinder for $Re_c = 4$.

increasing size of the cylinder. Figure 5.8 (c) demonstrates the same result as of 5.7 (c) for having the same reason.

The variations of C_D, C_L and *Nu* for different values of *Re* are displayed in Figs. 5.9 (a), (b) and (c) respectively. The obvious fact that the drag coefficient decreases with increasing Reynolds number at higher Reynolds number is shown in Fig. 5.9 (a). Increase of *Re* keeping the rotational speed constant increases the upward dislocation of the stagnation point. Therefore, for smaller speed ratios, the effect of velocity increase is much higher than the effect of rotational speed and hence, drag coefficient decreases with larger slopes [98]. Figure 5.9 (b) shows that the effect of *Re* on lift coefficient is almost negligible as the values are close to zero. Because of higher velocity of inlet fluid parallel to the circular cylinder, vertical lift force is much less and probably due to the turbulence of fluid it gives arbitrary results. Increasing values of Nusselt number means the increasing heat transfer for higher Reynolds number. This is depicted in Fig. 5.9 (c). High velocity fluid takes away more heats from the cylinder surface.

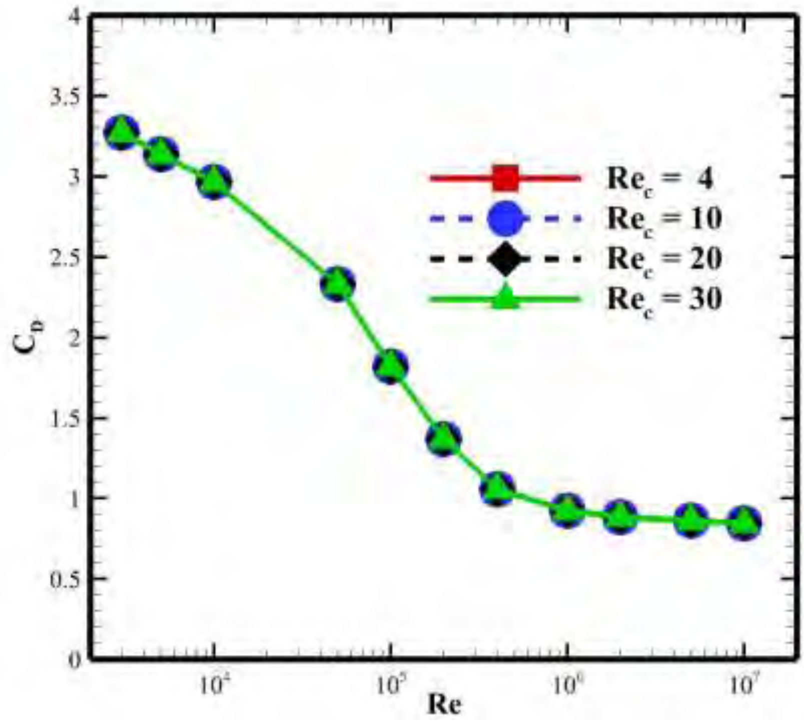

(a)

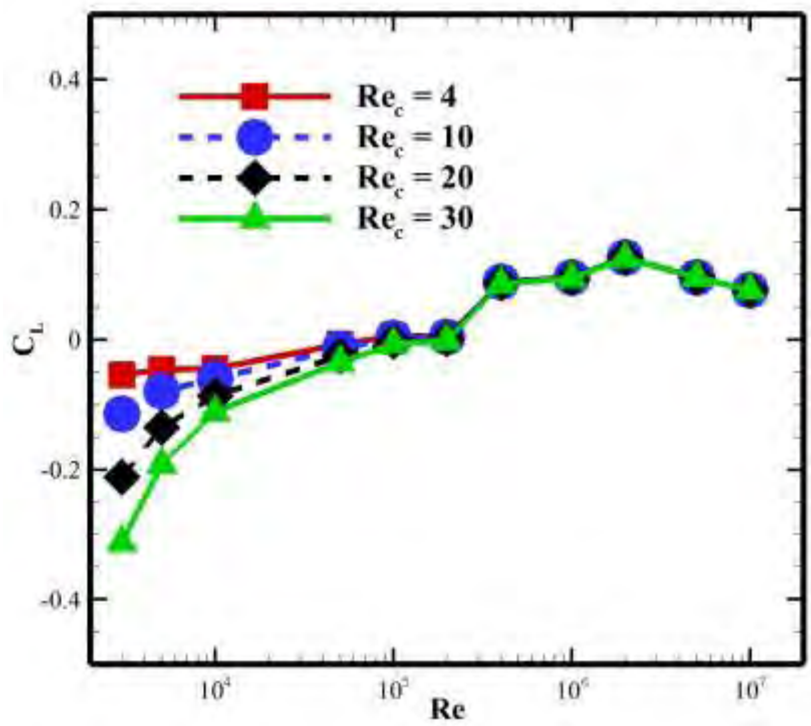

(b)

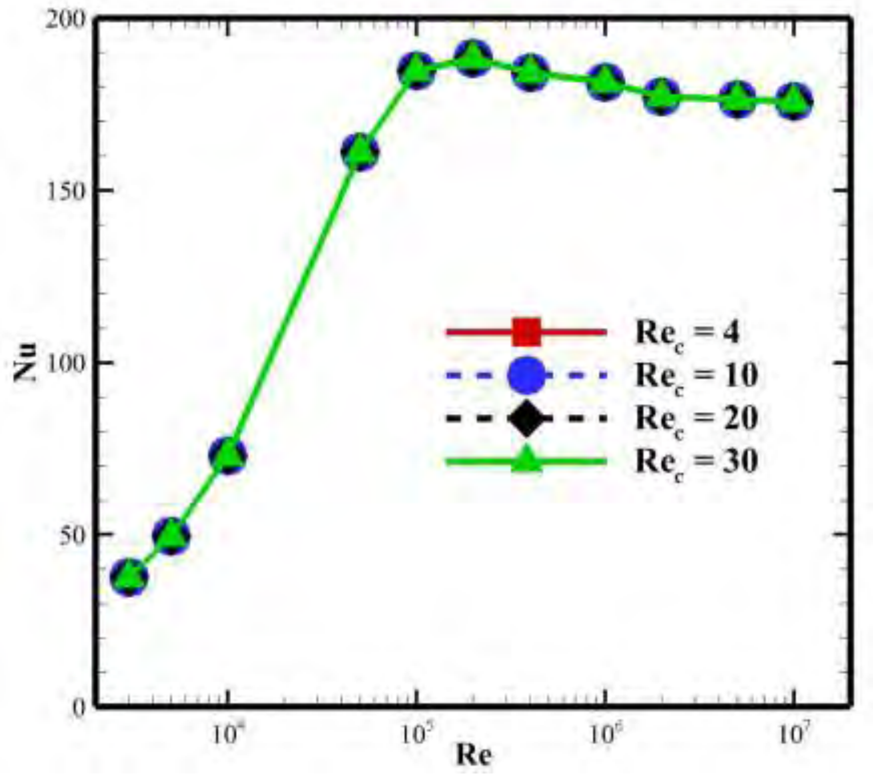

(c)

FIGURE 5.10: Effects of Re_c on (a) C_D, (b) C_L and (c) Nu as a function of Re for $\beta = 0.1$ and CCW rotational direction of the cylinder.

But after a certain values of Reynolds number, Nusselt number keeps decreasing. Initially with the increase of mean flow Reynolds number, due to greater contacts with cylinder heat transfer enhances. Along with this collision among fluid particles becomes higher for turbulent flow. This increases the heat transition rate and thus contribute to increasing *Nu*. After the values of $Re \geq 2\times10^5$, Nusselt number decreases.

Figure 5.10 depicts the effect of Re_c as a function of Re on drag coefficient, lift coefficient and Nusselt number. Changing the values of Re_c has no effect on C_D and *Nu*. These are shown in Fig. 5.10 (a) and 5.10 (c) respectively. This is probably due to the higher mean flow inlet velocity comparing with the relatively lower rotational velocity of the cylinder which nullifies the effect of rotational velocity. For the case of lift coefficient, at higher values of Re, there are no effect of Re_c, but some variations are present at lower Reynolds number. This is shown in

Fig. 5.10 (b). But if we increase the rotational velocity of the cylinder, it will probably affect the flow fields and thermal fields.

In this study, we have considered variational speed ratio instead of making it constant by changing both the mean flow inlet velocity and the rotational speed simultaneously which is more practical in this type of problem. The fact that the variation of drag coefficient in respect to experimental study [90] is about 7-8% whereas there is no such variation for lift coefficient [90] are shown in Table 5.1. And the variation of *Nu* found is less than 3% [100, 101] which is shown in Table 5.2. So, we can conclude that our results with variable speed ratio concept matches the experimental results well enough to describe the scenario.

Table 5.1: Variation of drag and lift coefficients with experimental study

	Re	Takayama and Aoki (2004)	Present
Drag Coefficient	1.8×10^5	1.25	1.34
Lift Coefficient	1.8×10^5	0	0

Table 5.2: Comparison of Nu with experimental study

Re	Ouali et al. (2006)	Present
5000	50	49.5
10000	95	91.3

Chapter 6

Concluding Remarks and Future Scopes

The present two-dimensional, incompressible, steady laminar and turbulent flow past a rotating circular cylinder has provided new information regarding the effect of blockage ratio, mean fluid velocity, rotational direction of the cylinder and rotational speed of the cylinder. These are summarized in the first four sections and section 6.5 discusses further numerical research opportunities to be taken to further investigate the thermal performance of the confined channel due to the cylinder.

6.1 Effects of Blockage Ratio

The effects of blockage ratio on the flow field, thermal field and performance parameters are summarized below:

- With the increasing size of the cylinder, eddies are formed at larger rate because flow restrictions become greater for large cylinder. So, flow fields affect significantly by blockage ratio.
- Thermal fields and pressure fields at the downstream of the channel also significantly depend on the blockage ratio.
- Drag coefficients are higher for smallest cylinder in laminar case and opposite for turbulent flow case.
- Lift coefficients are higher for laminar zone but no regular pattern is found for turbulent flow.
- For laminar flow, Nu is greater for smallest cylinder but opposite for the case of turbulent flow.

6.2 Effect of Mean Fluid Velocity

- Both thermal field, pressure field and flow fields are significantly influenced by the mean fluid velocity.
- Drag coefficient decreases with the increase of Reynolds number.
- Lift coefficient approaches to zero for higher Reynolds number for laminar flow but for turbulent flow it shows arbitrary value around zero.
- *Nu* increases with the increase of Reynolds number up to a certain range in turbulent zone, after that following a decreasing pattern it remains almost constant.

6.3 Effect of Rotational Direction of the Cylinder

- This phenomenon has very little or no effect on thermal, flow and pressure fields.
- Drag coefficient and *Nu* remains the same for either rotation of the cylinder.
- Lift coefficient has showed the opposite value for either rotation of the cylinder.

6.4 Effect of Cylinder Speed

- Cylinder speed greatly influenced the thermal, flow and pressure fields.
- Drag and Lift coefficient shows a little difference for lower Reynolds number but for higher one these values are similar.
- *Nu* remains constant for all speed of the cylinder.

6.5 Future Research Scopes

The present study has hopefully developed our understanding of the flow field, thermal fields and performance parameters of two-dimensional, incompressible, steady laminar and turbulent flow past a rotating circular cylinder. So, a great amount of investigation is required to provide more to the following issue. The future scopes of the present study are summarized as follows:

- Different types of nanofluid can be introduced to the channel.

- The present work has been carried out for steady state. Therefore, the work can be extended for transient case.
- Effect of higher blockage ratios can be studied her on.
- Investigations can be carried out for heat fluxes too.
- More rotational speed of the cylinder can be introduced.
- The investigation can be extended for three-dimensional steady or unsteady cases.
- Experimental study of this type of problem is an urgent need.

Bibliography

[1] Chen, J. H., Pritchard, W. G. and Tavener, S. J., "Bifurcation for flow past a cylinder between parallel planes," *J. Fluid Mech*. Vol. 284, pp. 23-41, 1995.

[2] Huang P. Y. and Feng, J., "Wall effects on the flow of viscoelastic fluids around a circular cylinder," *J. of Non-Newtonian Fluid Mech.*, vol. 60, no. 2–3, pp. 179–198, 1995.

[3] Anagnostopoulos P. and Iliadis G., "Numerical study of the blockage effects on viscous flow past a circular cylinder," *Int. J. Numer. Meth. Fluids*, vol. 22, pp. 1061–1074, 1996.

[4] Zovatto L. and Pedrizzetti G., "Flow about a circular cylinder between parallel walls," *J. Fluid Mech.*, vol. 440, pp. 1–25, 2001.

[5] Chakraborty J., Verma N., and Chhabra R. P., "Wall effects in flow past a circular cylinder in a plane channel: a numerical study," *Chem. Engg. and Process.*, vol. 43, no. 12, pp. 1529–1537, 2004.

[6] Sahin M. and Owens R. G., "A numerical investigation of wall effects up to high blockage ratios on two-dimensional flow past a confined circular cylinder," *Phys. of Fluids*, vol. 16, no. 5, pp. 1305–1320, 2004.

[7] Wen C. Y., Yeh C. L., Wang M. J., and Lin C. Y., "On the drag of two-dimensional flow about a circular cylinder," *Phys. of Fluids*, vol. 16, no. 10, pp. 3828–3831, 2004.

[8] Dipankar A. and Sengupta T. K., "Flow past a circular cylinder in the vicinity of a plane wall," *J. of Fluids and Struct.*, vol. 20, no. 3, pp. 403–423, 2005.

[9] Kumar B. and Mittal S., "Effect of blockage on critical parameters for flow past a circular cylinder," *Int. J. Numer. Meth. Fluids*, vol. 50, no. 8, pp. 987–1001, 2006.

[10] Rehimi, F., Aloui, F., Nasrallah, S. B., Doubliez, L., and Legrand, J., "Experimental investigation of a confined flow downstream of a circular cylinder centred between two parallel walls," J. Fluid Struct. Vol. 24, pp. 855–882, 2008.

[11] Singha S. and Sinhamahapatra K. P., "Flow past a circular cylinder between parallel walls at low Reynolds numbers," *Ocean Engg.*, vol. 37, pp. 757–769, 2010.

[12] Sen S., Mittal S., and Biswas G., "Numerical Simulation of Steady Flow Past a Circular Cylinder," *Int. Conf. of Fluid Mech.*, pp. 11, 2010.

[13] Mettu S., Verma N., and Chhabra R. P., "Momentum and heat transfer from an asymmetrically confined circular cylinder in a plane channel," *Heat Mass Transfer*, vol. 42, no. 11, pp. 1037–1048, 2006.

[14] Rajani B.N., Gowda R.V.P. and Ranjan P., "Numerical Simulation of Flow past a Circular Cylinder with Varying Tunnel Height to Cylinder Diameter at Re 40," *Int. J. of Comput. Engg. Research*, vol. 3, no. 1, pp. 188-194, 2013.

[15] Nidhul K., Sunil A. S., and Benphil C. P., "Effect of Domain Size and Grid Spacing on Flow Past a Circular Cylinder at Low Reynolds Number," *Int. J. of Engg. Research and Tech.*, vol. 3, no. 8, pp. 1365–1368, 2014.

[16] Sun D. W. and Sun B. X., "The Research on Flow Past a Cylinder," *Int. Conf. of Mech. and Mechanical Engg.*, vol. 105, pp. 1047–1050, 2016.

[17] Deepakkumar R., Jayavel S., and Tiwari S., "Computational Study of Fluid Flow Characteristics past Circular Cylinder due to Confining Walls with Local Waviness," *J. of Phys.*, vol. 759, p. 7, 2016.

[18] Mehdi H., Namdev V., Kumar P., and Tyagi A., "Numerical Analysis of Fluid Flow around a Circular Cylinder at Low Reynolds Number," *J. of Mechanical and Civil Engg.*, vol. 13, no. 3, pp. 94–101, 2016.

[19] Zhang W., Jiang Y., Li L., and Chen G., "Effects of wall suction/blowing on two-dimensional flow past a confined square cylinder," *SpringerPlus*, vol. 5, no. 1, pp. 985–994, 2016.

[20] Mathupriya P., Chan L., Hasini H., and Ooi A., "Numerical Investigations of Flow Over a Confined Circular Cylinder," *Australian Fluid Mech. Conf.*, p. 4, 2018.

[21] Doreti L. K. and Dineshkumar L., "Control techniques in flow past a cylinder- A Review," *Mater. Sci. Engg.*, vol. 377, no. 1, 2018.

[22] Cavanagh K. and Wulandana R., "2D Flow Past a Confined Circular Cylinder with Sinusoidal Ridges," *COMSOL Conf.*, p. 6, 2019.

[23] Glauert M. B., "The flow past a rapidly rotating circular cylinder," *Proc. R. Soc. Lond. A*, vol. 242, no. 1228, pp. 108–115, 1957.

[24] Ingham D. B., "Steady flow past a rotating cylinder," *Computers & Fluids*, vol. 11, no. 4, pp. 351–366, 1983.

[25] Ingham D. B. and Tang T., "A numerical investigation into the steady flow past a rotating circular cylinder at low and intermediate Reynolds number," J. Comput. Phys, vol. 87, pp. 91-107, 1990.

[26] Tang T. and Ingham D. B., "On steady flow past a rotating circular cylinder at Reynolds numbers 60 and 100," Computers & Fluids, vol. 19, no. 2, pp. 217–230, 1991.

[27] Chew Y. T., Cheng M., and Luo S. C., “A numerical study of flow past a rotating circular cylinder using a hybrid vortex scheme,” *J. Fluid Mech.*, vol. 299, pp. 35–71, 1995.

[28] Kang S., Choi H., and Lee S., “Laminar flow past a rotating circular cylinder,” *Phys. of Fluids*, vol. 11, no. 11, p. 11, 1999.

[29] Barnes F. H., “Vortex shedding in the wake of a rotating circular cylinder at low Reynolds numbers,” *J. Phys. D: Appl. Phys.*, vol. 33, no. 23, pp. 141–144, 2000.

[30] Jagad P., Mohamed M. S. and Samtaney R., “Flow Past a Circular Cylinder on Curved Surfaces,” *Phys. Fluid. Dyn.*, 2018.

[31] Tokumaru P. T. and Dimotakis P. E., “The lift of a cylinder executing rotary motions in a uniform flow,” J. Fluid Mech., vol. 255, no. 1, p. 1, 1993.

[32] Stojković D., Breuer M., and Durst F., “Effect of high rotation rates on the laminar flow around a circular cylinder,” *Phys. Fluids*, vol. 14, no. 9, pp. 3160–3178, 2002.

[33] Stojković D., Schön P., Breuer M., and Durst F., “On the new vortex shedding mode past a rotating circular cylinder,” *Phys. Fluids*, vol. 15, no. 5, pp. 1257–1260, 2003.

[34] Lam K. M., “Vortex shedding flow behind a slowly rotating circular cylinder,” *Journal of Fluids and Structures*, vol. 25, no. 2, pp. 245–262, 2009.

[35] Mittal S. and Kumar B., “Flow past a rotating cylinder,” *J. Fluid Mech.*, vol. 476, pp. 303–334, 2003.

[36] Cliffe K. A. and Tavener S. J., “The effect of cylinder rotation and blockage ratio on the onset of periodic flows,” *J. Fluid Mech.*, vol. 501, pp. 125–133, 2004.

[37] Kang S., “Laminar flow over a steadily rotating circular cylinder under the influence of uniform shear,” *Phys. of Fluids*, vol. 18, no. 4, pp. 1–13, 2006.

[38] Sojoudi A. and Saha S. C., “Shear Thinning and Shear Thickening Non- Newtonian Confined Fluid Flow over Rotating Cylinder,” *American J. Fluid Dynamics*, vol. 2, no. 6, pp. 117–121, 2013.

[39] Kumar S., Cantu C., and Gonzalez B., “Flow Past a Rotating Cylinder at Low and High Rotation Rates,” *J. Fluids Eng.*, vol. 133, no. 4, pp. 1–9, 2011.

[40] Rao A., Stewart B. E., Thompson M. C., Leweke T., and Hourigan K., “Flows past rotating cylinders next to a wall,” *J. of Fluids and Struct.*, vol. 27, no. 5–6, pp. 668–679, 2011.

[41] Shaafi K., Naik S. N., and Vengadesan S., "Effect of rotating cylinder on the wake-wall interactions," *Ocean Engg.*, vol. 139, pp. 275–286, 2017.

[42] Sengupta T. K. and Patidar D., "Flow past a circular cylinder executing rotary oscillation: Dimensionality of the problem," *Phys. Fluids*., vol. 30, no. 9, pp. 1-12, 2018.

[43] Badr H. M., Dennis S. C. R., and Young P. J. S., "Steady and unsteady flow past a rotating circular cylinder at low Reynolds numbers," *Computers & Fluids*, vol. 17, no. 4, pp. 579–609, 1989.

[44] Paramane S. B. and Sharma A., "Numerical investigation of heat and fluid flow across a rotating circular cylinder maintained at constant temperature in 2-D laminar flow regime," *Int. J Heat Mass Trans.*, vol. 52, no. 13–14, pp. 3205–3216, 2009.

[45] Paramane S. B. and Sharma A., "Heat and fluid flow across a rotating cylinder dissipating uniform heat flux in 2D laminar flow regime," *Int. J. of Heat Mass Trans.*, vol. 53, no. 21–22, pp. 4672–4683, 2010.

[46] Prasad K., Paramane S. B., Agrawal A., and Sharma A., "Effect of Channel-Confinement and Rotation on the Two-Dimensional Laminar Flow and Heat Transfer across a Cylinder," *Numer. Heat Trans.*, vol. 60, no. 8, pp. 699–726, 2011.

[47] Sharma V. and Dhiman K., "Heat transfer from a rotating circular cylinder in the steady regime: Effects of Prandtl number," *Therm sci*, vol. 16, no. 1, pp. 79–91, 2012.

[48] Sharma M. K., Dewangan C. L., and Verma P., "Convective Heat Transfer Across Rotating Cylinder at Unsteady Laminar Flow Regime," *Int. J. Engg. Research*, vol. 3, no. 20, p. 4, 2015.

[49] Roshko A., "Experiments on the flow past a circular cylinder at very high Reynolds number," J. Fluid Mech., vol. 10, no. 3, pp. 345–356, 1961.

[50] Yazdi M. J. E. and Khoshnevis A. B., "Experimental study of the flow across an elliptic cylinder at subcritical Reynolds number," *Eur. Phys. J. Plus*, vol. 133, pp. 533-544, 2018.

[51] Ford C. L. and Winroth P. M., "On the scaling and topology of confined bluff-body flows," *J. Fluid Mech.*, vol. 876, pp. 1018-1040, 2019.

[52] Arumuru V., Agrawal A. and Prabhu S. V., "Experimental investigations on flow over a circular cylinder placed in a circular pipe," Phys. Fluids., vol. 32, no. 9, pp. 1-12, 2020.

[53] Maryami R., Ali S. A. S., Azarpeyvand M. and Afshari A., "Turbulent flow interaction with a circular cylinder," Phys. Fluids, vol. 32, no. 1, pp. 1-18, 2020.

[54] Islam W. S. and Raghavan V. R., "Numerical Simulation of High Sub-critical Reynolds Number Flow Past a Circular Cylinder," *Int. Conf. Boundary and Inter. Layers*, pp. 1-8, 2006.

[55] Benim A. C., "RANS Predictions of Turbulent Flow Past a Circular Cylinder over the Critical Regime," *Int. Conf. Fluid Mech. Aero.*, pp. 232–237, 2007.

[56] Rahman M. M., Karim M. M., and Alim M. A., "Numerical investigation of unsteady flow past a circular cylinder using 2-D finite volume method," *J. nav. arch. mar. engg.*, vol. 4, no. 1, pp. 27–42, 2007.

[57] Parnaudeau P., Carlier J., Heitz D., and Lamballais E., "Experimental and numerical studies of the flow over a circular cylinder at Reynolds number 3900," *Phys. Fluids*, vol. 20, no. 8, pp. 1–14, 2008.

[58] Ong M. C., Utnes T., Holmedal L. E., Myrhaug D., and Pettersen B., "Numerical simulation of flow around a smooth circular cylinder at very high Reynolds numbers," *Marine Struct.*, vol. 22, no. 2, pp. 142–153, 2009.

[59] Yagmur S., Dogan S., Aksoy M. H., Canli E., and Ozgoren M., "Experimental and Numerical Investigation of Flow Structures around Cylindrical Bluff Bodies," *EPJ Web of Conf.*, vol. 92, pp. 1–7, 2015.

[60] Yuce M. I. and Kareem D. A., "A Numerical Analysis of Fluid Flow Around Circular and Square Cylinders," *J. American Water Works Asso.*, vol. 108, pp. 546–554, 2016.

[61] Daneshi M., "Numerical Investigation of the Fluid Flow around and Past a Circular Cylinder by Ansys Simulation," *Int. J. Advanced Sci. Tech.*, vol. 92, pp. 49–58, 2016.

[62] Tabata M. and Fujima S., "Finite-element analysis of high Reynolds number flows past a circular cylinder," *J. Comput. Appl. Math.*, vol. 38, pp. 411–424, 1991.

[63] Tutar M. and Holdø A. E., "Computational modelling of flow around a circular cylinder in sub-critical flow regime with various turbulence models," *Int. J. Numer. Meth. Fluids*, vol. 35, pp. 763–784, 2001.

[64] Young M. E. and Ooi A., "Turbulence Models and Boundary Conditions for Bluff Body Flow," *Australian Fluid Mech. Conf.*, pp. 1–4, 2004.

[65] Dong S. and Karniadakis G. E., "DNS of flow past a stationary and oscillating cylinder at," *J. Fluids Struct.*, vol. 20, no. 4, pp. 519–531, 2005.

[66] Rodríguez I., Lehmkuhl O., Piomelli U., Chiva J., Borrell R., and Oliva A., "Numerical simulation of roughness effects on the flow past a circular cylinder," *J. Phys.: Conf. Ser.*, vol. 745, pp. 1–8, 2016.

[67] Xie J. and Wang X., "Modelling Two-Dimensional Flow Around a Circular Cylinder with Different Roughness Height," in *Proceedings of the 2016 2nd International Conference on Architectural, Civil and Hydraulics Engineering (ICACHE 2016)*, Kunming City, China, 2016, pp. 228–233, 2021.

[68] Pang A. L. J., Skote M., and Lim S. Y., "Modelling high Re flow around a 2D cylindrical bluff body using the k-ω (SST) turbulence model," *Progress in Comput. Fluid Dynamics*, vol. 16, no. 1, pp. 48–57, 2016.

[69] Plata M. L. Naddei F. and Couaillier V., "LES of the flow past a circular cylinder using a multiscale discontinuous Galerkin method," *Int. Conf. Turbul. Inter.*, 2018.

[70] Yao J., Lou W., Shen G., Guo Y. and Xing Y., "Influence of Inflow Turbulence on the Flow Characteristics around a Circular Cylinder," *Appl. Sci.*, vol. 9, no. 17, pp. 3595-3614, 2019.

[71] Kumar P. and Singh S. K., "Flow past a bluff body subjected to lower subcritical Reynolds number," *J. Ocean Engg. Sci.*, vol. 5, pp. 173-179, 2020.

[72] Ooi A., Chan L., Lu W., Cao Y., Philip J., Leontini J. and Skvortsov A.., "Turbulent Flow Over a Confined Cylinder at Re=3,900," in *Proceedings of the 22nd Australasian Fluid Mechanics Conference AFMC2020*, Brisbane, Australia, 2020, pp. 1–4, 2020.

[73] Sowoud K. M., AL-Filfily A. A. and Abed B. H., "Numerical investigation of 2D Turbulent flow past a circular cylinder at lower subcritical Reynolds number," *Int. Conf. Sustainable Engg. Tech.*, vol. 881, pp. 1-11, 2020.

[74] Sooraj P., Ramagya M. S., Khan M. H., Sharma A. and Agrawal A., "Effect of superhydrophobicity on the flow past a circular cylinder in various flow regimes," *J. Fluid Mech.*, vol. 897, pp. 1-31, 2020.

[75] Kravchenko A. G. and Moin P., "Numerical studies of flow over a circular cylinder at ReD=3900," *Phys. Fluids*, vol. 12, no. 2, pp. 403–417, 2000.

[76] Breuer M., "A challenging test case for large eddy simulation: high Reynolds number circular cylinder ¯ow," *Int. J. Heat Fluid Flow*, vol. 21, pp. 648–654, 2000.

[77] Catalano P., Wang M., Iaccarino G., and Moin P., "Numerical simulation of the flow around a circular cylinder at high Reynolds numbers," *Int. J. Heat Fluid Flow*, vol. 24, no. 4, pp. 463–469, 2003.

[78] Rodríguez I., Lehmkuhl O., Chiva J., Borrell R., and Oliva A., "On the flow past a circular cylinder from critical to super-critical Reynolds numbers: Wake topology and vortex shedding," *Int. J. Heat Fluid Flow*, vol. 55, pp. 91–103, 2015.

[79] Sidebottom W., Ooi A., and Jones D., "A Parametric Study of Turbulent Flow Past a Circular Cylinder Using Large Eddy Simulation," *J. Fluids Engg.*, vol. 137, no. 9, pp. 1–13, 2015.

[80] Zhang C., Moreau S. and Sanjosé M., "Turbulent flow and noise sources on a circular cylinder in the critical regime," AIP adv., vol. 9, no. 8, pp. 1-17, 2019.

[81] Sanjital S. and Goldstein R. J., "Forced convection heat transfer from a circular cylinder in crossflow to air and liquids," *Int. J. Heat & Mass Trans.*, vol. 47, pp. 4795–4805, 2004.

[82] Shao J. and Zhang C., "Numerical analysis of the flow around a circular cylinder using RANS and LES," *Int. J. Comput. Fluid Dynamics*, vol. 20, no. 5, pp. 301–307, 2006.

[83] Ma H. and Duan Z., "Similarities of Flow and Heat Transfer around a Circular Cylinder," *Symmetry*, vol. 12, no. 4, pp. 658-670, 2020.

[84] Badr H. M., Coutanceau M., Dennis S. C. R., and Ménard C., "Unsteady flow past a rotating circular cylinder at Reynolds numbers 10^3 and 10^4," *J. Fluid Mech.*, vol. 220, pp. 459–484, 1990.

[85] Cheng M., Chew Y. T., and Luo S. C., "Discrete vortex simulation of the separated flow around a rotating circular cylinder at high Reynolds number," *Finite Elements in Analysis and Design*, vol. 18, no. 1–3, pp. 225–236, 1994.

[86] Nair M. T., Sengupta T. K., and Chauhan U. S., "flow past rotating cylinders at high reynolds numbers using higher order upwind scheme," *Computers & Fluids*, vol. 27, no. 1, pp. 47–70, 1998.

[87] Dierich M., Gersten K., and Schlottmann F., "Turbulent flow around a rotating cylinder in a quiescent fluid," *Experiments in Fluids*, vol. 25, no. 5–6, pp. 455–460, 1998.

[88] Chou M. H., "Numerical study of vortex shedding from a rotating cylinder immersed in a uniform flow field," *Int. J. Numer. Meth. Fluids*, vol. 32, pp. 545–567, 2000.

[89] Elmiligui A., Abdol-Hamid K., Massey S., and Pao S., “Numerical Study of Flow Past a Circular Cylinder Using RANS, Hybrid RANS /LES and PANS Formulations,” in *22nd Applied Aerodynamics Conference and Exhibit*, pp. 1–17, 2004.

[90] Takayama S. and Aoki K., “Flow characteristics around a rotating circular cylinder with arc grooves,” *Proc. Schl. Eng.*, vol. 29, pp. 9-14, 2004.

[91] Hwang J. Y., Yang K. S., and Bremhorst K., “Direct Numerical Simulation of Turbulent Flow Around a Rotating Circular Cylinder,” *J. Fluids Engg.*, vol. 129, no. 1, pp. 40–47, 2007.

[92] Cheng M. and Luo L. S., “Characteristics of two-dimensional flow around a rotating circular cylinder near a plane wall,” *Phys. Fluids*, vol. 19, no. 6, pp. 1–17, 2007.

[93] Dol S. S., Kopp G. A., and Martinuzzi R. J., “The suppression of periodic vortex shedding from a rotating circular cylinder,” *J. Wind Engg. Industrial Aerodynamics*, vol. 96, no. 6–7, pp. 1164–1184, 2008.

[94] Karabelas S. J., “Large Eddy Simulation of high-Reynolds number flow past a rotating cylinder,” *Int. J. Heat Fluid Flow*, vol. 31, no. 4, pp. 518–527, 2010.

[95] Karabelas S. J., Koumroglou B. C., Argyropoulos C. D., and Markatos N. C., “High Reynolds number turbulent flow past a rotating cylinder,” *Appl. Math. Modelling*, vol. 36, no. 1, pp. 379–398, 2012.

[96] Yao Q., Zhou C. Y., and Wang C., “Numerical Study of the Flow past a Rotating Cylinder at Supercritical Reynolds Number,” in *Proceedings of the 2016 4th International Conference on Mechanical Materials and Manufacturing Engineering*, pp. 813–816, 2016.

[97] Mgaidi A. M., Rafie A. S. M., Ahmad K. A., Zahari R., Hamid M. F. A., and Marzuki O. F., “Numerical and experimental analyses of the flow around a rotating circular cylinder at subcritical regime of reynolds number using k-ε and k-ω-sst turbulent models,” *Asian Research Publishing Network*, vol. 13, no. 3, p. 7, 2018.

[98] Ezadi Yazdi M. J., Rad A. S., and Khoshnevis A. B., “Features of the flow over a rotating circular cylinder at different spin ratios and Reynolds numbers: Experimental and numerical study,” *Eur. Phys. J. Plus*, vol. 134, no. 5, pp. 189–210, 2019.

[99] Chen W., Rheem C. K., Lin Y. and Li Y., “Experimental investigation of the whirl and generated forces of rotating cylinders in still water and in flow,” *Int. J. Naval Arch. Ocean Engg.*, vol. 12, pp. 531-540, 2020.

[100] Ozerdem B., "Measurement of convective heat transfer coefficient for a horizontal cylinder rotating in quiescent air," *Int. Comn. Heat & Mass Trans.*, vol. 27, Issue. 3, pp. 389-395, 2000.

[101] Seghir-Ouali S., Saury D., Harmand S., Phillipart O. and Laloy D., "Convective heat transfer inside a rotating cylinder with an axial air flow," *Int. J. Thermal Sci.*, vol. 45, pp. 1166–1178, 2006.

[102] Eighnam R. I., "Experimental and numerical investigation of heat transfer from a heated horizontal cylinder rotating in still air around its axis," *Ain Shams Engg. J.*, vol. 5, pp. 177-185, 2014.

[103] Launder B.E and Spalding D.B., "The numerical computation of turbulent flows," *Computer Methods in Appl. Mech. Engg.*, vol. 3, pp. 269-289, 1974.

[104] Wilcox, D. C., "Turbulence modeling for CFD (Vol. 2)," DCW Industries La Canada, CA., 1994.

[105] Wilcox D.C., "Reassessment of the scale determining equation for advanced turbulence models," *American Institute of Aeronautics and Astronautics Journal.* Vol. 26, no. 11, pp. 1299-1310, 1988.

[106] Abe K., Kondoh T., and Nagano Y., "A New Turbulence Model for Predicting Fluid Flow and Heat Transfer in Separating and Reattaching Flows — I. Flow Field Calculations", *Int. J. Heat and Mass Transfer*, vol. 37, no. 1, pp. 139–151, 1994.

[107] Mollik T. and Roy B., "*Turbulence Modeling of Channel Flow and Heat Transfer: A Comparison with DNS Data*," M. Sc. Engg. Thesis, Department of Mechanical Engineering, Bangladesh University of Engineering and Technology, 2016.

[108] Zienkiewicz O.C., Taylor R. L. and Zhu J. Z. (2005), *The Finite Element Method: Its Basis and Fundamentals*. Edition: Sixth, Publisher: Elsevier.

[109] Basak T. and Ayappa K.G., "Influence of Internal Convection during Microwave Thawing of Cylinders," *J. American Institute Chem. Engg.,* pp. 835-850, vol. 47, 2001.

[110] Chung T. J. (1927) *Computational Fluid Dynamics*. Cambridge University Press; 0 edition.

[111] Hoerner S. F. (1965) *Fluid-Dynamic Drag*. American Institute of Aeronautics and Astronautics, New York.